VIRGINIA POLYTECHNIC INSTITUTE
AND STATE UNIVERSITY

The Charles E. Via, Jr. Department
of Civil and Environmental Engineering
Blacksburg, VA 24061

Structural Engineering and Materials

COMPUTATIONAL STUDY OF TENSION FIELD ACTION IN GABLE FRAME PANEL ZONES

Gengrui Wei
Graduate Research Assistant

Ioannis Koutromanos, Ph.D.
Assistant Professor

Thomas M. Murray, Ph.D., P.E.
Emeritus Professor

Matthew R. Eatherton, Ph.D., S.E.
Associate Professor

Report No. CE/VPI-ST-17/03

April 2018

EXECUTIVE SUMMARY

Past experiments have shown that thin panel zones in the knee joint of a gable frame are capable of developing tension field action (TFA) when there are full depth column web stiffeners and the joint is subjected to negative bending (top flange of the rafter is in tension). Conversely, experiments on knee joints subjected to positive bending have shown that a tension field can partially, but not fully develop. This report describes an analytical and computational study that investigates the shear strength of thin panel zones subjected to positive bending.

A plastic mechanism model was developed to predict the post-buckling shear strength of panel zones subjected to positive bending. The model is based on plastic mechanism analysis and accounts for partially developed TFA. Using this model, a prediction equation for panel zone shear strength was derived and was found to be a function of three design parameters: flange flexural strength, panel aspect ratio, and panel slenderness.

A literature review of past tests on knee joints with thin panel zones found twenty applicable previous tests. Twelve tests on knee joints with full depth column web stiffeners subjected to negative bending verified that full tension field action developed. Four tests on knee joints with partial depth column web stiffeners subjected to negative bending developed a shear strength comparable to the shear buckling strength without tension field action. Four knee joints with full depth column web stiffeners subjected to positive bending developed approximately two times their shear buckling strength, but only about 70% of the total strength expected if tension field action fully formed. A finite element (FE) model was created for two of these specimens and was shown to accurately capture the strength and buckling behavior from the experiments.

A parametric computational study was then conducted on fifty-six prototype knee joint configurations, to quantify the effect of the three primary design parameters on panel zone shear strength and to validate the derived equation. The range of design variables considered in the computational study were based on responses from an industry survey administered by MBMA. Several sub-studies were also conducted to investigate the effect of other variables on TFA in the panel zone such as: different flange thicknesses on different sides of the panel zone, varying frame

width and roof height, prismatic versus tapered sections, orientation of end-plate connection (horizontal, vertical, sloped), and variations in roof slope.

Two types of load-displacement response were obtained, some that experienced hardening (i.e. increasing in strength) after the mechanism formed, and others that experienced softening associated with larger flange deformations. It was found that configurations with normalized flange flexural strength less than 0.05 exhibited softening. There are three reasons to be cautious with configurations that produce softening response including: 1) the cumulative plastic strains were larger than the models with hardening behavior and thus softening joints may be more prone to fracture, 2) the panel zone shear strength is expected to be more sensitive to initial imperfections and residual stresses, and 3) the consequences of reaching this limit state are worse because it is a brittle failure mode.

A modification to the derived panel zone shear strength equation was calibrated based on computational study results to account for boundary conditions. The computational study showed that, for the range of dimensions and parameters considered in this study, the modified equation can predict the panel zone shear strength with an average error of 1% with reasonably high confidence (corresponding to a standard deviation of 4%). The final proposed equations for panel zone shear strength, V_{PZ}, of gable frame knee joints subjected to positive bending including partial tension field action are provided. However, the use of TFA in positive bending is not recommended for configurations that will produce softening (normalized flange flexural strength less than 0.05), until further testing is conducted.

ACKNOWLEDGEMENTS

This work was supported by the Metal Building Manufacturers Association (MBMA) and the American Iron and Steel Institute (AISI). The authors appreciate the help from Dean Jorgenson, President of Metal Building Software, Inc. for conducting the design of five prototype metal building gable frames. Special thanks also go out to the industry survey respondents for providing valuable information on the industry practice. Thanks also to the MBMA advisory group for their input, and to Advanced Research Computing (ARC) at Virginia Tech for support on supercomputing resources.

TABLE OF CONTENTS

Contents

CHAPTER 1 INTRODUCTION

1.1 Overview

Metal building systems are popular for low-rise buildings because they are associated with fast construction and cost efficiency. One of the main components of a metal building are gable frames which resist lateral and gravity loads. A gable frame consists of columns and rafters usually connected by an end-plate connection. The corner regions of a gable frame are sometimes referred to as knee joints and the column web in the knee joint is the panel zone. As the knee joint undergoes bending, the panel zone is subjected to significant shear forces.

The AISC *Specification* (AISC 2016a) allows beam webs to be designed considering tension field action (TFA) for interior panels (between transverse stiffeners) with an aspect ratio less than 3 and a web slenderness greater than a certain limit. Contrary to an interior beam web panel that has two opposing edges that rigidly anchor the tension field, the knee joint panel zone has two adjacent sides capable of fully anchoring the tension field. The outside flanges bounding the exterior corner of the panel zone may not be stiff enough to allow the development of full TFA when the knee joint is subjected to positive bending (tension on the bottom flange of the rafter). AISC Design Guide 16 (Murray and Shoemaker 2002) does not allow TFA for negative bending when the column web stiffeners are partial depth (see Figure 1-1c) based on work by Murray (1986) or in knee joints subjected to positive bending (see Figure 1-1d) based on work by Young and Murray (1996). In knee joints with full depth column web stiffeners subjected to negative bending (see Figure 1-1a) and joints with rafters on both sides (see Figure 1-1b), the AISC Design Guide 16 allows TFA.

While design guidelines do not currently consider TFA for positive bending (Figure 1-1d), some TFA will partially develop. Results from previous research programs have demonstrated additional post-buckling strength of the panel zone beyond the shear buckling strength. However, the amount of TFA, the consistency of this level of action, and the design parameters that affect this action are not well understood. The present report describes a computational study that investigates the behavior of gable frame knee joint panel zones subjected to positive bending, wherein the tension field is oriented from the interior to the exterior corners of the panel zone. The

study is also aimed at examining whether the strength attributed to a partially developed tension field can be consistently predicted and thus incorporated in design calculations.

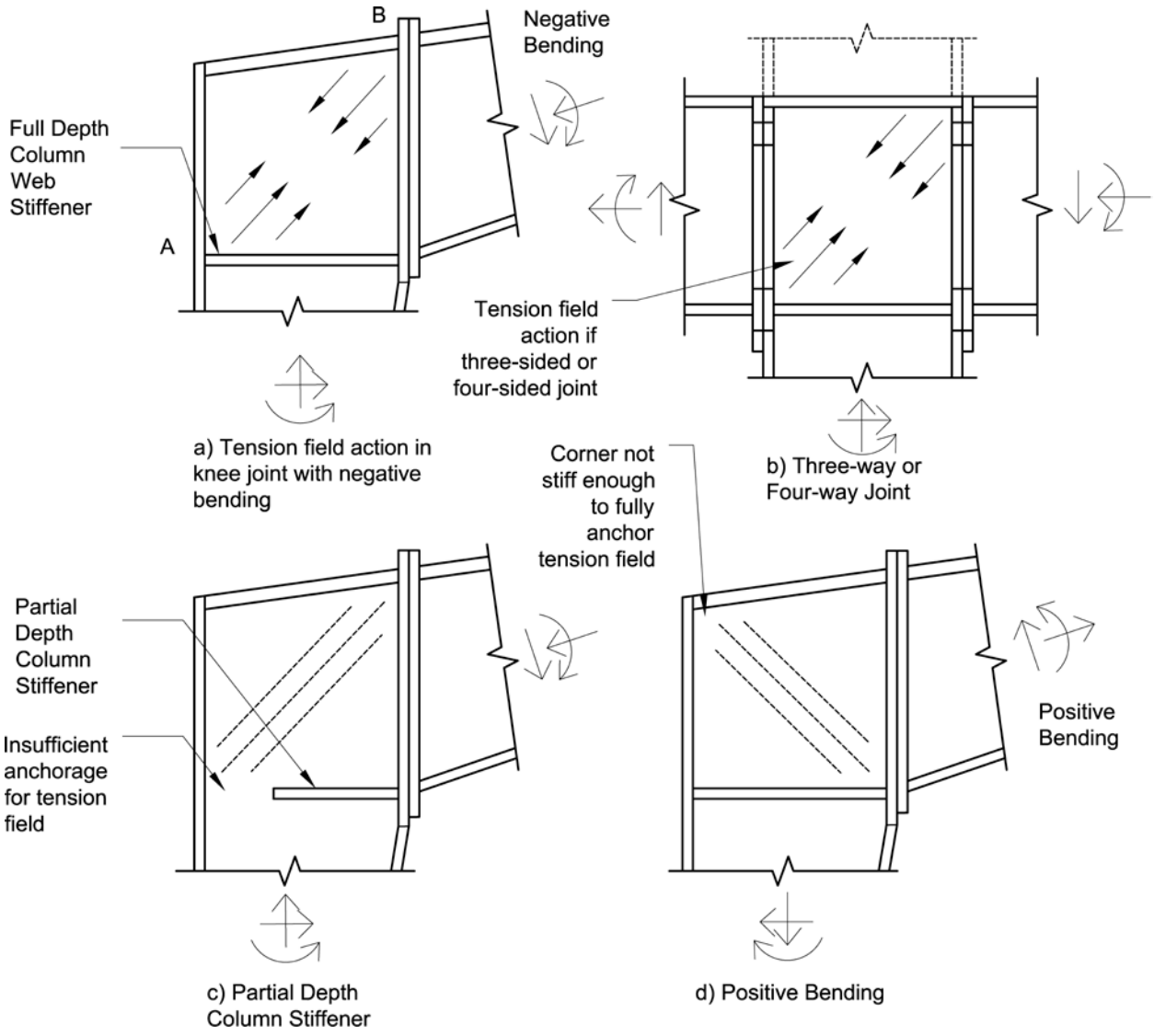

Figure 1-1 Variation of Panel Zone Configurations and Resulting Tension Fields

1.2 Scope of Research

A theoretical model was created based on plastic analysis to predict the post-buckling shear strength of panel zones due to partially developed TFA, for cases where the knee joint is subjected to positive bending. Using this model, an equation was derived to predict the panel zone shear

strength associated with partially developed TFA. The panel zone shear strength was found to depend on three design parameters, namely, flange flexural strength, panel aspect ratio, and panel slenderness. A parametric computational study involving fifty-six prototype knee joint configurations was conducted to quantify the effect of the aforementioned three design parameters on panel zone shear strength.

In developing the prototype knee joints for the parametric finite element method (FEM) study, the responses from an industry survey were used as a reference to determine the range of each configuration parameter. This study did not examine prototype configurations with partial depth stiffeners in the panel zone, for two reasons: 1) Available test data from the literature indicates that TFA does not develop for this type of knee joint configuration (see Chapter 2) and 2) The industry survey revealed that partial depth stiffeners in the panel zone are rarely used in practice (see Chapter 4). Therefore, the parametric finite element (FE) study only focused on the tension field action in panel zones of knee joints with full depth stiffeners subjected to positive bending.

Several sub-studies were also conducted to investigate the effect of different configurations on panel zone shear strength including variations such as: different flange / stiffener thicknesses on different sides of the panel zone, varying bay width and roof height, prismatic versus tapered sections, orientation of end-plate connection (horizontal, vertical, sloped), and variations in roof slope. The design of prototype configurations for these sub-studies is discussed in Chapter 4.

1.3 Organization of This Report

This report provides a literature review, derives an equation for characterizing TFA for knee joints subjected to positive moments, validates the use of a finite element modeling scheme for the computational analysis of prototype knee joints, conducts a parametric computational study, and provides several recommendations for designers. The report is organized into the following chapters:

- Chapter 1 introduces the present study and describes the motivation for investigating the post-buckling behavior of the panel zone in knee joints. It also summarizes the contents of this report.

- Chapter 2 provides a review of the literature relevant to this study. Both experimental programs and computational studies focusing on resistance of knee joints are presented in this chapter.
- Chapter 3 presents the derivation of equations for predicting the post-buckling shear strength of panel zones subjected to positive bending.
- Chapter 4 describes the methodology adopted in this study. It also provides an introduction to the industry survey and the philosophy of designing the prototype configurations for the studies.
- Chapter 5 validates the finite element modeling approach against available test data.
- Chapter 6 provides the results of the FE study. It also analyses and discusses the agreement of the predicted shear strength of each configuration from the derived equation to the one obtained from the FE analysis results.
- Chapter 7 summarizes the contents of this report. It provides some conclusions and design recommendations drawn from this research.
- Appendices provide the details of the industry survey questionnaire and responses from the participants, the design output of five prototype gable frames, and a database of results from the FE study.

CHAPTER 2 LITERATURE REVIEW

2.1 Introduction

Tension field action (TFA) can be developed in an appropriately stiffened thin panel subjected to shear. Such action leads to development of additional shear strength after the panel buckles. A significant amount of experimental research has been dedicated to studying the post-buckling shear behavior of stiffened steel panels. However, the majority of experimental tests have been conducted on interior joints with beams on both sides of a column, which are outside the focus of the present study. Only a limited number of tests have been conducted on knee joints of metal building gable frames.

One related study of note was conducted on end panels of plate girders. Kim and Uang (2015) experimentally and analytically investigated the shear strength of end panels in steel plate girders. They derived an analytical model and an accompanying shear strength equation which was tailored to the 2014 AASHTO provisions and accounted for the development of partial TFA. They deduced that the top flange and bearing stiffeners will be acting together with a portion of the web to enable the development of the tension field. The design equation was calibrated/validated using the results of the experimental tests and results of a parametric finite element analytical study. Their model is specifically tailored to the end panel regions of simply supported girders. For this reason, the developed equations may not be applicable to knee joint panel zones, but the study instead is an example of a similar research approach as the present study.

2.2 Experimental Programs

2.2.1 Summary

Previous experimental research of the structural behavior of metal building gable frame knee joints is summarized in Table 2-1.

Table 2-1 Experimental Programs Involving Metal Building Gable Frame Knee Joints

Specimen Type	Author(s)	Specimens	Summary
Knee joint	Jenner et al. (1985)	8 knee joint specimens with different panel zone dimensions and partial/full-depth stiffeners, 2 full frames.	Carried out frame assembly test to study the behavior of the knee joints and full frame tests to verify manufacturer's design procedure.
	Spangler and Murray (1989)	7 specimens with open-web truss-type rafters, full-length stiffeners, varied panel zone dimensions and slenderness.	Conducted tests of seven frame assemblies subjected to a single applied force. Conducted limit state analysis for all specimens and compared to test results.
	Scheer et al. (1991)	10 specimens with a scale of 1:2 to 1:4, varied web slenderness, flange thickness and ratios of the internal forces M/N and M/Q.	Conducted ten tests on square knee joints subjected to negative bending moment to analyze their behavior.
	Young and Murray (1997)	4 specimens with different panel zone dimensions and numbers and diameters of bolts.	Carried out four tests of the knee joint area of typical metal building frames to study the significance of tension field action under positive bending.
	Cristutiu (2010)	3 joint configurations with varying depths, widths and thicknesses of column and rafter sections. 2 specimens of each configuration were tested: monotonic and cyclic loading.	Investigated different beam-to-column joints for portal frames with tapered column and haunched rafter to establish their sensitivity due to the variation of different components of the joint.
Full frame	Forest and Murray (1982)	4 sets of 2 standard frames with varying clear spans, design loads, eave heights, frame spacing and roof slopes.	Conducted tests on standard manufactured rigid frames to determine the structural strength and stiffness of the frames.
	Hong and Uang (2012)	2 full-scale moment frames with non-compact, web-tapered members, 2 stages of testing: gravity load test and cyclic load test.	Cyclic testing of a full-scale metal building with built-up, web-tapered members was carried out to develop a seismic design procedure for this type of moment frame system.
	Uang et al. 2011	3 specimens consisting of one full bay (two frames) with 60' clear span and 20' eave height .	Shake table testing. Buildings were subjected to white noise and scaled ground motions up to three times the design basis earthquake

The full frame tests demonstrated that tension field action can develop, but did not provide sufficient panel zone shear force measurements to use in this study. For instance, Uang et al. (2011) conducted shake-table tests on metal building specimens, which included four gable frame panel

zones. Two of the panel zones included a vertically oriented end-plate connection, and the other two had a horizontally oriented plate. The observed response of the specimens indicated that joint panel regions can potentially serve as inelastic energy dissipation components, and that TFA can indeed develop in such regions.

Three of these testing programs (Young and Murray 1997, Sheer et al. 1991, and Jenner et al. 1985) provided sufficient documentation and data to evaluate the degree of tension field action that developed in the panel zones. The panel zone shear strengths from these three testing programs are evaluated in the following section.

2.2.2 Calculation of Shear Capacities

2.2.2.1 Young and Murray (1997)

Four tests were conducted on knee joints with full depth stiffeners subjected to positive bending (see Figure 2-1). The critical section regarding shear demand is determined to be at the top cross section of the column, as shown in Figure 2-2. The nominal shear strength, V_n, considering full tension field action can be calculated with AISC 360-16 Eq. G2-7 (AISC 2016a) as follows:

$$V_n = 0.6F_y A_w \left[C_{v2} + \frac{1 - C_{v2}}{1.15\sqrt{1 + (a/h)^2}} \right] \tag{2-1}$$

where

F_y = yield stress of the panel web plate material

A_w = overall area of the panel zone web plate at the section under consideration = $d_v\, t_w$

d_v = overall depth of the column at the section under consideration

t_w = panel zone web plate thickness

a = shortest side of the panel zone (see Figure 2-2 for an example)

h = longest side of the panel zone (see Figure 2-2 for an example)

C_{v2} = web shear buckling coefficient, determined as follows:

When $1.10\sqrt{k_v E/F_y} < h/t_w \le 1.37\sqrt{k_v E/F_y}$

$$C_{v2} = \frac{1.10\sqrt{k_v E / F_y}}{h/t_w} \tag{2-2}$$

When $h/t_w > 1.37\sqrt{k_v E/F_y}$

$$C_{v2} = \frac{1.51 k_v E}{(h/t_w)^2 F_y} \tag{2-3}$$

where

$$k_v = 5 + \frac{5}{(a/h)^2} = 5.34 \text{ when } a/h > 3.0 \tag{2-4}$$

Eq. (2-1) can be rewritten as:

$$V_n = V_{cr} + V_{TFA} \tag{2-5}$$

where V_{cr} is the predicted shear buckling strength of the panel web plate, and V_{TFA} is the predicted shear strength developed by the tension field action:

$$V_{cr} = 0.6 F_y A_w C_{v2} \tag{2-6}$$

$$V_{TFA} = \frac{0.6 F_y A_w (1 - C_{v2})}{1.15\sqrt{1 + (a/h)^2}} \tag{2-7}$$

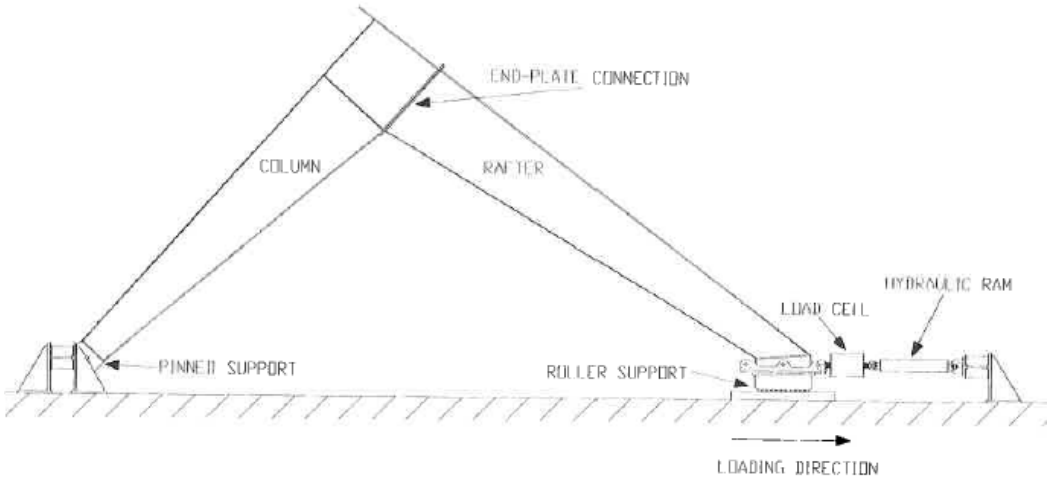

Figure 2-1 Test setup for all knee tests [from (Young and Murray 1997)]

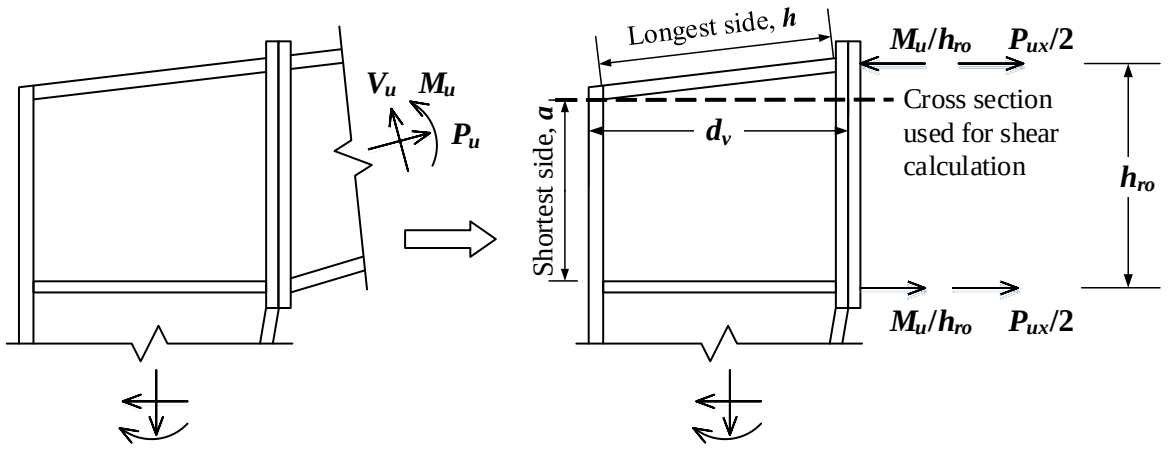

Figure 2-2 Identifying the cross section used for calculation of panel zone shear subjected to positive bending

Figure 2-2 shows that the section used to calculate the shear was a horizontal section across the top of the panel zone. It is noted that the horizontal section is an arbitrary choice and that the shear strength and shear demand can be calculated along any section of the panel zone as long as all shear forces and areas are calculated consistently. In some cases, engineers may want to calculate shear strength along the top sloping edge of the panel zone or the vertical outside edge of the panel zone, but since the definitions of the dimensions *a* and *h* are irrespective of the section chosen, and the shear stress is constant around the perimeter of the panel zone, all sections should result in the same ratio of shear strength to shear demand.

The predicted and experimental shear strength of the knee joints are provided in Table 2-2. V_{exp} is the experimental shear strength of the knee joints calculated with the test results as follows:

$$V_{exp} = V_u = \frac{M_u}{h_{ro}} - \frac{P_{ux}}{2} \tag{2-8}$$

where

M_u = Moment at the rafter face of the panel zone determined with maximum applied force

P_{ux} = Horizontal component of the axial tension force in the rafter determined by maximum applied force (Note that the calculations used P_u instead of P_{ux} for simplicity; it was found that this introduced only a 0.2% error in the calculation of V_{exp}).

h_{ro} = distance between the center lines of the rafter flanges at the rafter face of the panel zone

It can be observed from the results that the experimental shear strength of all specimens exceeded the predicted shear strength corresponding to buckling (as indicated by the fact that the ratio V_{exp}/V_{cr} is greater than 1.0), but was less than the predicted shear strength corresponding to full TFA (as indicated by the fact that the ratio $V_{exp}/(V_{cr}+V_{TFA})$ is less than 1.0). Therefore, TFA was partially developed in these test specimens.

Table 2-2 Predicted and Experimental Shear Strengths of Knee Joints

Specimen #	1	2	3	4
V_{exp} (kips)	43.2	46.8	119	148
V_{exp}/V_{cr}	1.18	1.48	2.33	3.68
$V_{exp}/(V_{cr}+V_{TFA})$	0.64	0.64	0.67	0.77

2.2.2.2 Jenner et al. (1985)

Eight knee joint tests were conducted with full or partial depth stiffeners subjected to negative bending (see Figure 2-3). The experimental shear strength and the predicted shear strengths of the knee joints are provided in Table 2-3. Specimens # 1 and 2 did not fail in panel web buckling and thus are not useful in evaluating TFA. For knee joints with full-depth stiffeners, TFA can fully develop (as indicated by the fact that the ratio $V_{exp}/(V_{cr}+V_{TFA})$ has values close to 1.0). However, for partial depth stiffeners, the ratio $V_{exp}/(V_{cr}+V_{TFA})$ has values less than 1.0, which indicates that TFA did not fully develop in these knee joints with partial depth stiffeners.

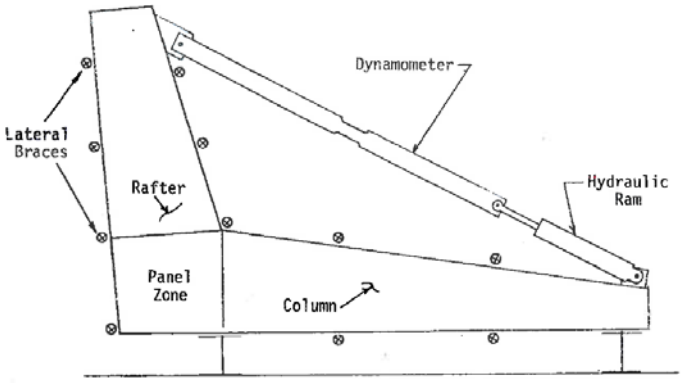

Figure 2-3 Test setup [from (Jenner et al. 1985)]

Table 2-3 Predicted and Experimental Shear Strengths of Knee Joints

	Partial Depth Stiffeners						Full Depth	
Specimen #	1	2	3	4	5	6	7	8
V_{exp} (kips)	36.8	55.7	54.7	95.2	81.8	120.8	94.9	85.2
V_{exp} / V_{cr}	N/A*	N/A	0.76	1.10	1.32	0.60	3.07	2.48
$V_{exp} / (V_{cr} + V_{TFA})$	N/A	N/A	0.48	0.57	0.70	0.33	0.97	0.96

*N/A: The specimen did not fail in panel zone web buckling.

2.2.2.3 Scheer et al. (1991)

Ten tests were conducted on knee joints with full-depth stiffeners, subjected to negative bending (see Figure 2-4). The experimental shear strengths and predicted shear strengths of the knee joints are provided in Table 2-4. It can be observed from the results that TFA was fully developed in this type of knee joint (as indicated by the fact that the average ratio $V_{exp} / (V_{cr} + V_{TFA})$ is 1.03 and very close to 1.0).

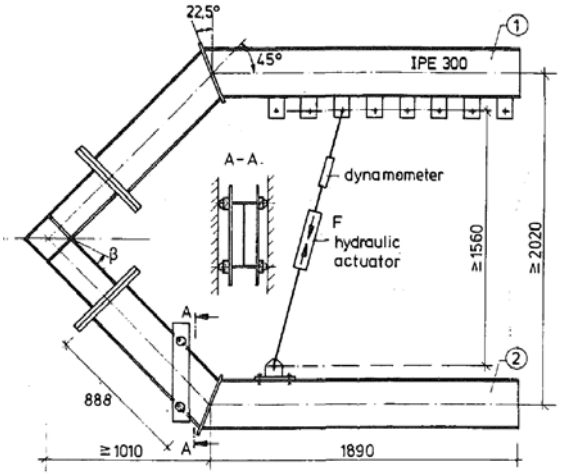

Figure 2-4 Test setup [from (Scheer et al. 1991)]

Table 2-4 Predicted and Experimental Shear Strengths of Knee Joints

Specimen #	1	2	3	4	5	6	7	8	9	10
V_{exp} (kN)	20.2	29.0	27.7	31.2	32.5	20.8	23.1	22.7	25.0	27.9
V_{exp} / V_{cr}	1.48	2.84	2.09	1.60	0.99	1.60	2.37	2.32	3.84	4.30
$V_{exp} / (V_{cr} + V_{TFA})$	0.84	1.35	1.18	1.04	0.88	0.90	1.11	1.09	0.90	1.01

2.2.2.4 Summary

Table 2-5 summarizes the shear strength calculation for twenty knee joint tests. As mentioned above, TFA can fully develop in knee joints subjected to negative bending with full-depth stiffeners, but does not develop in knee joints with partial-depth stiffeners. Knee joints with full-depth column web stiffeners exhibit partial TFA when subjected to positive bending. Further investigation is deemed necessary to reliably estimate the amount of TFA for such cases.

Table 2-5 Summary of Calculation Results

Bending Type	Column Web Stiffener	Number of Specimens	Average V_{exp} / V_{cr}	Average $V_{exp} / (V_{cr} + V_{TFA})$
Negative Bending	Full Depth	12	2.42	1.02
Negative Bending	Partial Depth	4	0.95	0.52
Positive Bending	Full Depth	4	2.17	0.68

2.3 Computational Studies

A number of computational studies focused on knee joints are summarized in Table 2-6. No positive bending or partial depth stiffeners were considered in these studies.

Table 2-6 Computational Studies Involving Metal Building Gable Frame Knee Joints

Author(s)	Models	Summary
Baumberger (2005)	8 models (SAP200): 2 rafter slopes with varying member sizes (depths).	Determined the forces in panel zone using finite element analysis and compared results with design procedure. Proposed equations for determining panel zone shear strength.
Cristutiu (2010)	36 models (ANSYS) with varying dimensions and steel grades of column, rafter and end plate.	Investigated different beam-to-column joints for portal frames with tapered column and haunched rafter to establish their sensitivity due to the variation of different components of the joint.
Gillman (2004)	7 models (SAP2000) with similar dimensions but varying rafter slopes.	Developed a design procedure for steel gable frames with a relatively steep pitch using shear values obtained from finite element analysis.
Liu and Li (2012)	2 sets of 16 models (ANSYS) in total with varied connection types, end-plate thicknesses, and bolt strengths.	Conducted finite element analysis to analyze the initial stiffness of end-plate connections of steel portal frames.
Sullivan and Charney (2006)	6 models (DIANA) with or without different types of stiffeners.	Carried out a series of finite element analyses to investigate the behavior and strength of the knee joints and to determine whether or not various types of stiffeners are required to provide required strength.

CHAPTER 3 DERIVATION OF EQUATIONS

3.1 Starting Assumptions

A theoretical model is established based on plastic analysis to predict the post-buckling shear strength of a knee joint panel zone subjected to positive bending. The model is based on the following assumptions:

1) The panel zone web plate is simply supported along its four edges by the panel zone flanges (similar assumption by Porter et al. 1975).
2) Plastic hinges develop in the panel zone flanges at the corner. These hinges lead to a mechanism in the panel zone after it buckles (see Rockey 1971, Porter et al. 1975).
3) The tensile stress in the tension field is uniformly distributed and its orientation, defined by an angle θ is parallel to the diagonal of the panel plate (Rockey 1971).
4) Panel edges on the rafter and column sides are rigid in-plane, but these two edges can undergo rigid body rotation relative to one another.
5) The shear strength associated with buckling V_{cr} remains constant after the panel buckles (Porter et al. 1975).

3.2 Critical Shear Stress at Buckling

Figure 3-1 shows a knee joint configuration that will be used in the proposed theoretical model. Parameters h_c and h_r in this figure correspond to the width and height of the panel web plate, while d_c and d_r correspond to the full width and full height of the section, and t_w is the thickness of the panel zone web plate.

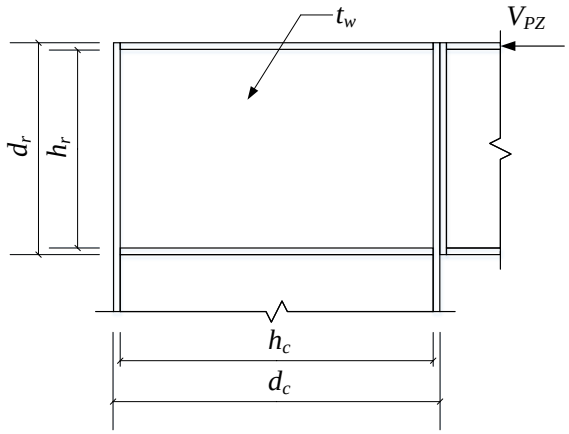

Figure 3-1 Knee joint configuration for the theoretical model

The shear strength, V_{PZ}, of the panel zone considering the contribution of TFA is given by:

$$V_{PZ} = V_{cr} + V_{TFA} \tag{3-1}$$

where the shear strength at buckling, V_{cr}, is given by:

$$V_{cr} = A_v \tau_{cr} = d_c t_w \tau_{cr} \tag{3-2}$$

and V_{TFA} is the post-buckling shear strength due to TFA.

For a simply supported rectangular plate, the critical shear stress at buckling, τ_{cr}, is given by Equation 9-7 in Timoshenko and Gere (1961):

$$\tau_{cr} = K\left[\frac{\pi^2 E}{12\left(1-\mu^2\right)}\right]\left(\frac{t_w}{h_c}\right)^2 \tag{3-3}$$

where *K* is a buckling coefficient, given by Equation 4.3 in Ziemian (2010):

$$K = \begin{cases} 5.34 + 4\left(\dfrac{h_c}{h_r}\right)^2 & \text{for } \dfrac{h_c}{h_r} < 1.0 \\ 5.34\left(\dfrac{h_c}{h_r}\right)^2 + 4 & \text{for } \dfrac{h_c}{h_r} > 1.0 \end{cases} \tag{3-4}$$

3.3 Tensile Stress of the Tension Field

For a plate undergoing shear buckling and then tension yielding along the TFA diagonal, the web stresses acting in directions $-\theta$ and $90° - \theta$ relative to the bottom flange (see Figure 3-2) are given by:

$$\begin{aligned} \sigma_\xi &= \left(-\tau_{cr}\right) sin\, 2\left(-\theta\right) + \sigma_t^y = \tau_{cr}\, sin\, 2\theta + \sigma_t^y \\ \sigma_\eta &= \left(-\tau_{cr}\right) sin\, 2\left(90° - \theta\right) = -\tau_{cr}\, sin\, 2\theta \\ \tau &= \left(-\tau_{cr}\right) cos\, 2\left(-\theta\right) = -\tau_{cr}\, cos\, 2\theta \end{aligned} \tag{3-5}$$

where θ is the angle of the tension field (taken as equal to the panel zone corner to corner angle). Using the Von Mises yield criterion, the material yields when the effective stress, σ_{mc}, becomes equal to the yield stress, σ_{yw}, with

$$\sigma_{mc} = \sqrt{\sigma_{\xi}^2 + \sigma_{\eta}^2 - \sigma_{\zeta}\sigma_{\eta} + 3\tau^2} \tag{3-6}$$

Substituting Eq. (3-5) into (3-6) and rearranging the terms results in the following expression for the diagonal tension field stress when the plate yields. The web plate will be assumed to resist this level of diagonal stress in the mechanism described in the next section.

$$\sigma_t^y = -\frac{3}{2}\tau_{cr}\, sin\, 2\theta + \sqrt{\sigma_{yw}^2 + \tau_{cr}^2\left(\left(\frac{3}{2} sin\, 2\theta\right)^2 - 3\right)} \tag{3-7}$$

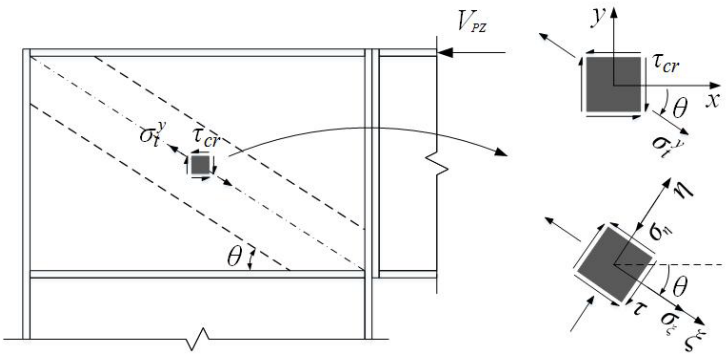

Figure 3-2 Stress transformation of a square element on the diagonal of the panel web

3.4 Plastic Analysis

Figure 3-3 shows the proposed failure mechanism for a thin knee joint panel zone subjected to pure shear.

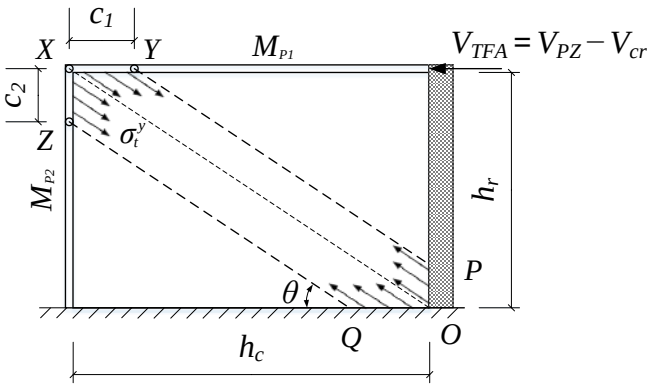

Figure 3-3 Proposed failure mechanism for a panel zone subjected to pure shear

Plastic hinges develop in the flanges at locations of maximum bending moment, where the shear force is zero (locations identified by dimensions c_1 and c_2 in Figure 3-3). The locations of these plastic hinges are obtained by considering the equilibrium of the flanges over segments X – Y and X – Z in Figure 3-3. If the moment strength of the flanges are taken as M_{P1} and M_{P2}, moment equilibrium about point X produces the following equations:

$$c_1\left(\sigma_t^y t_w\right) sin^2\theta\left(\frac{c_1}{2}\right) = M_{P1} + M_{P,min} \tag{3-8}$$

$$c_2\left(\sigma_t^y t_w\right) cos^2\theta\left(\frac{c_2}{2}\right) = M_{P2} + M_{P,min} \tag{3-9}$$

where $M_{P1} = \frac{\sigma_{yf} b_{f1} t_{f1}^2}{4}$, $M_{P2} = \frac{\sigma_{yf} b_{f2} t_{f2}^2}{4}$ and $M_{P,min} = min\left(M_{P1}, M_{P2}\right)$ define the plastic moment of the flange sections.

Solving Equations (3-8) and (3-9) for c_1 and c_2, respectively, gives equations that locate the flange plastic hinges:

$$c_1 = \frac{1}{sin\theta}\sqrt{\frac{2\left(M_{P1} + M_{P,min}\right)}{\sigma_t^y t_w}} \tag{3-10}$$

$$c_2 = \frac{1}{cos\theta}\sqrt{\frac{2\left(M_{P2} + M_{P,min}\right)}{\sigma_t^y t_w}} \tag{3-11}$$

Plastic mechanism analysis can then be conducted using virtual work. Virtual rotations ϕ_1 and ϕ_2 are assumed at the plastic hinges associated with the mechanism shown in Figure 3-4. The external and internal virtual work done by these virtual rotations must be equal to each other. It is worth mentioning that the work done by the panel zone tension field force is treated as external work because the work balance is conducted on the flanges as a rigid frame for which the panel zone is external.

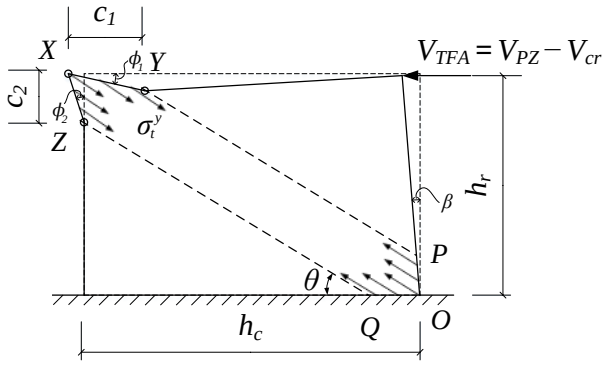

Figure 3-4 Mechanism with virtual displacements

$$
\begin{aligned}
W_{ext} &= V_{TFA}\left(c_2\phi_2\right) && \cdots \text{ work done by } V_{TFA} \\
&\quad -\sigma_t^y t_w \left(c_1 \sin\theta\right)\cos\theta \cdot c_2\phi_2 + \sigma_t^y t_w \left(c_1 \sin\theta\right)\sin\theta \cdot \frac{1}{2} c_1\phi_1 && \cdots \text{ work done on XY} \\
&\quad -\sigma_t^y t_w \left(c_2 \cos\theta\right)\cos\theta \cdot \frac{1}{2} c_2\phi_2 && \cdots \text{ work done on XZ} \\
&\quad +\sigma_t^y t_w \left(c_2 \cos\theta\right)\cos\theta \cdot \frac{1}{2} c_2\beta && \cdots \text{ work done on OP} \\
W_{int} &= M_{P,min}\left(\phi_1 + \phi_2\right) && \cdots \text{ work done at plastic hinge X} \\
&\quad + M_{P1}\left(\phi_1 + \beta\right) && \cdots \text{ work done at plastic hinge Y} \\
&\quad + M_{P2}\phi_2 && \cdots \text{ work done at plastic hinge Z}
\end{aligned}
\tag{3-12}
$$

where

$$
\begin{aligned}
c_1\phi_1 &= \left(h_c - c_1\right)\beta \\
c_2\phi_2 &= h_r\beta
\end{aligned}
\tag{3-13}
$$

The principle of virtual work is stated as:

$$
W_{ext} = W_{int} \tag{3-14}
$$

Substituting Eq.'s (3-10) (3-11) (3-12) & (3-13) into Eq. (3-14) and simplifying, one obtains:

$$V_{TFA} = \frac{M_{P1} - M_{P2} - M_{P,min}}{h_r} + \cos\theta\sqrt{2\sigma_t^y t_w}\left(\sqrt{M_{P1} + M_{P,min}} + \sqrt{M_{P2} + M_{P,min}}\right) \tag{3-15}$$

From Figure 3-4, the angle θ is found to be equal to:

$$\theta = arctan\frac{h_r}{h_c} \tag{3-16}$$

Plugging Eq. (3-16) into Eq. (3-7) and Eq. (3-15) leads to:

$$\sigma_t^y = -\frac{3h_c h_r \tau_{cr}}{h_c^2 + h_r^2} + \sqrt{\sigma_{yw}^2 + \tau_{cr}^2\left(\left(\frac{3h_c h_r}{h_c^2 + h_r^2}\right)^2 - 3\right)} \tag{3-17}$$

$$V_{TFA} = \frac{M_{P1} - M_{P2} - M_{P,min}}{h_r} + \frac{h_c}{\sqrt{h_c^2 + h_r^2}}\sqrt{2\sigma_t^y t_w}\left(\sqrt{M_{P1} + M_{P,min}} + \sqrt{M_{P2} + M_{P,min}}\right) \tag{3-18}$$

where τ_{cr} is given by Eq. (3-3).

Next, the stress τ_{cr} is written as $\tau_{cr} = C_v\tau_y$, where $\tau_y = \frac{\sigma_{yw}}{\sqrt{3}}$ and

$$C_v = \sqrt{3}K\left[\frac{\pi^2 E \big/ \sigma_{yw}}{12\left(1-\mu^2\right)}\right]\left(\frac{t_w}{h_c}\right)^2 \tag{3-19}$$

Equation (3-17) can be rewritten as:

$$\sigma_t^y = C_t\sigma_{yw} \tag{3-20}$$

where

$$C_t = -\frac{\sqrt{3}C_v h_c h_r}{h_c^2 + h_r^2} + \sqrt{1 + \frac{C_v^2}{3}\left(\left(\frac{3h_c h_r}{h_c^2 + h_r^2}\right)^2 - 3\right)} \tag{3-21}$$

Substituting Eq. (3-20) into Eq. (3-18) and normalizing both sides by $V_y = \sigma_{yw}h_c t_w$, produces:

$$\frac{V_{TFA}}{V_y} = \left(\frac{h_c}{6h_r}\right)\frac{M_{P1} - M_{P2} - M_{P,min}}{h_c^2 t_w \sigma_{yw}/6} + \frac{h_c}{\sqrt{h_c^2 + h_r^2}}\sqrt{\frac{C_t}{3}}\left(\sqrt{\frac{M_{P1} + M_{P,min}}{t_w h_c^2 \sigma_{yw}/6}} + \sqrt{\frac{M_{P2} + M_{P,min}}{t_w h_c^2 \sigma_{yw}/6}}\right) \tag{3-22}$$

Note that $M_y = \frac{t_w h_c^2 \sigma_{yw}}{6}$ is the corresponding yield moments of the panel plate cross sections parallel to the shear force direction. Therefore, it is recommended that the following normalized parameters are introduced:

$$M_{P1}^* = \frac{M_{P1}}{M_y} \tag{3-23}$$

$$M_{P2}^* = \frac{M_{P2}}{M_y} \tag{3-24}$$

where $M_y = \frac{t_w h_c^2 \sigma_{yw}}{6}$.

Equation (3-22) can now be rewritten as:

$$V_{TFA} = \left[\left(\frac{h_c}{6h_r} \right) \left(M_{P1}^* - M_{P2}^* - M_{P,min}^* \right) + \frac{h_c}{\sqrt{h_c^2 + h_r^2}} \sqrt{\frac{C_t}{3}} \left(\sqrt{M_{P1}^* + M_{P,min}^*} + \sqrt{M_{P2}^* + M_{P,min}^*} \right) \right] h_c t_w \sigma_{yw} \tag{3-25}$$

or:

$$V_{TFA} = \left[\left(\frac{1}{6 \tan\theta} \right) \left(M_{P1}^* - M_{P2}^* - M_{P,min}^* \right) + \cos\theta \sqrt{\frac{C_t}{3}} \left(\sqrt{M_{P1}^* + M_{P,min}^*} + \sqrt{M_{P2}^* + M_{P,min}^*} \right) \right] h_c t_w \sigma_{yw} \tag{3-26}$$

When $M_{P1}^* = M_{P2}^* = M_P^*$ (or $M_{P1} = M_{P2} = M_P$), Eq. (3-26) reduces to:

$$V_{TFA} = \left[-\frac{M_P^* \cot\theta}{6} + 2\cos\theta \sqrt{\frac{2C_t M_P^*}{3}} \right] h_c t_w \sigma_{yw} \tag{3-27}$$

In Chapter 6, these derived equations are compared to finite element analysis results and a modification factor for boundary conditions is found necessary. The final equations including the calibrated modification factor will be given in Chapter 7.

CHAPTER 4 METHODOLOGY

4.1 Introduction

The methodology adopted in this study to characterize tension field action (TFA) in panel zones is schematically summarized in Figure 4-1. The accuracy of the theoretical model presented in the previous chapter is validated through finite element analyses (FEA). A parametric investigation was conducted, involving different prototype configurations which were established using an industry survey. The finite element modeling scheme has been validated against data from previously conducted experimental tests which are available in the literature. By comparing the results from the FE study to the prediction from the derived equations, conclusions can be drawn and recommendations can be made.

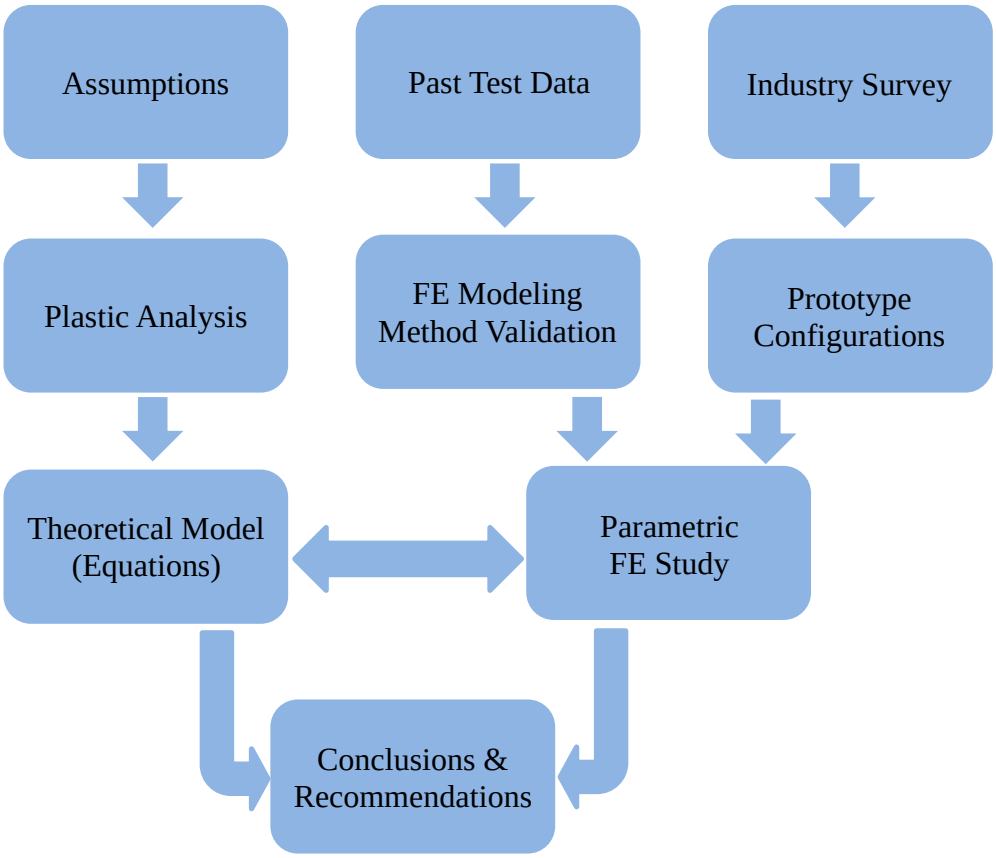

Figure 4-1 Illustration of the methodology

4.2 Industry Survey

The range of panel zone parameters to be investigated were determined in collaboration with MBMA. To ensure that the prototype configurations of the parametric study represent current design and construction practice, an industry survey was conducted to collect input from metal building manufacturers. A total of nine respondents (two from the same manufacturer), contributed to this survey. The survey included nine details regarding design of knee joints, including the web and flange thickness, the use of panel zone stiffeners and continuity plates, the orientation of the column-to-rafter bolted end-plate connection, column adjacent to the panel zone, rafter adjacent to the panel zone, and roof slope. The following sections summarize the survey and the provided responses. Further details regarding the survey are provided in Appendix A. Most of the respondents use A572 Gr. 55, A529 Gr. 55, or ASTM A1011 for the panel zone material. Grade 55 steel was used in the computational parametric study.

4.2.1 Panel Zone

4.2.1.1 Dimensions and Material

Table 4-1 provides a summary of the survey responses regarding the in-plane dimensions and thickness of the panel zone. The table includes the mean, median and standard deviation obtained from the survey responses, as well as the range of values adopted in the present study.

Table 4-1 Summary of Industry Survey on Panel Zone Dimensions

			Mean	Median	std	For Study
Panel zone	Panel web thickness	Min (in.)	0.131	0.134	0.005	0.1644-0.25
		Max (in.)	0.667	0.625	0.153	
		Typical min	0.157	0.135	0.039	
		Typical max	0.389	0.313	0.197	
	Panel height	Min (in.)	9.11	10.0	2.20	24-48
		Max (in.)	72.0	70.0	18.8	
		Typical min	16.0	18.0	5.20	
		Typical max	45.4	48.0	11.5	
	Panel width	Min (in.)	8.44	8.00	1.88	24-48
		Max (in.)	70.7	62.0	19.3	
		Typical min	14.7	12.0	5.57	
		Typical max	46.7	48.0	15.1	

Table 4-1 (Continued) Summary of Industry Survey on Panel Zone Dimensions

			Mean	Median	std	For Study
Panel zone	Panel aspect ratios	Min	0.50	0.50	0.18	0.67-1.50
		Max	2.80	2.50	1.35	
		Typical min	0.86	0.90	0.18	
		Typical max	1.49	1.23	0.70	
	Panel zone flange width	Min (in.)	5.11	5.00	0.33	5-16
		Max (in.)	16.1	15.0	3.69	
		Typical min	5.67	6.00	0.50	
		Typical max	10.7	10.0	3.00	
	Panel zone flange thickness	Min (in.)	0.216	0.250	0.043	0.25-1.5
		Max (in.)	1.42	1.50	0.306	
		Typical min	0.271	0.250	0.063	
		Typical max	0.806	0.750	0.331	

4.2.1.2 Web and Flanges

Table 4-2 summarizes survey information pertaining to the thickness of the panel web and knee joint flanges. The panel zone web can be either part of the web of one of the connected frame members (with the same thickness), or an inserted plate with a different thickness from the member webs. Few of the respondents use doubler plates. The flanges should have the same thickness as the flanges of the connected frame members, and the vertical flanges may have different dimensions from the top flange.

Table 4-2 Summary of Industry Survey on Panel Zone Web and Flanges

		Percentage of agreement	For Study
Panel Zone Web Options	Part of one of the connected frame members, same thickness.	88.9%	Yes
	Inserted plate, thickness can differ from connected frame members.	100%	Different thickness not considered
	Doubler plate is permitted, when needed.	11.1%	No doubler plates
Panel Zone Flange Options	Part of one of the connected frame members, same thickness.	88.9%	For main study
	Both flanges, vertical and top, same dimensions	0%	Vary Thicknesses in a Sub-Study

4.2.1.3 Panel Zone Stiffeners and Column/Rafter Web Stiffeners

The responses regarding the use of panel zone stiffeners that cross the panel zone and of column or rafter web stiffeners that align with the column or rafter flanges are summarized in Table 4-3. Given the responses that panel zone stiffeners are not common and because it is less likely that tension field action develops in panel zone with stiffeners, these stiffeners were not considered in the computational study. Based on the survey responses, the column or rafter web stiffeners on the side of the panel zone were oriented horizontal (for vertical end-plate connections) or vertical (for horizontal end-plate connections).

Table 4-3 Summary of Industry Survey on Panel Zone Stiffeners and Column/Rafter Web Stiffeners

<table>
<tr><td colspan="3"></td><td>Percentage</td><td>For Study</td></tr>
<tr><td rowspan="8">Panel Zone Stiffeners (crossing the panel zone)</td><td colspan="2">Used in approx. what percent of your buildings?</td><td>21.4%</td><td rowspan="8">No panel zone stiffeners considered</td></tr>
<tr><td rowspan="3">Orientation</td><td>Horizontal</td><td>100%</td></tr>
<tr><td>Vertical</td><td>42.9%</td></tr>
<tr><td>Diagonal</td><td>71.4%</td></tr>
<tr><td rowspan="2">Stiffener location</td><td>One side</td><td>85.7%</td></tr>
<tr><td>Both sides</td><td>71.3%</td></tr>
<tr><td rowspan="2">Stiffener welding</td><td>Long edge</td><td>66.7% Continuous
50% Intermittent</td></tr>
<tr><td>Short edges</td><td>83.3% Both edges
50% One edge</td></tr>
<tr><td rowspan="4">Column or Beam Web Stiffeners (aligned with column/rafter flanges)</td><td colspan="2">Aligned with rafter flange or horizontal?</td><td>100% Horizontal
33.3% Aligned</td><td>Horizontal</td></tr>
<tr><td colspan="2">Aligned with column flange or vertical?</td><td>85.7% Vertical
42.9% Aligned</td><td>Vertical</td></tr>
<tr><td colspan="2">How often are they partial depth?</td><td>Rarely</td><td rowspan="2">No partial depth</td></tr>
<tr><td colspan="2">How often are they full depth?</td><td>Almost always</td></tr>
</table>

4.2.2 End-Plate Connection Orientation

Table 4-4 provides a summary of the responses regarding the orientation of end-plate connections.

Table 4-4 Summary of Industry Survey on End-Plate Connection Orientation

			Percentage	For Study
Column-Rafter Bolted End-Plate Connection Orientation	Orientation varies?		77.8% Yes	Yes
	Orientation used	Horizontal	15.7%	Focus on vertical, sub-study on others.
		Vertical	48.6%	
		Sloped (Perpendicular to roof slope)	35.7%	
		Other	0.11%	

4.2.3 Column and Rafter Adjacent to the Panel Zone

The responses regarding the dimensions of the columns and rafters adjacent to the panel zone are almost the same as the corresponding ones for panel zone dimensions in Section 4.2.1. This is reasonable, because in practice, dimensions of the columns are often designed to be the same as the panel zone for convenience and cost saving purpose.

4.2.4 Roof Slope

Table 4-5 provides a summary of the responses for roof slope.

Table 4-5 Summary of Industry Survey on Roof Slope

		Mean	Median	std	For Study
Roof Slope	Min (deg.)	0.79	1.19	0.60	Focus on 2:12, substudy on 0:12 and 4:12
	Max (deg.)	34.0	31.7	10.2	
	Typical min (90%) (deg.)	2.84	2.40	1.68	
	Typical max (90%) (deg.)	18.0	18.4	4.75	

4.3 Prototype Configurations

4.3.1 Parametric Study with Three Varied Primary Design Variables

The panel strength obtained with the theoretical model of Chapter 3 primarily depends on three dimensionless variables, namely, panel web slenderness, $\max(h_c, h_r)/t_w$, panel web aspect ratio h_r/h_c, and the panel flange flexural strength parameter M_P^*. The range for the values of these variables in the prototype structures has been determined based on the industry survey results. Table 4-6 summarizes the values of the dimensionless variables for the 56 prototype knee joints.

Each prototype structure corresponds to a different combination of the three variables, to allow the individual assessment of the effect of each variable. The configurations of the prototype knee joints are summarized in Table 4-7. It is worth mentioning that, for all prototype structures, the flange parameter is identical for both flanges at the corner edges of the panel zone (i.e. the flanges on the two outside edges of the knee joint are assumed identical). All prototype configurations have a roof slope of 2:12 and a vertical end-plate connection. No stiffener is used in the panel zone.

Table 4-6 Values and Combinations of Three Variables

$\frac{\max(h_c, h_r)}{t_w}$	h_r/h_c	M_P^*	$\frac{\max(h_c, h_r)}{t_w}$	h_r/h_c	M_P^*	$\frac{\max(h_c, h_r)}{t_w}$	h_r/h_c	M_P^*	$\frac{\max(h_c, h_r)}{t_w}$	h_r/h_c	M_P^*
144	0.67	0.010	192	0.67	0.010	256	0.67	0.010	292	0.67	0.010
	0.75	0.005 0.010 0.050 0.100		0.75	0.005 0.010 0.050 0.100		0.75	0.005 0.010 0.050 0.100		0.75	0.005 0.010 0.050 0.100
	1.00	0.005 0.010 0.050 0.100		1.00	0.005 0.010 0.050 0.100		1.00	0.005 0.010 0.050 0.100		1.00	0.005 0.010 0.050 0.100
	1.33	0.005 0.010 0.050 0.100		1.33	0.005 0.010 0.050 0.100		1.33	0.005 0.010 0.050 0.100		1.33	0.005 0.010 0.050 0.100
	1.50	0.010		1.50	0.010		1.50	0.010		1.50	0.010

Note: h_c = column web height; h_r = rafter web height; t_w = panel web thickness; M_P^* = flange parameter as defined in Chapter 3.

Because this study focuses on the behavior of the panel zone, the columns and rafters are assumed to have the same cross-sectional dimensions (i.e., web height and thickness, flange width and thickness) as the corresponding dimensions of the panel zone. This is also consistent with industry practice as found in the survey.

The lengths of the columns (height of the building) for all prototype configurations are set equal to 15 ft. The rafter length is determined in such a way that the rafter of the knee joint extends to the nearest inflection point when subjected to a combination of typical gravity loads (D + L). The rafter length (distance from column to rafter inflection point) that is used in the computational model of the knee joint is given in Table 4-7.

To evaluate this method for choosing rafter length, a total of five prototype structures (four corresponding to extreme values in Table 4-7 and one based on average values of member dimensions and sectional modulus) were designed by Mr. Dean Jorgenson of Metal Building Software, Inc. in a reversed way. Specifically, the length of the frame members and member tapers were back-calculated given the knee joint dimensions and the design loads. A substudy was conducted to investigate the effects of column and rafter length and whether the sections being tapered has a substantial effect on panel zone behavior. Results provided in Chapter 6 show that these variables have a negligible impact on the shear strength of the panel zone. This allowed the models in the parametric study to use idealized lengths and prismatic sections.

Table 4-7 Prototype Configurations for Parametric Study

Model #	$\frac{\max(h_c, h_r)}{t_w}$	Panel aspect ratio h_r/h_c	M_P^*	Panel web thickness t_w (in.)	Panel height h_r (in.)	Panel width h_c (in.)	Panel flange width b_f (in.)	Panel flange thickness t_f (in.)	End-plate thickness t_p (in.)	Column length l_c (ft)	Rafter length l_r (ft)
1	144	0.67	0.010	0.2500	24	36	6	0.625	0.875	15	18.5
2	144	0.75	0.005	0.2500	27	36	8	0.375	0.750	15	17.0
3	144	0.75	0.010	0.2500	27	36	6	0.625	0.875	15	19.5
4	144	0.75	0.050	0.2500	27	36	10	1.000	1.125	15	29.5
5	144	0.75	0.100	0.2500	27	36	14	1.250	1.250	15	38.5
6	144	1.00	0.005	0.2500	36	36	8	0.375	0.750	15	20.5
7	144	1.00	0.010	0.2500	36	36	6	0.625	0.875	15	23.0
8	144	1.00	0.050	0.2500	36	36	10	1.000	1.125	15	34.5
9	144	1.00	0.100	0.2500	36	36	14	1.250	1.250	15	45.0
10	144	1.33	0.005	0.2500	36	27	6	0.313	0.750	15	18.5
11	144	1.33	0.010	0.2500	36	27	9	0.375	0.750	15	21.5
12	144	1.33	0.050	0.2500	36	27	10	0.750	1.000	15	31.0
13	144	1.33	0.100	0.2500	36	27	12	1.000	1.125	15	38.0
14	144	1.50	0.010	0.2500	36	24	6	0.375	0.750	15	20.5
15	192	0.67	0.010	0.2500	32	48	10	0.625	0.875	15	26.0
16	192	0.75	0.005	0.2500	36	48	8	0.500	0.875	15	23.0
17	192	0.75	0.010	0.2500	36	48	10	0.625	0.875	15	27.5
18	192	0.75	0.050	0.2500	36	48	12	1.250	1.250	15	41.5
19	192	0.75	0.100	0.2500	36	48	16	1.500	1.375	15	52.5
20	192	1.00	0.005	0.2500	48	48	8	0.500	0.875	15	27.5
21	192	1.00	0.010	0.2500	48	48	10	0.625	0.875	15	33.0
22	192	1.00	0.050	0.2500	48	48	12	1.250	1.250	15	49.5
23	192	1.00	0.100	0.2500	48	48	16	1.500	1.375	15	62.5
24	192	1.33	0.005	0.2500	48	36	8	0.375	0.750	15	24.5

Table 4-7 (Continued) Prototype Configurations for Parametric Study

Model #	$\frac{\max(h_c, h_r)}{t_w}$	Panel aspect ratio h_r/h_c	M_P^*	Panel web thickness t_w (in.)	Panel height h_r (in.)	Panel width h_c (in.)	Panel flange width b_f (in.)	Panel flange thickness t_f (in.)	End-plate thickness t_p (in.)	Column length l_c (ft)	Rafter length l_r (ft)
25	192	1.33	0.010	0.2500	48	36	6	0.625	0.875	15	27.5
26	192	1.33	0.050	0.2500	48	36	10	1.000	1.125	15	41.0
27	192	1.33	0.100	0.2500	48	36	14	1.250	1.250	15	53.5
28	192	1.50	0.010	0.2500	48	32	6	0.500	0.875	15	26.0
29	256	0.67	0.010	0.1875	32	48	8	0.625	0.875	15	22.5
30	256	0.75	0.005	0.1875	36	48	6	0.500	0.750	15	19.5
31	256	0.75	0.010	0.1875	36	48	8	0.625	0.875	15	24.0
32	256	0.75	0.050	0.1875	36	48	14	1.000	1.125	15	39.5
33	256	0.75	0.100	0.1875	36	48	14	1.500	1.375	15	48.5
34	256	1.00	0.005	0.1875	48	48	6	0.500	0.750	15	22.5
35	256	1.00	0.010	0.1875	48	48	8	0.625	0.875	15	28.0
36	256	1.00	0.050	0.1875	48	48	14	1.000	1.125	15	46.5
37	256	1.00	0.100	0.1875	48	48	14	1.500	1.375	15	57.5
38	256	1.33	0.005	0.1875	48	36	6	0.375	0.750	15	21.0
39	256	1.33	0.010	0.1875	48	36	6	0.500	0.750	15	23.0
40	256	1.33	0.050	0.1875	48	36	8	1.000	1.000	15	35.5
41	256	1.33	0.100	0.1875	48	36	10	1.250	1.125	15	44.0
42	256	1.50	0.010	0.1875	48	32	9	0.375	0.625	15	23.0
43	292	0.67	0.010	0.1644	32	48	10	0.500	0.750	15	21.5
44	292	0.75	0.005	0.1644	36	48	9	0.375	0.625	15	18.5
45	292	0.75	0.010	0.1644	36	48	10	0.500	0.750	15	23.0
46	292	0.75	0.050	0.1644	36	48	12	1.000	1.125	15	36.0
47	292	0.75	0.100	0.1644	36	48	16	1.250	1.250	15	47.0
48	292	1.00	0.005	0.1644	48	48	9	0.375	0.625	15	21.0
49	292	1.00	0.010	0.1644	48	48	10	0.500	0.750	15	26.5
50	292	1.00	0.050	0.1644	48	48	12	1.000	1.125	15	42.5
51	292	1.00	0.100	0.1644	48	48	16	1.250	1.250	15	55.5
52	292	1.33	0.005	0.1644	48	36	5	0.375	0.625	15	18.5
53	292	1.33	0.010	0.1644	48	36	10	0.375	0.625	15	22.0
54	292	1.33	0.050	0.1644	48	36	12	0.750	1.000	15	37.0
55	292	1.33	0.100	0.1644	48	36	14	1.000	1.125	15	46.5
56	292	1.50	0.010	0.1644	48	32	8	0.375	0.625	15	21.5

4.3.2 Sub-studies

A total of four sub-studies were also conducted to investigate the impact of several additional variables on the knee joint panel zone shear resistance.

4.3.2.1 Sub-study on Column and Rafter Lengths, and Use of Tapered Sections

The prototype structures considered in the main parametric study used fixed column height and prismatic members. In real buildings, a range of column heights are possible and members are typically tapered. To investigate the effect of these differences, a substudy was conducted with 15 configurations as shown in Table 4-8.

4.3.2.2 Sub-study on Flange Flexural Strength Parameter

In the main parametric study, the dimensions of the two flanges at the exterior edges of the panel zone are assumed identical. A sub-study was performed with 24 knee joint configurations to examine whether the derived equations are valid for cases where the dimensions for the two flanges are different. Table 4-9 summarizes the prototype configurations for this substudy.

Table 4-8 Prototype Configurations from Practical Design and Researchers' Preliminary Design

Model #	Panel web thickness t_w (in.)	Panel height h_r (in.)	Panel width h_c (in.)	Panel flange width b_f (in.)	Panel flange thickness t_f (in.)	End-plate thickness t_p (in.)	**Column length l_c (ft)**	**Rafter length l_r (ft)**
8	0.2500	36	36	10	1.0000	1.125	**15.00**	**34.50**
8MP	0.2500	36	36	10	1.0000	1.125	**28.75**	**23.24**
8MT	0.2500	36	36	10	1.0000	1.125	**28.75**	**23.24**
10	0.2500	36	27	6	0.3125	0.75	**15.00**	**18.50**
10MP	0.2500	36	27	6	0.3125	0.75	**14.72**	**16.61**
10MT	0.2500	36	27	6	0.3125	0.75	**14.72**	**16.61**
23	0.2500	48	48	16	1.5000	1.375	**15.00**	**62.50**
23MP	0.2500	48	48	16	1.5000	1.375	**26.83**	**30.36**
23MT	0.2500	48	48	16	1.5000	1.375	**26.83**	**30.36**
28	0.2500	48	32	6	0.5000	0.875	**15.00**	**26.00**
28MP	0.2500	48	32	6	0.5000	0.875	**19.75**	**22.54**
28MT	0.2500	48	32	6	0.5000	0.875	**19.75**	**22.54**
29	0.1875	32	48	8	0.6250	0.875	**15.00**	**22.50**
29MP	0.1875	32	48	8	0.6250	0.875	**15.30**	**15.77**
29MT	0.1875	32	48	8	0.6250	0.875	**15.30**	**15.77**

Note: Configurations with Model #8, 10, 23, 28, and 29 are extracted from Table 4-7, all with prismatic column and rafter sections, which are considered to be the four extreme cases and one average case. "MT" represents the designed configurations provided by MBMA (tapered sections). "MBMA prismatic" represent the same configurations as "MP" except that prismatic sections are used.

Table 4-9 Prototype Configurations with Different Flange Parameters for Panel Zone

Model #	$\frac{\max(h_c, h_r)}{t_w}$	Panel aspect ratio h_r/h_c	M_{P1}^*	M_{P2}^*	Panel web thickness t_w (in.)	Panel height h_r (in.)	Panel width h_c (in.)	Panel flange width b_f (in.)	Panel flange thickness t_{f1} (in.)	Panel flange thickness t_{f2} (in.)	End-plate thickness t_p (in.)	Column length l_c (ft)	Rafter length l_r (ft)
1A	144	0.75	**0.005**	**0.010**	0.2500	27	36	8	0.375	0.500	0.750	15	17.0
1B	144	0.75	**0.010**	**0.005**	0.2500	27	36	8	0.500	0.375	0.750	15	17.0
2A	144	1.00	**0.005**	**0.010**	0.2500	36	36	8	0.375	0.500	0.750	15	20.5
2B	144	1.00	**0.010**	**0.005**	0.2500	36	36	8	0.500	0.375	0.750	15	20.5
3A	144	1.33	**0.005**	**0.010**	0.2500	36	27	6	0.313	0.500	0.750	15	18.5
3B	144	1.33	**0.010**	**0.005**	0.2500	36	27	6	0.500	0.313	0.750	15	18.5
4A	192	0.75	**0.005**	**0.010**	0.2500	36	48	8	0.500	0.750	0.875	15	23.0
4B	192	0.75	**0.010**	**0.005**	0.2500	36	48	8	0.750	0.500	0.875	15	23.0
5A	192	1.00	**0.005**	**0.010**	0.2500	48	48	8	0.500	0.750	0.875	15	27.5
5B	192	1.00	**0.010**	**0.005**	0.2500	48	48	8	0.750	0.500	0.875	15	27.5
6A	192	1.33	**0.005**	**0.010**	0.2500	48	36	8	0.375	0.500	0.750	15	24.5
6B	192	1.33	**0.010**	**0.005**	0.2500	48	36	8	0.500	0.375	0.750	15	24.5
7A	256	0.75	**0.005**	**0.010**	0.1875	36	48	6	0.500	0.750	0.750	15	19.5
7B	256	0.75	**0.010**	**0.005**	0.1875	36	48	6	0.750	0.500	0.750	15	19.5
8A	256	1.00	**0.005**	**0.010**	0.1875	48	48	6	0.500	0.750	0.750	15	22.5
8B	256	1.00	**0.010**	**0.005**	0.1875	48	48	6	0.750	0.500	0.750	15	22.5
9A	256	1.33	**0.005**	**0.010**	0.1875	48	36	6	0.375	0.500	0.750	15	21.0
9B	256	1.33	**0.010**	**0.005**	0.1875	48	36	6	0.500	0.375	0.750	15	21.0
10A	292	0.75	**0.006**	**0.010**	0.1644	36	48	10	0.375	0.500	0.750	15	23.0
10B	292	0.75	**0.010**	**0.006**	0.1644	36	48	10	0.500	0.375	0.750	15	23.0
11A	292	1.00	**0.006**	**0.010**	0.1644	48	48	10	0.375	0.500	0.750	15	26.5
11B	292	1.00	**0.010**	**0.006**	0.1644	48	48	10	0.500	0.375	0.750	15	26.5
12A	292	1.33	**0.004**	**0.010**	0.1644	48	36	10	0.250	0.375	0.625	15	22.0
12B	292	1.33	**0.010**	**0.004**	0.1644	48	36	10	0.375	0.250	0.625	15	22.0

Note: Configurations with model numbers are not related to those with the same numbers in Table 4-7.

4.3.2.3 Sub-study on Orientation of End-Plate Connection

Another substudy was focused on the effect of the orientation of the end-plate connection. The prototype configurations for this substudy are provided in Table 4-10.

Table 4-10 Prototype Configurations with Different Orientations of End-Plate Connection

Model #	$\frac{\max(h_c, h_r)}{t_w}$	Panel aspect ratio h_r/h_c	M_P^*	Panel web thickness t_w (in.)	Panel height h_r (in.)	Panel width h_c (in.)	Panel flange width b_f (in.)	Panel flange thickness t_f (in.)	End-plate thickness t_p (in.)	Column length l_c (ft)	Rafter length l_r (ft)	**End-plate orientation**
6	144	1.00	0.005	0.25	36	36	8	0.375	0.750	15	20.5	**Vertical**
6H	144	1.00	0.005	0.25	36	36	8	0.375	0.750	15	20.5	**Horizontal**
6S	144	1.00	0.005	0.25	36	36	8	0.375	0.750	15	20.5	**Sloped**

Table 4-10 (Continued) Prototype Configurations with Different Orientations of End-Plate Connection

Model #	$\frac{\max(h_c, h_r)}{t_w}$	Panel aspect ratio h_r/h_c	M_P^*	Panel web thickness t_w (in.)	Panel height h_r (in.)	Panel width h_c (in.)	Panel flange width b_f (in.)	Panel flange thickness t_f (in.)	End-plate thickness t_p (in.)	Column length l_c (ft)	Rafter length l_r (ft)	**End-plate orientation**
25	192	1.33	0.01	0.25	48	36	6	0.625	0.875	15	27.5	**Vertical**
25H	192	1.33	0.01	0.25	48	36	6	0.625	0.875	15	27.5	**Horizontal**
25S	192	1.33	0.01	0.25	48	36	6	0.625	0.875	15	27.5	**Sloped**

Note: Configurations with Model #6 and #25 are extracted from Table 4-7, both with vertical end-plate connection. Model # containing "H" or "S" represents the same configuration as the corresponding one except that the end-plate connection is either horizontal or sloped (i.e. perpendicular to rafter).

4.3.2.4 Sub-study on Roof Slope

The fourth and final sub-study is focused on the effect of roof slope and involves the configurations provided in Table 4-11.

Table 4-11 Prototype Configurations with Different Roof Slopes

Model #	$\frac{\max(h_c, h_r)}{t_w}$	Panel aspect ratio h_r/h_c	M_P^*	Panel web thickness t_w (in.)	Panel height h_r (in.)	Panel width h_c (in.)	Panel flange width b_f (in.)	Panel flange thickness t_f (in.)	End-plate thickness t_p (in.)	Column length l_c (ft)	Rafter length l_r (ft)	**Roof slope**
6	144	1.00	0.005	0.25	36	36	8	0.375	0.750	15	20.5	**2:12**
6C	144	1.00	0.005	0.25	36	36	8	0.375	0.750	15	20.5	**0:12**
6D	144	1.00	0.005	0.25	36	36	8	0.375	0.750	15	20.5	**4:12**
25	192	1.33	0.010	0.25	48	36	6	0.625	0.875	15	27.5	**2:12**
25C	192	1.33	0.010	0.25	48	36	6	0.625	0.875	15	27.5	**0:12**
25D	192	1.33	0.010	0.25	48	36	6	0.625	0.875	15	27.5	**4:12**

Note: Configurations with Model #6 and 25 are extracted from Table 4-7, both with a roof slope of 2:12. Model # containing "C" or "D" represents the same configuration as the corresponding one except that the roof slope is either 0:12 or 4:12.

CHAPTER 5 FINITE ELEMENT MODELING APPROACH AND VALIDATION

5.1 Modeling Approach

The computational study is performed using the commercial finite element program *LS-DYNA* (LSTC 2016a; LSTC 2016b), which is capable of simulating structural response in the presence of material nonlinearity, large displacements and large strains. The models of the prototype structures employ shell elements with selectively reduced integration, using the formulation of Hughes and Liu (1981a; 1981b), to capture the inelastic hysteretic material behavior and the buckling of panel regions. As shown in Figure 5-1, refined three-dimensional shell element models simulate the connection regions, while the remainder of the frame members are modeled with much simpler frame (beam) elements, as this remainder of the frame is most likely to remain elastic during the loading and its behavior is not of primary interest in this study. The kinematics of the beam elements are also governed by the formulation of Hughes and Liu (1981). The aim of the modeling approach is to allow high-fidelity models for the connection regions which are the focus of the research, while entailing a computational cost which is as low as possible.

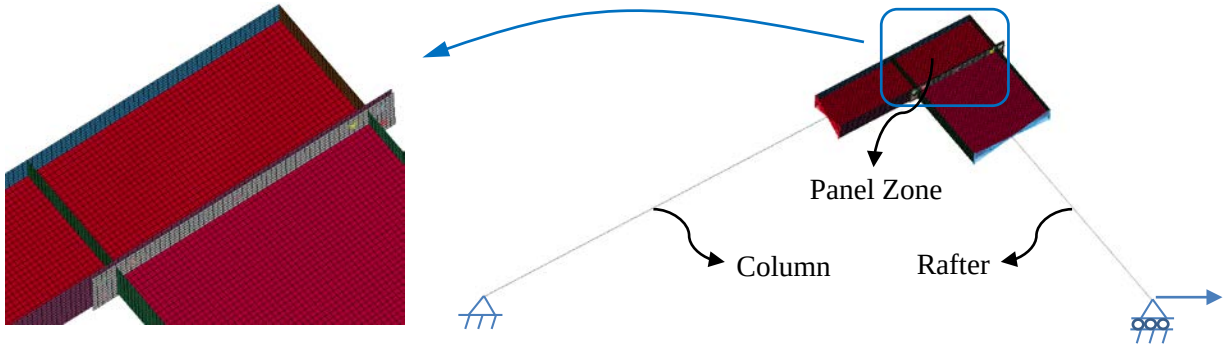

Figure 5-1 Finite element model with high-fidelity representation of the connection regions

The model shown in Figure 5-1 simulates a knee joint subjected to positive bending. The end of the beam (at the inflection point) and column (at the column base) are assumed to be points of zero moment. The application of loads as shown in Figure 5-1 produces relative magnitudes of axial force to bending moment in the members consistent with those in a real building. This configuration of loading is more accurate than applying only bending moments at the joint. Also,

because it holds the ratio of axial forces to bending moments relatively constant, it is considered more generalized than a full frame analysis that is dependent on specific loads and load combinations.

A mesh sensitivity study was performed to validate the finite element modeling approach. In general, a finer mesh (i.e., the use of a larger number of elements in a model, with each element having a smaller size) will lead to more accurate results. However, the computational cost will increase as the number of elements increases. Based on the mesh sensitivity study, an element size of 0.5 in. for the shell elements (e.g., 28×56 elements in a panel zone with 14 in. width and 28 in. height) was found to lead to practically converged results in terms of load-deformation response and deformed patterns/buckling modes, while also maintaining an acceptable computational cost.

An imperfection sensitivity study was also conducted (not shown here) to investigate the effect of initial out-of-plane imperfection of the panel web. The first buckling mode of the structure was obtained by eigenbuckling analysis, and an initial imperfection (based on this first mode) was introduced in the original geometry of each mesh. The imperfection values were scaled so that the maximum initial out-of-straightness of the panel web was equal to a certain fraction of the maximum dimension of the web plate. It was found that the stiffness of the structure was not significantly affected by the initial imperfection, but the peak load would decrease as the initial imperfection gets larger. In this study, the maximum initial out-of-straightness of the panel web is set to 1/72 times the maximum panel in-plane dimension, based on the tolerance allowed for deviations from a plane in the webs of built-up plate girders (according to MBMA) is 1/72 of the web depth (MBMA 2012). This value was also selected because it produced reasonable agreement with experimental results as described in the following section.

An elastoplastic constitutive relationship with elastic modulus, E = 29,000 ksi, yield stress equal to 55 ksi, linear kinematic hardening, and a hardening modulus of 400 ksi, was used to model the A572 Gr 55 steel material. The global equations of the structure were solved using an implicit, incremental/iterative scheme. The simulations adopted a displacement-controlled loading method, wherein the applied loads are introduced by applying a monotonically increasing displacement at the end of the rafter in the direction shown in Figure 5-1.

5.2 Validation Analyses

To validate the finite element modeling approach for this study, two specimens tested by Young and Murray (1997) were simulated, to ensure that the computational models can satisfactorily capture the load-displacement response and buckling modes.

Table 5-1 summarizes the information for the validation analyses. Detailed descriptions of the test specimens and testing program can be found in the report by Young and Murray (1997).

Table 5-1 Specimen Data Used for Modeling

Specimen #	1	2
Section type	Prismatic	Prismatic
Panel web yield stress, σ_{yw} (ksi)	71.9	70.3
Panel flange yield stress, σ_{yf} (ksi)	56.7	58.4
Panel width, h_c (in.)	12	14
Panel height, h_r (in.)	26	28
Panel web thickness, t_w (in.)	0.138	0.137
Panel flange width, b_f (in.)	6	6
Panel flange thickness, t_f (in.)	0.316	0.315
Experimental failure mode	Panel zone web buckling	Panel zone web buckling
Maximum applied load, F (kips)	16.9	21.9
Experimental panel zone shear strength, V_{exp} (kips)	43.2	46.8

5.3 Validation Analyses Results

5.3.1 Specimen 1

The analytically obtained force-displacement curve for specimen 1 is compared to the corresponding test data in Figure 5-2. The maximum applied forces obtained from the experiment and the FEA are 16.9 kips and 18.4 kips, respectively. The 8.9% error between the peak forces of the test and FEA results is most likely due to the existence of residual stress in the panel zone and surrounding flanges. At approximately 5 inches of applied displacement, a noticeable reduction of strength happened in the test specimen possibly due to the fracture of steel in the specimen, which is not captured in the FE model since it is beyond the scope of this study. Figure 5-3 shows the

deformed shape of the specimen in the test and the FE simulation. Overall, the FEA results agree reasonably well with the test data.

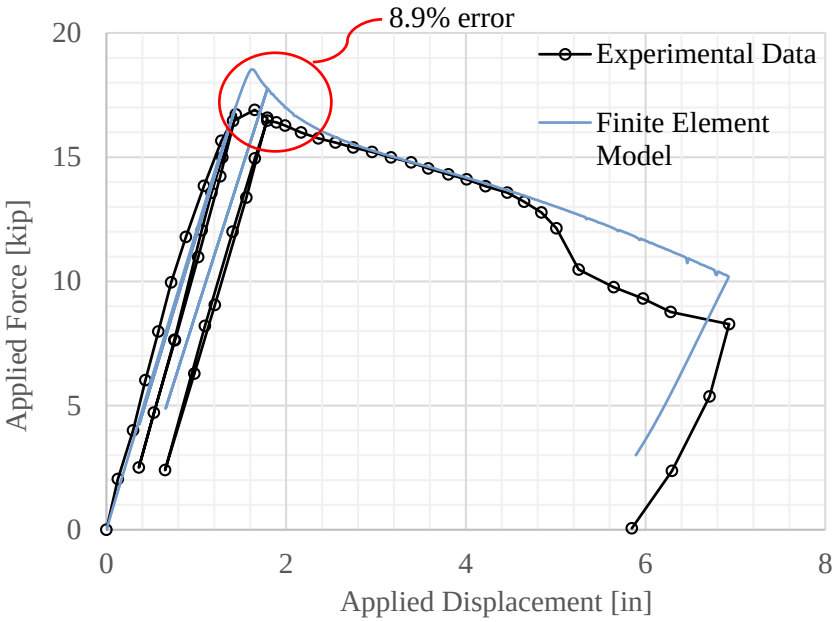

Figure 5-2 Applied force-displacement curves for Young and Murray (1997) Specimen 1

Figure 5-3 Deformed shapes of Young and Murray (1997) Specimen 1

5.3.2 Specimen 2

The comparison between the analytically obtained and experimentally recorded force-displacement curves for the second specimen is shown in Figure 5-4. The maximum applied forces obtained from the experiment and the FEA are 21.9 kips and 23.5 kips respectively, corresponding

to an error of 7.3%. This error is also attributed to the existence of residual stress in the panel zone and surrounding flanges. Figure 5-5 shows the deformed shape of the specimen in the test and the FE simulation. The agreement between the computational model and experimental test is deemed satisfactory.

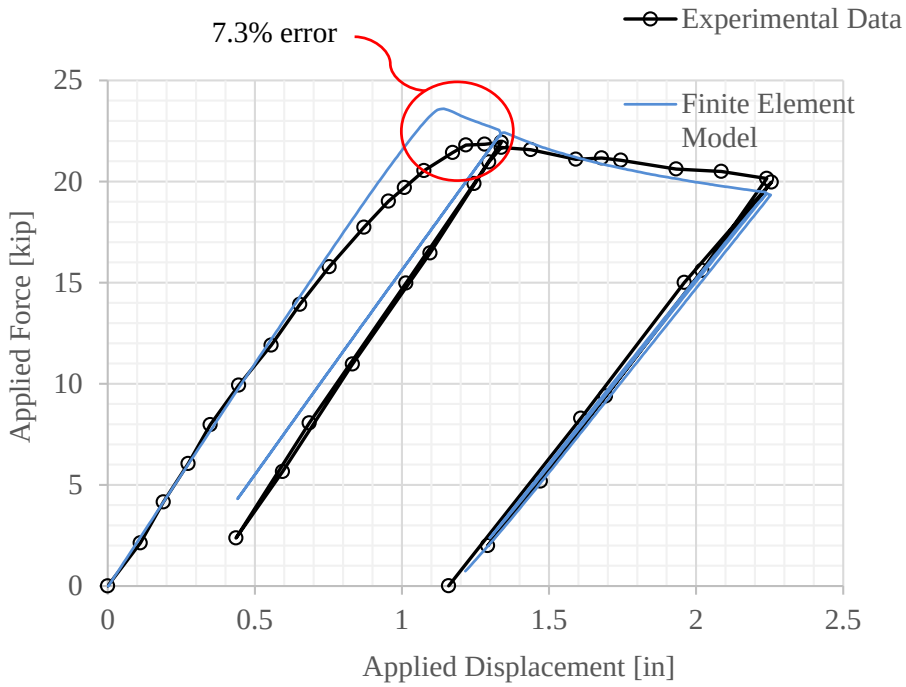

Figure 5-4 Applied force-displacement curves for Young and Murray (1997) Specimen 2

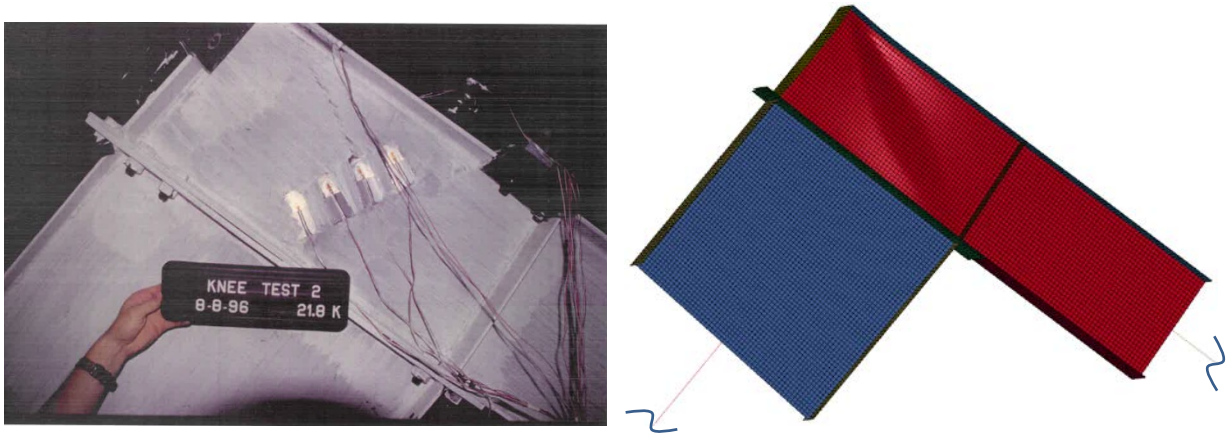

Figure 5-5 Deformed shapes of Young and Murray (1997) Specimen 2

CHAPTER 6 RESULTS AND DISCUSSION

6.1 Analytical Results for Prototype Structures

A parametric computational study with three varying variables specified in Chapters 3 and 4 and four sub-studies investigating several additional variables were performed to evaluate the impact of these variables on panel zone shear strength of knee joints and to validate the proposed theoretical model for the prediction of the strength. This section provides the finite element analysis results for these studies.

6.1.1 Parametric Study

The modeling scheme described in Chapter 5 was used to create 56 models for the prototype knee joint configurations described in Section 4.3.1. The maximum applied displacement in the models was equal to 10 inches (corresponding to a story drift of approximately 4% ~ 5% for most of the configurations).

Two types of load-displacement behavior, in terms of post-yielding response, were obtained, namely, softening where the strength begins degrading after reaching a peak strength at a relatively low level of deformation, and hardening where an initially elastic segment of the load-displacement curve reaches a threshold value of force, then the load-displacement curve retains a positive slope which is much lower than that of the elastic regime. In the models that experienced softening, the flanges on the outside of the panel zone were weaker and experienced large inelastic deformations. Conversely, the hardening response was related to strong flanges that exhibited less deformation. Softening was found to occur for flange flexural strength parameters, M_P^*, equal to 0.005 or 0.01, while hardening occurred when M_P^* was equal to 0.05 or 0.1. With an elastoplastic material model for steel, hardening responses are expected as the material hardens, as long as the flanges are adequately stiff to anchor the tension field action and allow the development of post-buckling strength in the panel zones.

Figure 6-1 shows the deformed shape and the effective plastic strain contours obtained at the end of the analysis for Model #10. This model is selected as an example of a softening load-deformation response. Noticeable flange plastic hinges occur in the vicinity of the panel zone

corner. The band of plastic strains along the diagonal of the panel indicates the formation of a tension field. The maximum effective plastic strain is 0.3698. In a real structure, this value of plastic deformation may not be reached, as the steel will be expected to fracture at a lower value of plastic strain. Therefore, the distribution of plastic strain can also be used to estimate where the material will fracture first. A detailed analysis of fracture behavior is beyond the scope of the present study.

Figure 6-2 shows the obtained force-displacement curve for Model #10. Softening occurs after the applied force reaches the peak value. The maximum applied force, F_{max}, is 39.9 kips. The corresponding story drift at the maximum applied force, calculated based on the geometry of the model, is 1.19%. The yield displacement, δ_y, determined by the intersection of the tangent line crossing the origin and the horizontal line crossing the peak of the curve (as shown in Figure 6-3), is 2.55 in.

There may be reasons to be cautious in the design of panel zones with softening behavior. The shear strength of panel zones that experience softening is expected to be more sensitive to initial imperfections and residual stresses. Well-anchored panels undergoing full tension field action can yield and strain-harden making it less sensitive to early buckling or yielding. The increased uncertainty associated with fracture and sensitivity of the strength of panel zones that soften warrants additional testing. See Section 6.4.1 and the Conclusions for additional discussion.

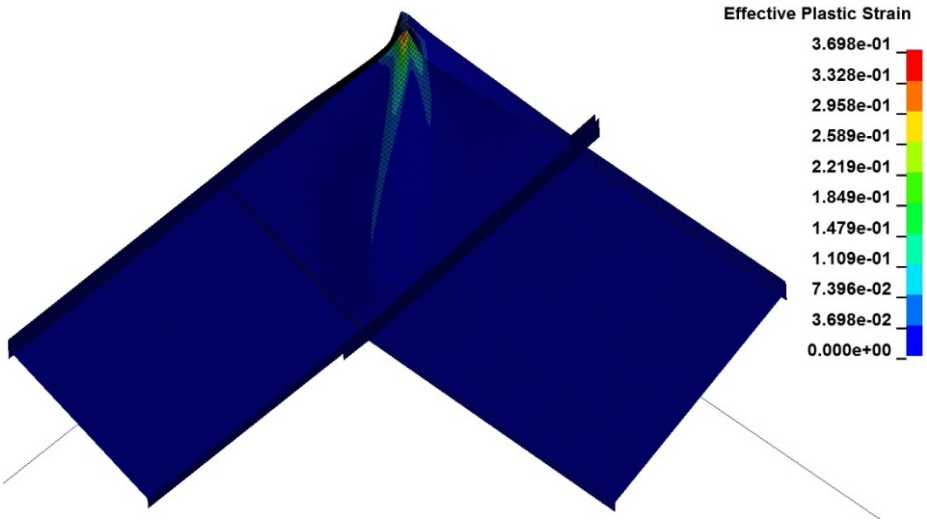

Figure 6-1 Deformed shape and effective plastic strain contours at the maximum applied displacement for Model #10

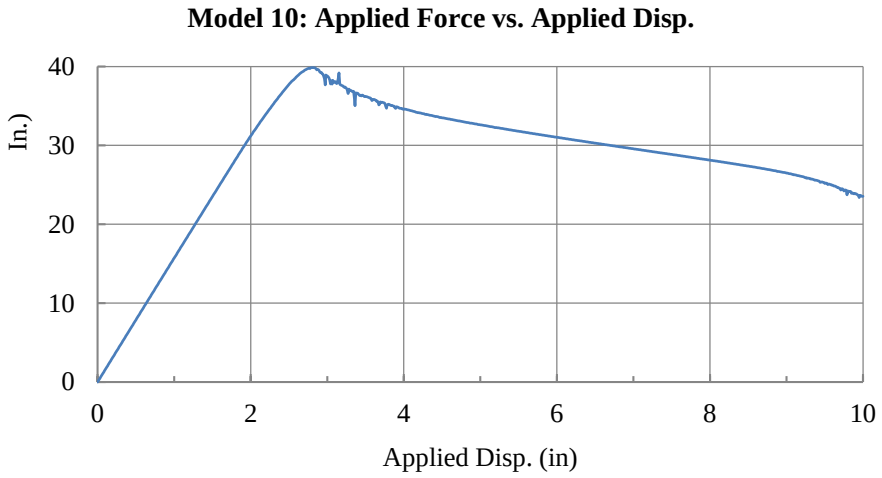

Figure 6-2 Applied force-displacement curve for Model #10

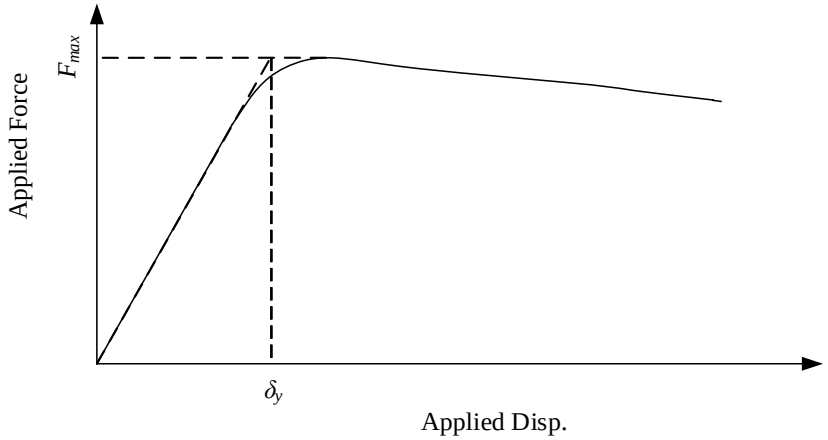

Figure 6-3 Definition of yield disp. for models with softening behavior

Figure 6-4 shows the deformed shape and the effective plastic strain contours at the end of the analysis for Model #8 which is an example of a model that exhibited hardening load-deformation response. It can be observed that plastic hinges still occur on the flanges of the panel zone at the corner, but they are less pronounced, and tension field development along the diagonal strip of the panel zone is deduced from the plastic strain contours. The maximum value of effective plastic strain is 0.1923 which is significantly less than Model #10 implying less potential for fracture.

Figure 6-5 shows the obtained force-displacement curve for Model #8. Hardening occurs after the occurrence of yielding. The yield displacement, δ_y, determined by the intersection of the tangent line crossing the origin and the tangent line for the post-yielding segment of the curve (as

shown in Figure 6-6), is 1.71 in. Since the load-displacement curve is always increasing, a definition of the obtained shear strength for models with hardening behavior is necessary. In this study, the maximum force for hardening response is defined as the force corresponding to a value of displacement equal to four times the yield displacement, as shown in Figure 6-6. This definition is based on a definition of ultimate shear strength for panel zones by Krawinkler (1978). According to the proposed definition, the maximum applied force for Model #8 is 56.9 kips and the corresponding story drift is 3.30%.

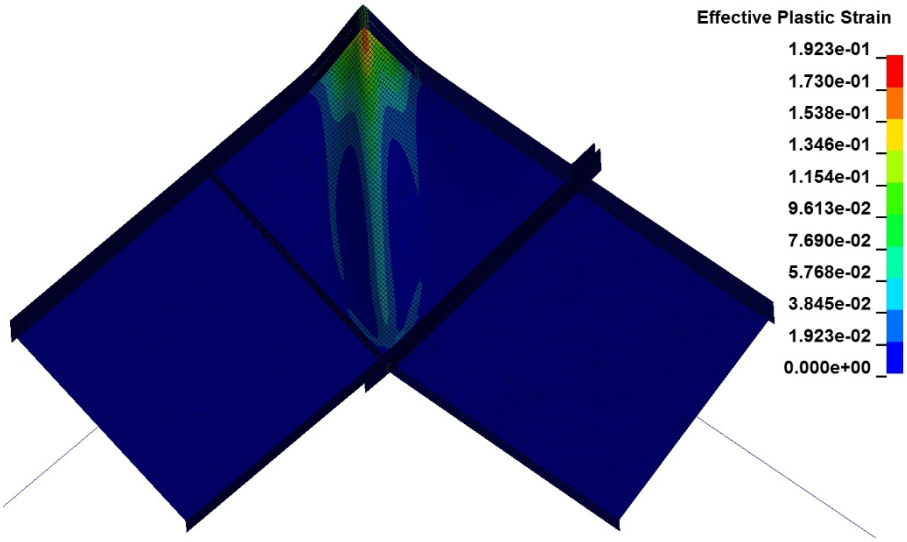

Figure 6-4 Deformed shape and effective plastic strain contours at the maximum applied displacement for Model #8

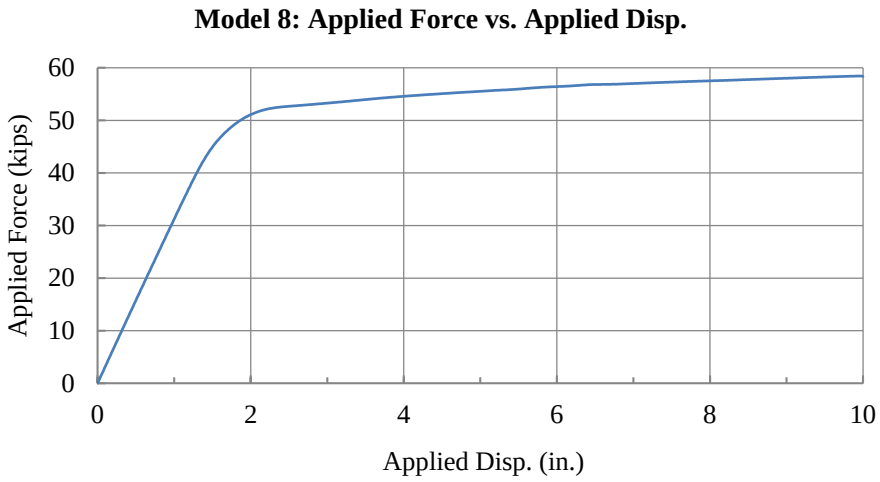

Figure 6-5 Applied force-displacement curve for Model #8

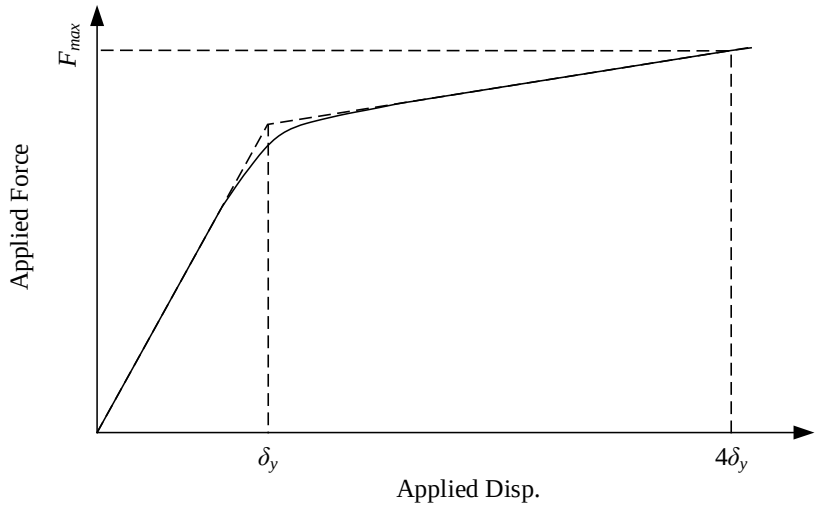

Figure 6-6 Definition of yield disp. and maximum applied force for models with hardening behavior

After the maximum applied force is obtained from the force-displacement curve, the maximum moment and axial force applied at the rafter face of the panel zone can be determined based on the geometry of the knee joint. The panel shear strength from the FEA results, V_{FEM}, is calculated using Eq. (2-8). The accuracy of the specific equation has been verified by comparing the calculated results of eight models to the maximum transverse forces acting on a section plane cut along their critical cross section (Figure 6-7), as presented in Table 6-1.

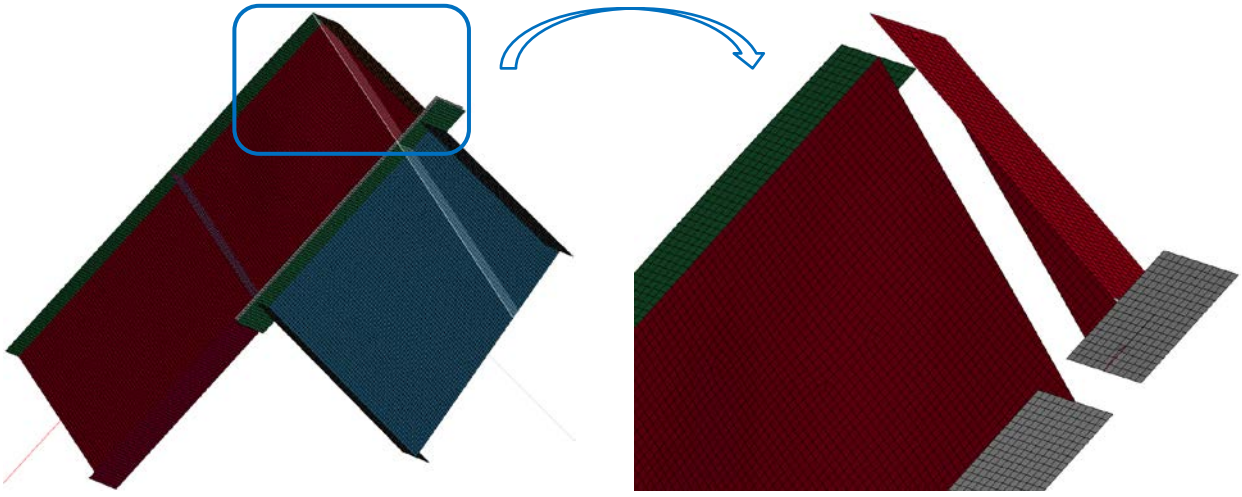

Figure 6-7 Cutting along the critical cross section to obtain maximum transverse (shear) force

Table 6-1 Validation of Eq. (2-8) for Calculating Shear Strength from FEA Results

Model #	Max applied force F_{max} (kips)	Moment at connection M_u (kip-ft)	Axial force at connection P_u (kips)	P.Z. shear strength $V_{FEM} = M_u/h_{r0} - P_u/2$ (kips)	P.Z. shear strength from cutting plane $V_{FEM,\,cut}$ (kips)	$\frac{V_{FEM}}{V_{FEM,\,cut}}$
1	40.4	422	33.4	189	201	0.94
2	42.8	432	34.5	172	182	0.95
3	42.4	455	35.4	180	191	0.94
4	51.2	636	46.5	250	235	1.06
5	61.8	819	58.0	319	306	1.04
6	48.0	534	40.3	156	159	0.98
7	47.8	557	41.2	162	165	0.98
8	56.9	750	52.6	217	213	1.02

Table 6-2 summarizes the FEA results of the 56 models. Further information on the results of the computational analyses is given in Appendix C. The results are used to evaluate the accuracy of the prediction equation in Section 6.2.

Table 6-2 FEA Results of Parametric Study (56 models)

Model #	Web thick-ness t_w (in.)	Panel web height h_r (in.)	Panel web width h_c (in.)	Panel flange width b_f (in.)	Panel flange thick-ness t_f (in.)	End-plate thick-ness t_p (in.)	Column length l_c (ft)	Rafter length l_r (ft)	Max applied force F_{max} (kips)	Story drift at F_{max} (%)	Yield disp. δ_y (in.)	P.Z. shear strength V_{FEM} (kips)
1	0.2500	24	36	6	0.625	0.875	15	18.5	40.4	1.16	2.14	189
2	0.2500	27	36	8	0.375	0.750	15	17.0	42.8	0.95	2.00	172
3	0.2500	27	36	6	0.625	0.875	15	19.5	42.4	1.11	2.04	180
4	0.2500	27	36	10	1.000	1.125	15	29.5	51.2	3.57	1.84	250
5	0.2500	27	36	14	1.250	1.250	15	38.5	61.8	3.64	1.82	319
6	0.2500	36	36	8	0.375	0.750	15	20.5	48.0	0.90	1.96	156
7	0.2500	36	36	6	0.625	0.875	15	23.0	47.8	1.02	1.94	162
8	0.2500	36	36	10	1.000	1.125	15	34.5	56.9	3.30	1.71	217
9	0.2500	36	36	14	1.250	1.250	15	45.0	68.7	3.25	1.65	276
10	0.2500	36	27	6	0.313	0.750	15	18.5	39.9	1.19	2.55	126
11	0.2500	36	27	9	0.375	0.750	15	21.5	38.3	0.96	2.07	129
12	0.2500	36	27	10	0.750	1.000	15	31.0	41.9	3.39	1.79	158
13	0.2500	36	27	12	1.000	1.125	15	38.0	49.3	3.28	1.69	195
14	0.2500	36	24	6	0.375	0.750	15	20.5	36.0	1.27	2.72	120
15	0.2500	32	48	10	0.625	0.875	15	26.0	55.7	1.11	1.86	218
16	0.2500	36	48	8	0.500	0.875	15	23.0	58.4	1.01	1.88	194
17	0.2500	36	48	10	0.625	0.875	15	27.5	58.4	1.03	1.76	207
18	0.2500	36	48	12	1.250	1.250	15	41.5	79.6	3.52	1.78	309
19	0.2500	36	48	16	1.500	1.375	15	52.5	94.9	3.54	1.76	383

Table 6-2 (Continued) FEA Results of Parametric Study (56 models)

Model #	Web thick-ness t_w (in.)	Panel web height h_r (in.)	Panel web width h_c (in.)	Panel flange width b_f (in.)	Panel flange thick-ness t_f (in.)	End-plate thick-ness t_p (in.)	Column length l_c (ft)	Rafter length l_r (ft)	Max applied force F_{max} (kips)	Story drift at F_{max} (%)	Yield disp. δ_y (in.)	P.Z. shear strength V_{FEM} (kips)
20	0.2500	48	48	8	0.500	0.875	15	27.5	65.3	0.82	1.75	172
21	0.2500	48	48	10	0.625	0.875	15	33.0	65.7	0.94	1.63	183
22	0.2500	48	48	12	1.250	1.250	15	49.5	89.4	3.18	1.64	270
23	0.2500	48	48	16	1.500	1.375	15	62.5	106.1	3.16	1.61	331
24	0.2500	48	36	8	0.375	0.750	15	24.5	54.6	0.93	2.01	141
25	0.2500	48	36	6	0.625	0.875	15	27.5	54.6	1.03	1.97	146
26	0.2500	48	36	10	1.000	1.125	15	41.0	63.1	3.17	1.67	187
27	0.2500	48	36	14	1.250	1.250	15	53.5	74.9	3.01	1.55	233
28	0.2500	48	32	6	0.500	0.875	15	26.0	50.2	1.08	2.22	133
29	0.1875	32	48	8	0.625	0.875	15	22.5	39.4	1.16	1.43	146
30	0.1875	36	48	6	0.500	0.750	15	19.5	40.1	0.75	1.43	124
31	0.1875	36	48	8	0.625	0.875	15	24.0	41.0	0.84	1.36	138
32	0.1875	36	48	14	1.000	1.125	15	39.5	57.2	2.93	1.49	222
33	0.1875	36	48	14	1.500	1.375	15	48.5	74.8	3.24	1.62	298
34	0.1875	48	48	6	0.500	0.750	15	22.5	44.6	0.68	1.31	109
35	0.1875	48	48	8	0.625	0.875	15	28.0	46.0	0.85	1.26	122
36	0.1875	48	48	14	1.000	1.125	15	46.5	64.1	2.67	1.38	192
37	0.1875	48	48	14	1.500	1.375	15	57.5	82.9	2.95	1.51	255
38	0.1875	48	36	6	0.375	0.750	15	21.0	36.1	0.74	1.53	87.5
39	0.1875	48	36	6	0.500	0.750	15	23.0	36.8	0.75	1.46	92.6
40	0.1875	48	36	8	1.000	1.000	15	35.5	46.1	2.63	1.41	132
41	0.1875	48	36	10	1.250	1.125	15	44.0	53.9	2.70	1.42	162
42	0.1875	48	32	9	0.375	0.625	15	23.0	33.2	0.77	1.43	84.3
43	0.1644	32	48	10	0.500	0.750	15	21.5	32.4	0.80	1.19	119
44	0.1644	36	48	9	0.375	0.625	15	18.5	32.9	0.63	1.11	100
45	0.1644	36	48	10	0.500	0.750	15	23.0	33.7	0.87	1.15	112
46	0.1644	36	48	12	1.000	1.125	15	36.0	50.1	2.75	1.41	190
47	0.1644	36	48	16	1.250	1.250	15	47.0	61.8	3.03	1.52	246
48	0.1644	48	48	9	0.375	0.625	15	21.0	36.3	0.71	1.01	86.3
49	0.1644	48	48	10	0.500	0.750	15	26.5	37.5	1.02	1.07	97.6
50	0.1644	48	48	12	1.000	1.125	15	42.5	56.1	2.62	1.37	165
51	0.1644	48	48	16	1.250	1.250	15	55.5	69.0	2.75	1.41	212
52	0.1644	48	36	5	0.375	0.625	15	18.5	30.6	0.64	1.36	69.9
53	0.1644	48	36	10	0.375	0.625	15	22.0	30.3	0.65	1.09	74.9
54	0.1644	48	36	12	0.750	1.000	15	37.0	39.2	2.37	1.26	114
55	0.1644	48	36	14	1.000	1.125	15	46.5	46.5	2.52	1.32	141
56	0.1644	48	32	8	0.375	0.625	15	21.5	28.0	0.68	1.29	69.2

6.1.2 Analytical Results for Sub-studies

The remainder of this Section will summarize the FEA results for the four sub-studies of prototype gable frame joints.

6.1.2.1 Sub-study on Column and Rafter Lengths, and Use of Tapered Sections

First a comparison between three models will be presented, then the results of all of the analyses in this substudy will be presented and conclusions made.

Figure 6-8 shows the deformed shape and the effective plastic strain contours obtained at the end of the analysis for Model #10, Model #10MP (which has the same configuration as Model #10 except that the lengths of column and rafter are different), and Model #10MT (which has the same configuration as Model #10MP except that tapered sections are used). The maximum effective plastic strain for Model #10 is 0.3698, for Model #10MP 0.3930, and for Model #10MT 0.3723. The deformed shape and plastic strain contours of the panel region for the three models are similar to each other.

Figure 6-9 shows the applied force-displacement curve for Model #10, Model #10MP, and Model #10MT. Softening occurs after the applied force reaches the peak value. For Model #10, the maximum applied force is 39.9 kips, obtained at a drift ratio of 1.19%, and the yield displacement is 2.55 in. For Model #10MP, the maximum applied force is 42.35 kips, obtained at a drift ratio of 1.11%, and the yield displacement is 2.33 in. For Model #10MT, the maximum applied force is 44.89 kips, obtained at a drift ratio of 1.63%, and the yield displacement is 2.98 in. It is observed that the force-displacement responses for the three models are close to each other, indicating a negligible impact of different column and rafter lengths, and the use of tapered section versus prismatic section, on the strength of panel zone knee joints.

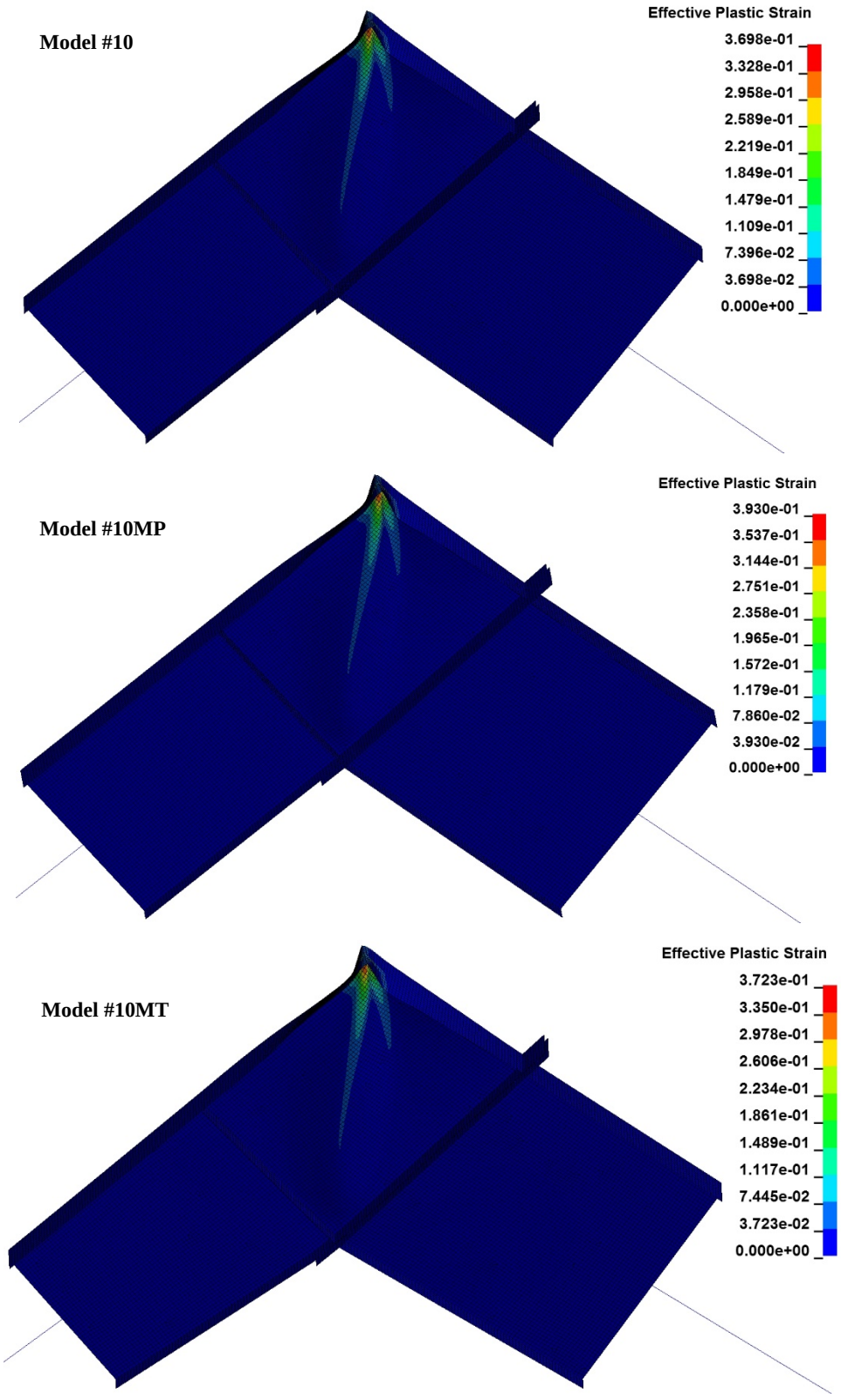

Figure 6-8 Deformed shapes and effective plastic strain contours at the maximum applied displacements for Model #10, Model #10MP, and Model #10MT

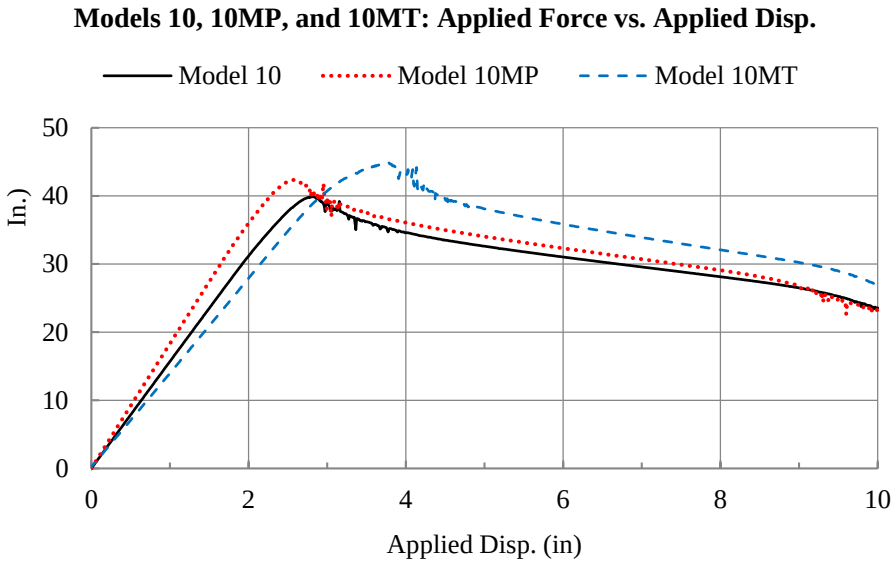

Figure 6-9 Applied force-displacement curves for Model #10, Model #10MP, and Model #10MT

Table 6-3 summarizes the FEA results of the 15 models for this sub-study. Further information of the results is given in Appendix C. For each triad of models in the sub-study (e.g., models 8, 8MP and 8MT), the configurations are similar to those of the main study, apart from the use of either different column and rafter lengths or prismatic member sections. The panel zone (P.Z.) shear strength for the three models in each set is very close to each other (with an average difference of 7% relative to the shear strength of configurations with tapered sections), i.e., different column and rafter lengths and the use of tapered sections have a negligible impact on the shear strength of the panel zone. It can also be concluded that idealization of member length and prismatic sections led to slightly conservative (smaller) values of shear strength.

Table 6-3 FEA Results of the Substudy – Column and Rafter Lengths, Tapered Section versus Prismatic Section (15 models)

Model #	Web thick-ness t_w (in.)	Panel web height h_r (in.)	Panel web width h_c (in.)	Panel flange width b_f (in.)	Panel flange thick-ness t_f (in.)	End-plate thick-ness t_p (in.)	Column length l_c (ft)	Rafter length l_r (ft)	Max applied force F_{max} (kips)	Story drift at F_{max} (%)	Yield disp. δ_y (in.)	P.Z. shear strength V_{FEM} (kips)	Ratio of V_{FEM} *
8	0.25	36	36	10	1.0000	1.125	15.00	34.50	56.9	3.30	1.71	217	94%
8MP	0.25	36	36	10	1.0000	1.125	28.75	23.24	44.5	4.49	2.14	221	95%
8MT	0.25	36	36	10	1.0000	1.125	28.75	23.24	46.6	4.47	2.01	231	100%
10	0.25	36	27	6	0.3125	0.750	15.00	18.50	39.9	1.19	2.55	126	95%
10MP	0.25	36	27	6	0.3125	0.750	14.72	16.61	42.4	1.11	2.33	125	94%
10MT	0.25	36	27	6	0.3125	0.750	14.72	16.61	44.9	1.63	2.98	133	100%

Table 6-3 (Continued) FEA Results of the Substudy – Column and Rafter Lengths, Tapered Section versus Prismatic Section (15 models)

Model #	Web thick-ness t_w (in.)	Panel web height h_r (in.)	Panel web width h_c (in.)	Panel flange width b_f (in.)	Panel flange thick-ness t_f (in.)	End-plate thick-ness t_p (in.)	Column length l_c (ft)	Rafter length l_r (ft)	Max applied force F_{max} (kips)	Story drift at F_{max} (%)	Yield disp. δ_y (in.)	P.Z. shear strength V_{FEM} (kips)	Ratio of V_{FEM} *
23	0.2500	48	48	16	1.500	1.375	15.00	62.50	106.1	1.19	2.55	331	89%
23MP	0.2500	48	48	16	1.500	1.375	26.83	30.36	85.9	4.40	1.58	347	94%
23MT	0.2500	48	48	16	1.500	1.375	26.83	30.36	91.7	4.46	1.96	370	100%
28	0.2500	48	32	6	0.500	0.875	15.00	26.00	50.2	1.08	2.22	133	92%
28MP	0.2500	48	32	6	0.500	0.875	19.75	22.54	44.4	1.38	2.70	134	92%
28MT	0.2500	48	32	6	0.500	0.875	19.75	22.54	48.0	1.99	3.93	144	100%
29	0.1875	32	48	8	0.625	0.875	15.00	22.50	39.4	1.16	1.43	146	92%
29MP	0.1875	32	48	8	0.625	0.875	15.30	15.77	45.7	0.72	1.08	145	91%
29MT	0.1875	32	48	8	0.625	0.875	15.30	15.77	50.2	0.82	1.18	160	100%

*: Ratios are relative to the shear strength of the corresponding configuration with tapered section.

6.1.2.2 Sub-study on Flange Flexural Strength Parameter

Table 6-4 provides the FEA results of the 24 models for this substudy. The deformed shapes of the models are similar to those with similar configurations in the parametric study, and thus are not provided here. All the models have flange flexural strength parameters smaller than 0.05, and a softening post-peak behavior is obtained in the corresponding force-displacement curves. It is also noted that the panel shear strength is almost the same for each pair of models (e.g., models 1A and 1B), with an average difference of less than 1%. More detailed information on the FEA results is presented in Appendix C.

Table 6-4 FEA Results of the Substudy – Flange Flexural Strength Parameter (24 models)

Model #	Web thick-ness t_w (in.)	Panel web height h_r (in.)	Panel web width h_c (in.)	Panel flange width b_f (in.)	Panel flange thick-ness t_{f1} (in.)	Panel flange thick-ness t_{f2} (in.)	End-plate thick-ness t_p (in.)	Column length l_c (ft)	Rafter length l_r (ft)	Max applied force F_{max} (kips)	Story drift at F_{max} (%)	Yield disp. δ_y (in.)	P.Z. shear strength V_{FEM} (kips)	Ratio of V_{FEM} *
1A	0.2500	27	36	8	0.375	0.500	0.750	15	17.0	43.4	0.93	1.93	174	100%
1B	0.2500	27	36	8	0.500	0.375	0.750	15	17.0	43.3	0.86	1.78	173	99%
2A	0.2500	36	36	8	0.375	0.500	0.750	15	20.5	48.2	0.85	1.85	157	100%
2B	0.2500	36	36	8	0.500	0.375	0.750	15	20.5	48.2	0.83	1.78	156	100%
3A	0.2500	36	27	6	0.313	0.500	0.750	15	18.5	40.4	0.99	2.21	128	100%
3B	0.2500	36	27	6	0.500	0.313	0.750	15	18.5	40.5	1.11	2.34	127	99%
4A	0.2500	36	48	8	0.500	0.750	0.875	15	23.0	59.8	0.96	1.82	199	100%
4B	0.2500	36	48	8	0.750	0.500	0.875	15	23.0	59.6	0.86	1.61	197	99%

Table 6-4 (Continued) FEA Results of the Substudy – Flange Flexural Strength Parameter (24 models)

Model #	Web thick-ness t_w (in.)	Panel web height h_r (in.)	Panel web width h_c (in.)	Panel flange width b_f (in.)	Panel flange thick-ness t_{f1} (in.)	Panel flange thick-ness t_{f2} (in.)	End-plate thick-ness t_p (in.)	Column length l_c (ft)	Rafter length l_r (ft)	Max applied force F_{max} (kips)	Story drift at F_{max} (%)	Yield disp. δ_y (in.)	P.Z. shear strength V_{FEM} (kips)	Ratio of V_{FEM} *
5A	0.2500	48	48	8	0.500	0.750	0.875	15	27.5	66.8	0.86	1.66	176	100%
5B	0.2500	48	48	8	0.750	0.500	0.875	15	27.5	66.7	0.80	1.55	175	99%
6A	0.2500	48	36	8	0.375	0.500	0.750	15	24.5	54.5	0.86	1.85	141	100%
6B	0.2500	48	36	8	0.500	0.375	0.750	15	24.5	55.3	0.90	1.98	143	101%
z7A	0.1875	36	48	6	0.500	0.750	0.750	15	19.5	41.1	0.73	1.39	127	100%
7B	0.1875	36	48	6	0.750	0.500	0.750	15	19.5	41.0	0.71	1.26	126	99%
8A	0.1875	48	48	6	0.500	0.750	0.750	15	22.5	45.7	0.70	1.25	112	100%
8B	0.1875	48	48	6	0.750	0.500	0.750	15	22.5	45.6	0.80	1.34	111	99%
9A	0.1875	48	36	6	0.375	0.500	0.750	15	21.0	36.7	0.69	1.43	89.0	100%
9B	0.1875	48	36	6	0.500	0.375	0.750	15	21.0	36.8	0.70	1.46	88.9	100%
10A	0.1644	36	48	10	0.375	0.500	0.750	15	23.0	31.2	0.76	1.23	104	100%
10B	0.1644	36	48	10	0.500	0.375	0.750	15	23.0	31.4	0.78	1.13	105	100%
11A	0.1644	48	48	10	0.375	0.500	0.750	15	26.5	35.0	0.82	1.11	91.3	100%
11B	0.1644	48	48	10	0.500	0.375	0.750	15	26.5	35.4	0.92	1.07	92.2	101%
12A	0.1644	48	36	10	0.250	0.375	0.625	15	22.0	28.1	0.97	1.83	69.8	100%
12B	0.1644	48	36	10	0.375	0.250	0.625	15	22.0	28.4	0.52	1.18	70.3	101%

*: Ratios are relative to the shear strength of the first model of each pair.

6.1.2.3 Sub-study on Orientation of End-Plate Connection

Figure 6-10 shows the deformed shapes and the effective plastic strain contours at the maximum applied displacement for Models #6, #6H, and #6S, which corresponds to different orientations of the end-plate connection. Table 6-5 summarizes the FEA results for this sub-study. For each triad of models, the highest panel shear strength is obtained for a vertical end-plate connection. The side of the panel zone with the end-plate is generally stiffer than the other three sides of the panel zone. While the reason for the variation in shear strength with different end-plate orientation is not well understood, it is hypothesized that the difference may be related to whether the side subjected to larger axial forces is the stiffer end-plate side or may be related to the length of the stiffer end-plate side. It is noted that the rafters evaluated in this study were subjected to axial tension and in general, the axial force in the rafter was larger than that in the column because the rafter was longer than the column and the model was loaded like a knee joint test. The average difference relative to the shear strength of the strongest configuration in each triad is 8%. For horizontal or sloped end-plate connections where the rafter experiences larger axial forces than the column, it may be necessary to reduce panel zone shear strength. The

accuracy of the prediction equation to capture these configurations will be evaluated in the next section and modifications for end-plate orientation will be discussed. Further information on the results of this sub-study is given in Appendix C.

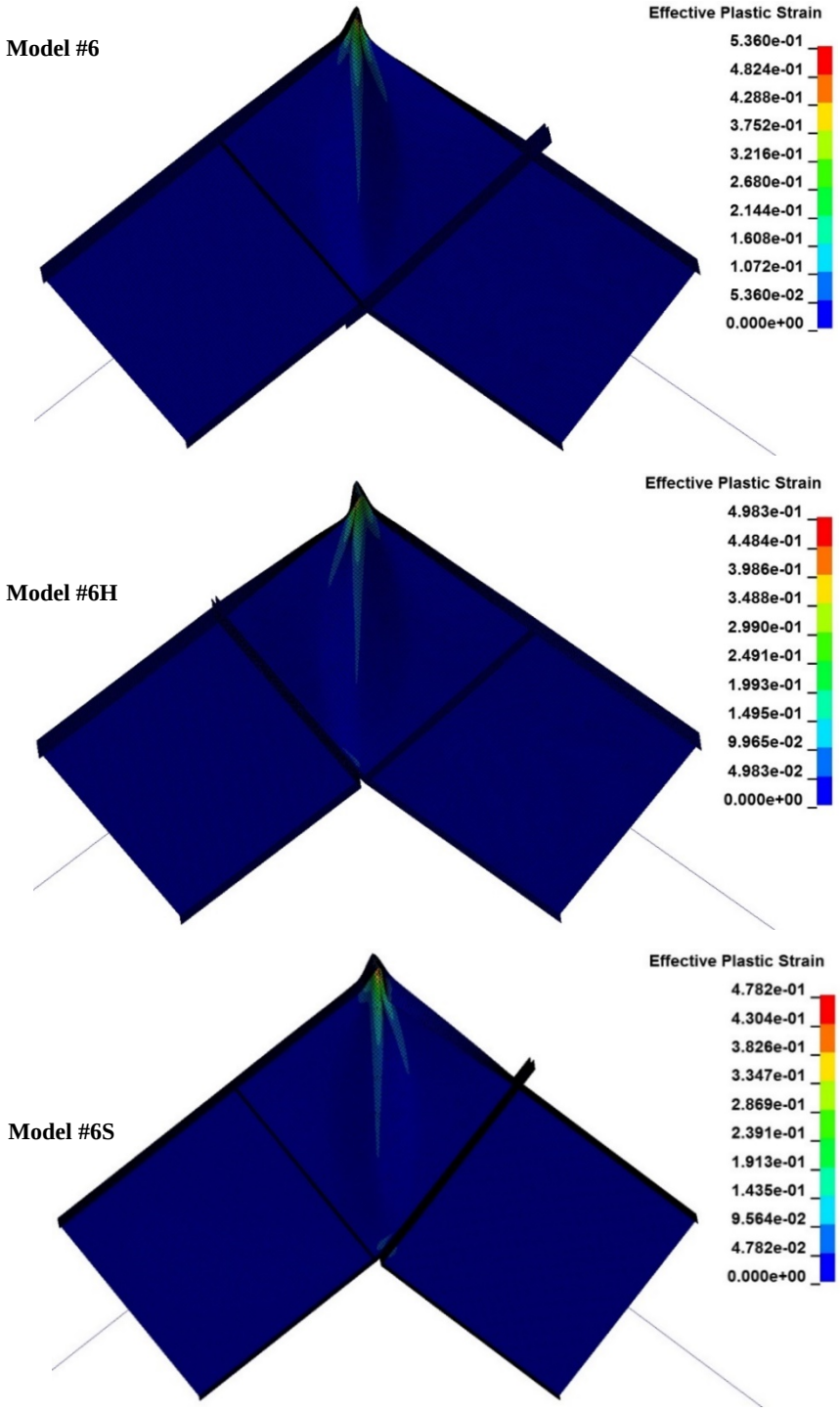

Figure 6-10 Deformed shapes and effective plastic strain contours at the maximum applied displacement for Model #6, Model #6H, and Model #6S

Table 6-5 FEA Results of the Substudy – Orientation of End-Plate Connection (4 models)

Model #	Web thick-ness t_w (in.)	Panel web height h_r (in.)	Panel web width h_c (in.)	Panel flange width b_f (in.)	Panel flange thick-ness t_f (in.)	End-plate thick-ness t_p (in.)	Column length l_c (ft)	Rafter length l_r (ft)	End -plate orient-ation	Max applied force F_{max} (kips)	Story drift at F_{max} (%)	Yield disp. δ_y (in.)	P.Z. shear strength V_{FEM} (kips)	Ratio of V_{FEM} *
6	0.25	36	36	8	0.375	0.750	15	20.5	Vert.	48.0	0.90	1.96	156	100%
6H	0.25	36	36	8	0.375	0.750	15	20.5	Horz.	43.5	0.99	1.90	141	91%
6S	0.25	36	36	8	0.375	0.750	15	20.5	Sloped	44.4	1.29	1.90	144	93%
25	0.25	48	36	6	0.625	0.875	15	27.5	Vert.	54.6	1.03	1.97	146	100%
25H	0.25	48	36	6	0.625	0.875	15	27.5	Horz.	49.5	1.54	1.99	133	91%
25S	0.25	48	36	6	0.625	0.875	15	27.5	Sloped	50.6	1.53	1.90	135	93%

6.1.2.4*: Ratios are relative to the shear strength of the model with vertical end-plate. Sub-study on Roof Slope

Figure 6-11 shows the deformed shapes and the effective plastic strain contours at the end of the analysis for Models #6C and #6D. Table 6-6 summarizes the results for the sub-study focusing on the effect of roof-slope. It is noted that the highest panel shear strength is obtained for a zero roof slope. This is probably due to the fact that the resistance of the end-plate connection to shear deformation is maximized when forces from the rafter flanges are perpendicular to the end-plate connection. Detailed information of the FEA results of this sub-study is given in Appendix C.

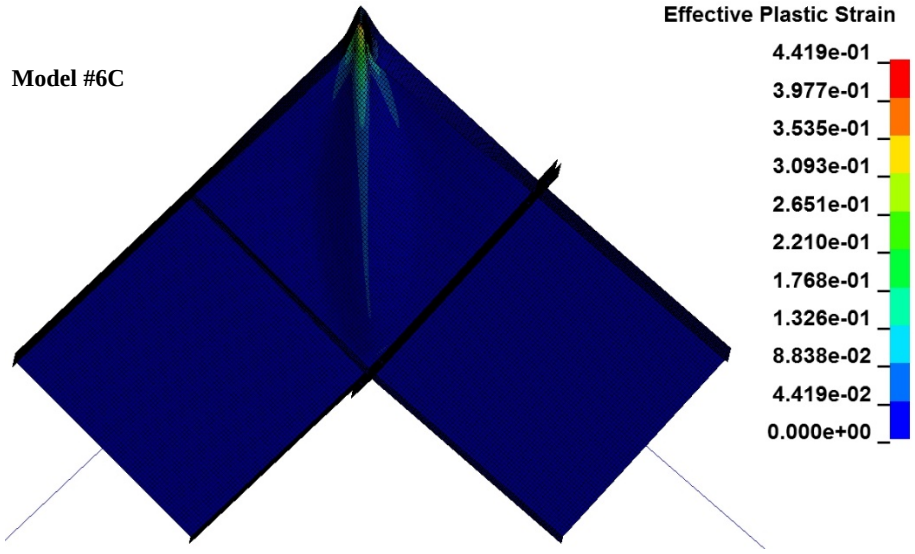

Figure 6-11 Deformed shape and effective plastic strain contours at the maximum applied displacement for Model #6C and Model #6D

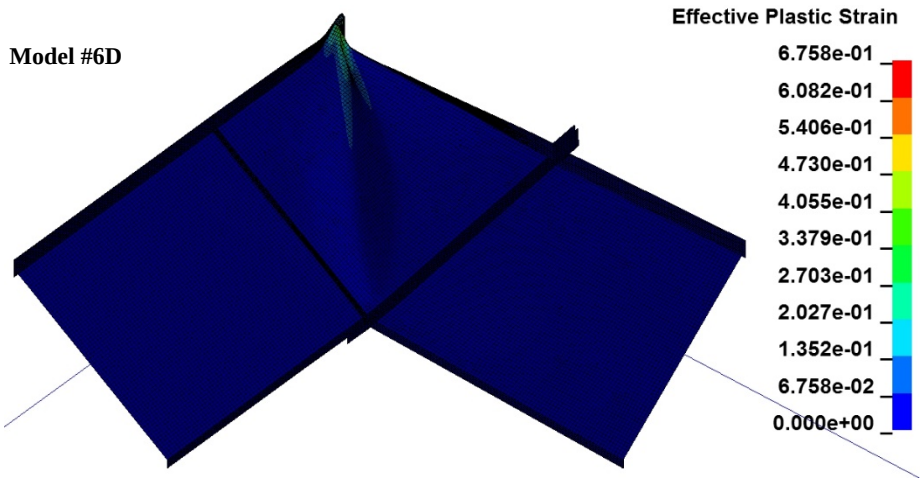

Figure 6-11 (Continued) Deformed shapes and effective plastic strain contours at the maximum applied displacement for Model #6C and Model #6D

Table 6-6 FEA Results of the Substudy – Roof Slope (4 models)

Model #	Panel web thickness t_w (in.)	Panel height h_r (in.)	Panel width h_c (in.)	Panel flange width b_f (in.)	Panel flange thickness t_f (in.)	End-plate thickness t_p (in.)	Column length l_c (ft)	Rafter length l_r (ft)	Roof slope	Max applied force F_{max} (kips)	Story drift at F_{max} (%)	Yield disp. δ_y (in.)	P.Z. shear strength V_{FEM} (kips)
6	0.25	36	36	8	0.375	0.750	15	20.5	2:12	48.0	0.90	1.96	156
6C	0.25	36	36	8	0.375	0.750	15	20.5	0:12	47.0	1.07	2.30	171
6D	0.25	36	36	8	0.375	0.750	15	20.5	4:12	49.9	0.86	1.68	142
25	0.25	48	36	6	0.625	0.875	15	27.5	2:12	54.6	1.03	1.97	146
25C	0.25	48	36	6	0.625	0.875	15	27.5	0:12	52.3	1.09	2.24	157
25D	0.25	48	36	6	0.625	0.875	15	27.5	4:12	58.7	0.99	1.75	138

6.2 Validation and Modification of Theoretical Model

In this section, the proposed theoretical model is first validated against available test data. Then the FEA results of the parametric study and the sub-studies are used to further validate and modify the theoretical model.

6.2.1 Validation against Test Data

Table 6-7 shows the test data and shear strength calculations of the two test specimens (Young and Murray 1997) used to validate the FE modeling approach. The predicted shear strength from the derived equations agrees well with the one obtained from the test results. However, only two test specimens are used for validation, and the derived equations overpredict the shear strength

by 14% for one of them. Further validation and modification of the theoretical model are therefore necessary.

Table 6-7 Validation of Theoretical Model against Test Data (Young and Murray 1997)

Specimen #	$\frac{\max(h_c, h_r)}{t_w}$	h_r/h_c	M_P^*	P.Z. shear strength from test V_{exp} (kips)	K	C_v	C_t	V_{TFA} (kips)	V_{cr} (kips)	P. Z. shear strength from derived eqns V_{PZ} (kips)	$\frac{V_{PZ}}{V_{exp}}$
1	188	2.17	0.036	43.2	6.19	0.52	0.58	11.7	37.4	49.1	114%
2	204	2.00	0.028	46.8	6.34	0.39	0.69	13.6	31.9	45.5	97%

6.2.2 Parametric Study

6.2.1.1 Validation of Derived Equations

The capability of the theoretical model described in Chapter 3 to predict the panel zone shear strength was checked by comparing the panel shear strength obtained from the 56 finite element models to the value obtained using Eqs. (3-1), (3-2), and (3-26), as shown in Table 6-8. The ratios of the shear strength obtained with the theoretical model and finite element analyses are also provided. The panel zone shear strength obtained from the FEA results is divided by a factor of 1.08 to obtain the expected "actual" panel zone shear strength. This modification is conducted because the validation analyses for the modeling scheme in Section 5.3 were found to overestimate the peak strength by an average 8%.

Table 6-8 Evaluating Preliminary Derived Equations – ***BEFORE MODIFICATION***

Model #	$\frac{\max(h_c, h_r)}{t_w}$	h_r/h_c	M_{P1}^*	M_{P2}^*	P.Z. shear strength from FEA V_{FEM} (kips)	K	C_v	C_t	V_{TFA} (kips)	V_{cr} (kips)	P. Z. shear strength from derived eqns V_{PZ} (kips)	$\frac{V_{PZ}}{V_{FEM}/1.08}$
1	144	0.67	0.011	0.011	189	16.0	0.64	0.41	43.7	182	226	129%
2	144	0.75	0.005	0.005	172	13.5	0.54	0.51	32.7	154	186	117%
3	144	0.75	0.011	0.011	180	13.5	0.54	0.51	46.8	154	200	120%
4	144	0.75	0.046	0.046	250	13.5	0.54	0.51	94.1	154	248	107%
5	144	0.75	0.101	0.101	319	13.5	0.54	0.51	136	154	289	98%
6	144	1.00	0.005	0.005	156	9.34	0.37	0.66	33.1	106	139	96%
7	144	1.00	0.011	0.011	162	9.34	0.37	0.66	47.5	106	154	103%
8	144	1.00	0.046	0.046	217	9.34	0.37	0.66	96.1	106	202	101%

Table 6-8 (Continued) Evaluating Preliminary Equations – ***BEFORE MODIFICATION***

Model #	$\frac{\max(h_c, h_r)}{t_w}$	h_r/h_c	$M_{P1}{}^*$	$M_{P2}{}^*$	P.Z. shear strength from FEA V_{FEM} (kips)	K	C_v	C_t	V_{TFA} (kips)	V_{cr} (kips)	P. Z. shear strength from derived eqns V_{PZ} (kips)	$\frac{V_{PZ}}{V_{FEM}/1.08}$
9	144	1.00	0.101	0.101	276	9.34	0.37	0.66	139	106	246	96%
10	144	1.33	0.005	0.005	126	7.59	0.54	0.51	17.8	115	133	114%
11	144	1.33	0.010	0.010	129	7.59	0.54	0.51	26.0	115	141	118%
12	144	1.33	0.046	0.046	158	7.59	0.54	0.51	53.6	115	169	115%
13	144	1.33	0.099	0.099	195	7.59	0.54	0.51	76.9	115	192	106%
14	144	1.50	0.009	0.009	120	7.12	0.64	0.41	17.7	121	139	126%
15	192	0.67	0.010	0.010	218	16.0	0.36	0.69	73.4	137	210	104%
16	192	0.75	0.005	0.005	194	13.5	0.30	0.73	52.6	115	168	93%
17	192	0.75	0.010	0.010	207	13.5	0.30	0.73	73.0	115	188	98%
18	192	0.75	0.049	0.049	309	13.5	0.30	0.73	156	115	271	95%
19	192	0.75	0.094	0.094	383	13.5	0.30	0.73	213	115	328	92%
20	192	1.00	0.005	0.005	172	9.34	0.21	0.81	49.0	79.7	129	81%
21	192	1.00	0.010	0.010	183	9.34	0.21	0.81	68.2	79.7	148	87%
22	192	1.00	0.049	0.049	270	9.34	0.21	0.81	147	79.7	226	91%
23	192	1.00	0.094	0.094	331	9.34	0.21	0.81	200	79.7	280	91%
24	192	1.33	0.005	0.005	141	7.59	0.30	0.73	29.7	86.3	116	89%
25	192	1.33	0.011	0.011	146	7.59	0.30	0.73	42.6	86.3	129	95%
26	192	1.33	0.046	0.046	187	7.59	0.30	0.73	86.6	86.3	173	100%
27	192	1.33	0.101	0.101	233	7.59	0.30	0.73	126	86.3	212	99%
28	192	1.50	0.009	0.009	133	7.12	0.36	0.69	30.6	91.1	122	99%
29	256	0.67	0.011	0.011	146	16.0	0.20	0.83	62.5	57.7	120	89%
30	256	0.75	0.005	0.005	124	13.5	0.17	0.85	42.6	48.6	91.1	79%
31	256	0.75	0.011	0.011	138	13.5	0.17	0.85	61.1	48.6	110	86%
32	256	0.75	0.049	0.049	222	13.5	0.17	0.85	126	48.6	175	85%
33	256	0.75	0.109	0.109	298	13.5	0.17	0.85	186	48.6	234	85%
34	256	1.00	0.005	0.005	109	9.34	0.12	0.90	38.6	33.6	72.2	72%
35	256	1.00	0.011	0.011	122	9.34	0.12	0.90	55.5	33.6	89.1	79%
36	256	1.00	0.049	0.049	192	9.34	0.12	0.90	115	33.6	149	84%
37	256	1.00	0.109	0.109	255	9.34	0.12	0.90	170	33.6	204	86%
38	256	1.33	0.005	0.005	87.5	7.59	0.17	0.85	24.0	36.4	60.5	75%
39	256	1.33	0.009	0.009	92.6	7.59	0.17	0.85	31.9	36.4	68.4	80%
40	256	1.33	0.049	0.049	132	7.59	0.17	0.85	72.4	36.4	109	89%
41	256	1.33	0.096	0.096	162	7.59	0.17	0.85	99.9	36.4	136	91%
42	256	1.50	0.010	0.010	84.3	7.12	0.20	0.83	26.7	38.4	65.2	84%
43	292	0.67	0.010	0.010	119	16.0	0.16	0.87	53.7	38.9	92.6	84%
44	292	0.75	0.005	0.005	100	13.5	0.13	0.89	37.4	32.7	70.1	76%

Table 6-8 (Continued) Evaluating Preliminary Equations – ***BEFORE MODIFICATION***

Model #	$\frac{\max(h_c, h_r)}{t_w}$	h_r/h_c	$M_{P1}{}^*$	$M_{P2}{}^*$	P.Z. shear strength from FEA V_{FEM} (kips)	K	C_v	C_t	V_{TFA} (kips)	V_{cr} (kips)	P. Z. shear strength from derived eqns V_{PZ} (kips)	$\frac{V_{PZ}}{V_{FEM}/1.08}$
45	292	0.75	0.010	0.010	112	13.5	0.13	0.89	52.2	32.7	85.0	82%
46	292	0.75	0.048	0.048	190	13.5	0.13	0.89	112	32.7	145	82%
47	292	0.75	0.099	0.099	246	13.5	0.13	0.89	159	32.7	191	84%
48	292	1.00	0.005	0.005	86.3	9.34	0.09	0.92	33.7	22.7	56.3	71%
49	292	1.00	0.010	0.010	97.6	9.34	0.09	0.92	47.1	22.7	69.8	77%
50	292	1.00	0.048	0.048	165	9.34	0.09	0.92	101	22.7	124	81%
51	292	1.00	0.099	0.099	212	9.34	0.09	0.92	144	22.7	167	85%
52	292	1.33	0.005	0.005	69.9	7.59	0.13	0.89	21.0	24.6	45.5	70%
53	292	1.33	0.010	0.010	74.9	7.59	0.13	0.89	29.5	24.6	54.1	78%
54	292	1.33	0.048	0.048	114	7.59	0.13	0.89	63.6	24.6	88.2	83%
55	292	1.33	0.099	0.099	141	7.59	0.13	0.89	90.4	24.6	115	88%
56	292	1.50	0.010	0.010	69.2	7.12	0.16	0.87	24.2	25.9	50.1	78%
											Average:	92%
											Standard deviation:	14%
											Percentage of models with 20% difference or less:	75%
											Percentage of models with 10% difference or less:	34%

The theoretical model equations were found to produce panel zone shear strength that were smaller than the shear strengths from the FE models by 8% on average. However, the standard deviation of this difference is large (14%) and there are cases where the prediction equations produce unconservative (larger) shear strength than the models. This is attributed to several idealized assumptions made during the formulation of the theoretical model, e.g., that the panel web plate is simply supported in the out-of-plane direction and rigidly anchored to resist in-plane deformation at the edges connected to the column and rafter, that the stress distribution across the tension field strip is uniform, and that the geometry of the panel zone is a rectangle as well.

Figure 6-12 shows that the accuracy of the panel zone shear strength prediction equation varies depending on the three primary design variables, and are rather scattered above and below the strength from FEA. For example, the ratio of predicted to FEA strength decreases as the panel web slenderness increases, and increases as the aspect ratio, $\max(h_r, h_c)/\min(h_r, h_c)$, increases. This dependency and variations can be attributed to the idealized boundary conditions.

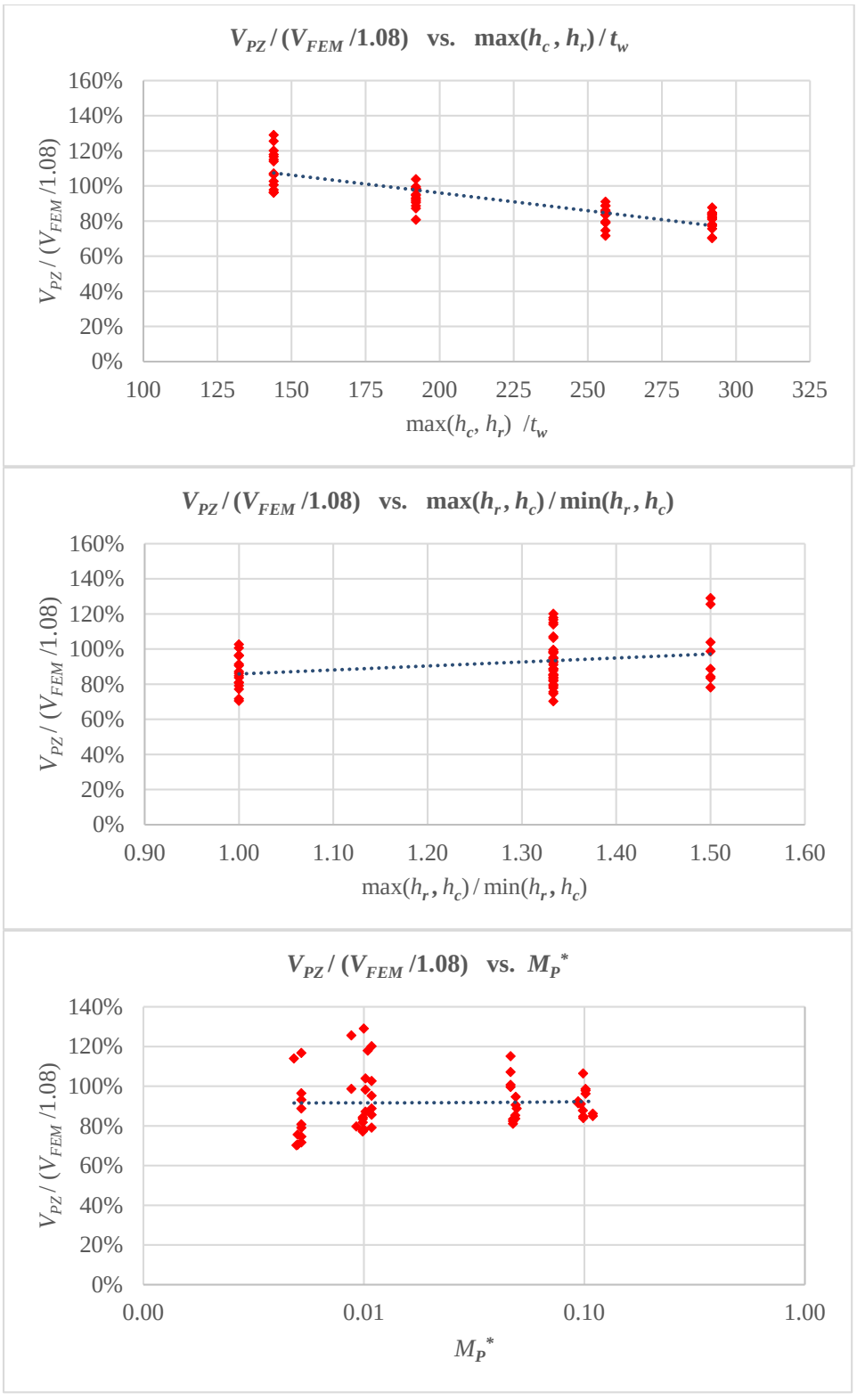

Figure 6-12 Ratios of predicted strength FE strength **before modification**

6.2.1.2 Modification of Theoretical Model

To improve the accuracy of the predicted panel zone shear strength with the theoretical model, a modification to the buckling strength is calibrated to account for boundary conditions. Specifically, the shear buckling coefficient, C_v, is modified to account for the limited accuracy of the idealized assumptions mentioned in Section 6.2.1.1. A modification with a first-order linear equation is made to C_v as follows:

$$C_v^* = C_1 C_v + C_2 \tag{6-1}$$

where C_1 and C_2 are constant coefficients determined by solving an optimization problem. The objective function for the optimization is set to the root mean square (RMS) of the differences between the V_{PZ} / (V_{FEM} /1.08) ratios and 1.0, which is desired to be minimum for optimized solution. A Generalized Reduced Gradient (GRG) nonlinear solving method (Lasdon et al. 1978) is adopted for the solution of the optimization problem and the optimal values of C_1 and C_2 were found to be equal to 0.50 and 0.17, respectively.

Table 6-9 shows the results for the 56 models calculated with the modified theoretical model compared to those obtained with the original equations of Chapter 3. The accuracy of the modified theoretical model is found to be significantly improved, and the error is less than 10% for all cases considered.

Table 6-9 Comparison of Results Calculated with Original and Modified Derived Equations – Parametric Study

Model #	P.Z. shear strength from FEA V_{FEM} (kips)	Original Equations					Modified Equations				
		C_v	V_{TFA} (kips)	V_{cr} (kips)	P. Z. shear strength from derived eqns V_{PZ} (kips)	$\frac{V_{PZ}}{V_{FEM}/1.08}$	C_v^*	V_{TFA} (kips)	V_{cr} (kips)	P. Z. shear strength from derived eqns V_{PZ} (kips)	$\frac{V_{PZ}}{V_{FEM}/1.08}$
1	189	0.64	43.7	182	226	129%	0.49	51.3	140	191	109%
2	172	0.54	32.7	154	186	117%	0.44	35.7	125	161	101%
3	180	0.54	46.8	154	200	120%	0.44	51.2	125	177	106%
4	250	0.54	94.1	154	248	107%	0.44	103	125	228	99%
5	319	0.54	136	154	289	98%	0.44	149	125	274	93%
6	156	0.37	33.1	106	139	96%	0.36	33.5	102	135	94%
7	162	0.37	47.5	106	154	103%	0.36	48.1	102	150	100%

Table 6-9 (Continued) Comparison of Results Calculated with Original and Modified Derived Equations – Parametric Study

Model #	P.Z. shear strength from FEA V_{FEM} (kips)	Original Equations					Modified Equations				
		C_v	V_{TFA} (kips)	V_{cr} (kips)	P. Z. shear strength from derived eqns V_{PZ} (kips)	$\frac{V_{PZ}}{V_{FEM}}/1.08$	$C_v{}^*$	V_{TFA} (kips)	V_{cr} (kips)	P. Z. shear strength from derived eqns V_{PZ} (kips)	$\frac{V_{PZ}}{V_{FEM}}/1.08$
8	217	0.37	96.1	106	202	101%	0.36	97.3	102	199	99%
9	276	0.37	139	106	246	96%	0.36	141	102	243	95%
10	126	0.54	17.8	115	133	114%	0.44	19.4	94.0	113	97%
11	129	0.54	26.0	115	141	118%	0.44	28.4	94.0	122	102%
12	158	0.54	53.6	115	169	115%	0.44	58.7	94.0	153	104%
13	195	0.54	76.9	115	192	106%	0.44	84.4	94.0	178	99%
14	120	0.64	17.7	121	139	126%	0.49	20.8	93.1	114	103%
15	218	0.36	73.4	137	210	104%	0.35	73.9	133	207	102%
16	194	0.30	52.6	115	168	93%	0.32	51.9	122	174	97%
17	207	0.30	73.0	115	188	98%	0.32	72.2	122	194	102%
18	309	0.30	156	115	271	95%	0.32	154	122	277	97%
19	383	0.30	213	115	328	92%	0.32	210	122	332	94%
20	172	0.21	49.0	79.7	129	81%	0.27	47.2	105	152	95%
21	183	0.21	68.2	79.7	148	87%	0.27	65.6	105	170	100%
22	270	0.21	147	79.7	226	91%	0.27	141	105	245	98%
23	331	0.21	200	79.7	280	91%	0.27	192	105	297	97%
24	141	0.30	29.7	86.3	116	89%	0.32	29.3	91.8	121	93%
25	146	0.30	42.6	86.3	129	95%	0.32	42.1	91.8	134	99%
26	187	0.30	86.6	86.3	173	100%	0.32	85.5	91.8	177	102%
27	233	0.30	126	86.3	212	99%	0.32	124	91.8	216	100%
28	133	0.36	30.6	91.1	122	99%	0.35	30.8	88.7	120	97%
29	146	0.20	62.5	57.7	120	89%	0.27	60.1	77.4	138	102%
30	124	0.17	42.6	48.6	91.1	79%	0.25	40.6	72.9	113	98%
31	138	0.17	61.1	48.6	110	86%	0.25	58.2	72.9	131	102%
32	222	0.17	126	48.6	175	85%	0.25	120	72.9	193	94%
33	298	0.17	186	48.6	234	85%	0.25	177	72.9	249	91%
34	109	0.12	38.6	33.6	72.2	72%	0.23	36.4	65.4	102	101%
35	122	0.12	55.5	33.6	89.1	79%	0.23	52.2	65.4	118	104%
36	192	0.12	115	33.6	149	84%	0.23	108	65.4	174	98%
37	255	0.12	170	33.6	204	86%	0.23	160	65.4	225	95%
38	87.5	0.17	24.0	36.4	60.5	75%	0.25	22.9	54.7	77.6	96%
39	92.6	0.17	31.9	36.4	68.4	80%	0.25	30.4	54.7	85.1	99%
40	132	0.17	72.4	36.4	109	89%	0.25	69.0	54.7	124	101%
41	162	0.17	99.9	36.4	136	91%	0.25	95.2	54.7	150	100%

Table 6-9 (Continued) Comparison of Results Calculated with Original and Modified Derived Equations – Parametric Study

Model #	P.Z. shear strength from FEA V_{FEM} (kips)	Original Equations					Modified Equations				
		C_v	V_{TFA} (kips)	V_{cr} (kips)	P. Z. shear strength from derived eqns V_{PZ} (kips)	$\frac{V_{PZ}}{V_{FEM}}/1.08$	$C_v{}^*$	V_{TFA} (kips)	V_{cr} (kips)	P. Z. shear strength from derived eqns V_{PZ} (kips)	$\frac{V_{PZ}}{V_{FEM}}/1.08$
42	84.3	0.20	26.7	38.4	65.2	84%	0.27	25.7	51.6	77.3	99%
43	119	0.16	53.7	38.9	92.6	84%	0.25	51.1	62.0	113	103%
44	100	0.13	37.4	32.7	70.1	76%	0.24	35.3	59.0	94.3	102%
45	112	0.13	52.2	32.7	85.0	82%	0.24	49.4	59.0	108	104%
46	190	0.13	112	32.7	145	82%	0.24	106	59.0	165	94%
47	246	0.13	159	32.7	191	84%	0.24	150	59.0	209	91%
48	86.3	0.09	33.7	22.7	56.3	71%	0.22	31.5	53.9	85.5	107%
49	97.6	0.09	47.1	22.7	69.8	77%	0.22	44.1	53.9	98.0	108%
50	165	0.09	101	22.7	124	81%	0.22	94.8	53.9	149	97%
51	212	0.09	144	22.7	167	85%	0.22	135	53.9	188	96%
52	69.9	0.13	21.0	24.6	45.5	70%	0.24	19.8	44.2	64.0	99%
53	74.9	0.13	29.5	24.6	54.1	78%	0.24	27.9	44.2	72.1	104%
54	114	0.13	63.6	24.6	88.2	83%	0.24	60.1	44.2	104	99%
55	141	0.13	90.4	24.6	115	88%	0.24	85.3	44.2	130	99%
56	69.2	0.16	24.2	25.9	50.1	78%	0.25	23.0	41.4	64.4	100%
					Average:	92%				Average:	99%
					Standard deviation:	14%				Standard deviation:	4%
					Percentage of models with 20% difference or less:	75%				Percentage of models with 20% difference or less:	100%
					Percentage of models with 10% difference or less:	34%				Percentage of models with 10% difference or less:	100%

The improvement of accuracy after modification is also reflected in Figure 6-13, which presents the relation of the panel zone shear strength values (obtained with the theoretical model and the finite element analyses) to the three design parameters. After modification, the ratios of predicted strength to the FEA results remain almost constant and equal to 1.0 as the three design variables are varied, as shown in Figure 6-13. Similar observations (regarding the beneficial effect of modification) are reached through Figure 6-14, which presents the relation between the panel shear strength ratio and the FE prediction of panel shear strength.

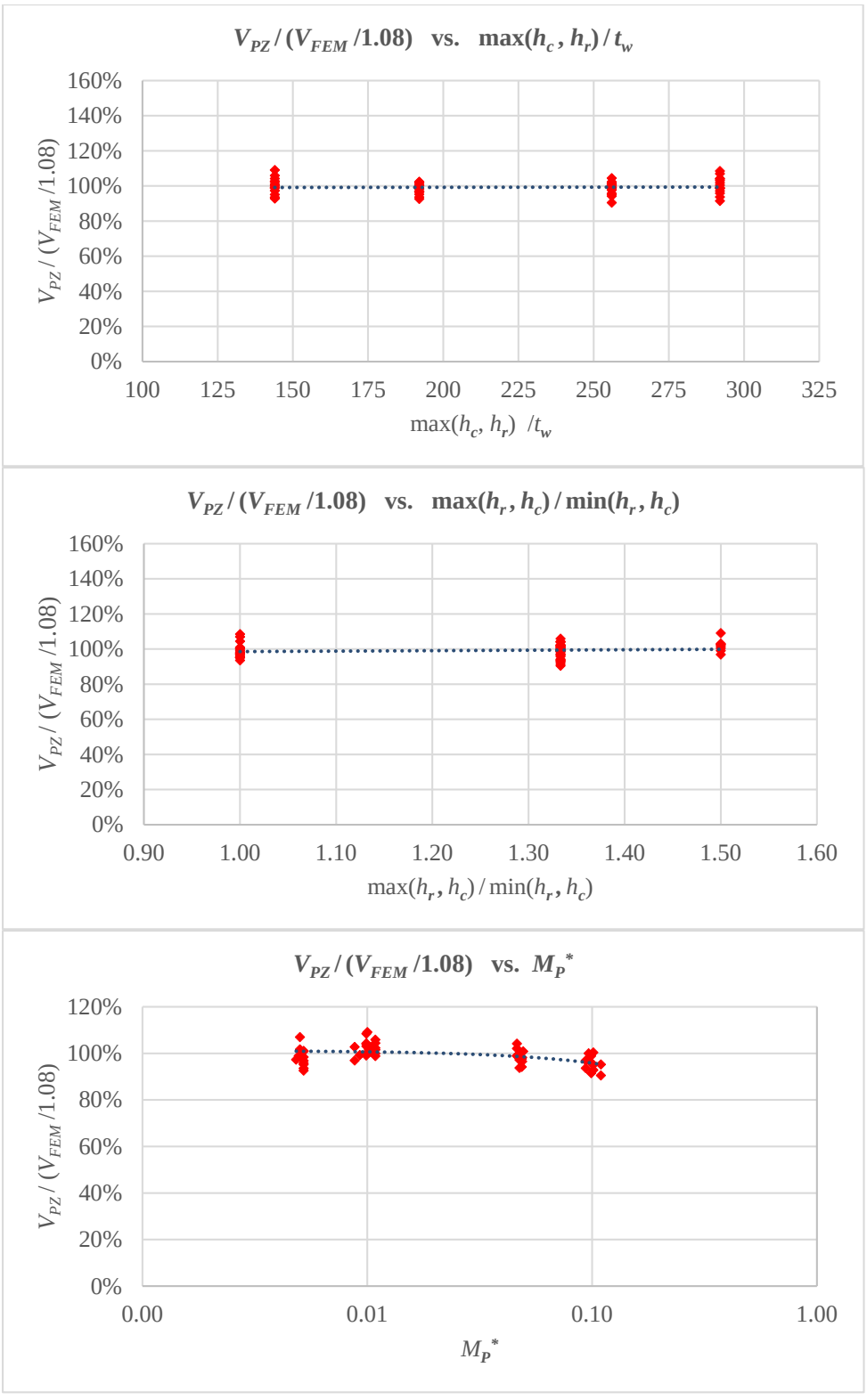

Figure 6-13 Ratios of predicted strength to FE strength **after modification**

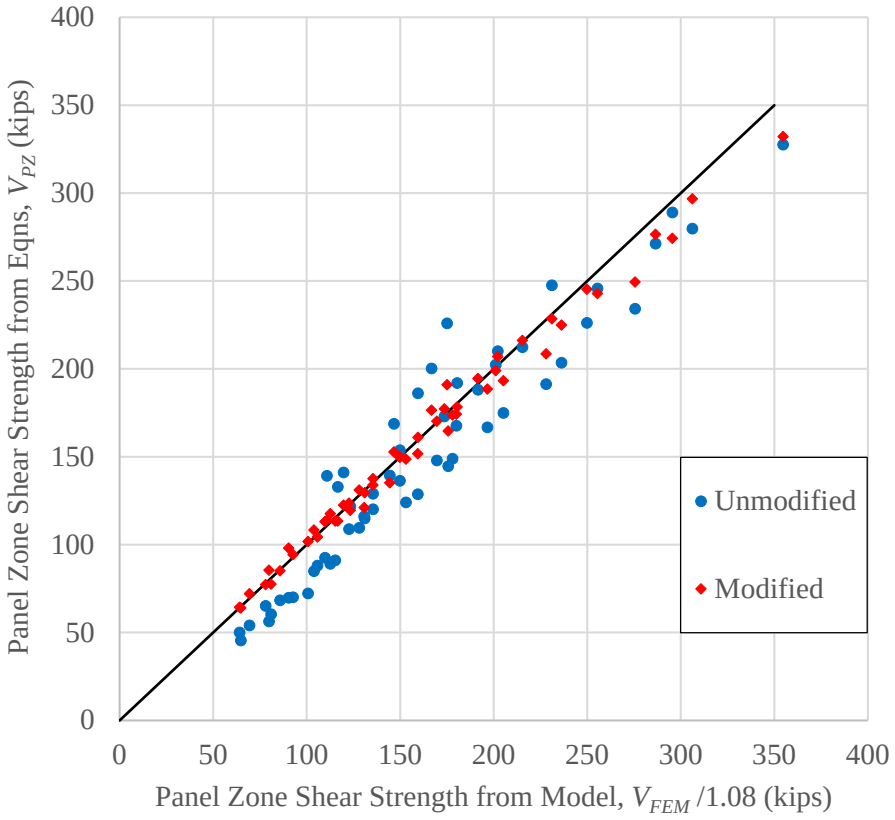

Figure 6-14 Evaluating Panel Zone Shear Strength Equations as Compared to FEA Results

Table 6-10 shows the shear strength calculations of the two test specimens (Young and Murray 1997) using the modified equations. The predicted shear strength from the modified equations agrees reasonably well with the one obtained from the test results, and average error of the prediction is also reduced.

Table 6-10 Validation of Theoretical Model against Test Data

Specimen #	$\frac{\max(h_c, h_r)}{t_w}$	h_r/h_c	M_P^*	P.Z. shear strength from test V_{exp} (kips)	K	C_v^*	C_t	V_{TFA} (kips)	V_{cr} (kips)	P. Z. shear strength from derived eqns V_{PZ} (kips)	$\frac{V_{PZ}}{V_{exp}}$
1	188	2.17	0.036	43.2	6.19	0.43	0.66	12.5	31.0	43.5	101%
2	204	2.00	0.028	46.8	6.34	0.37	0.71	13.8	29.8	43.6	93%

6.2.3 Sub-studies

This section presents the comparison between the results of the modified theoretical model and the FEA results, for each one of the four sub-studies.

6.2.2.1 Sub-study on Column and Rafter Lengths, and Use of Tapered Sections

Table 6-11 shows the results for the 15 models of the sub-study calculated with the theoretical model. It is observed that the predicted strength agrees well with the strength from the FEA. Almost all the 15 models have a difference less than 10% between the predicted shear strength using the modified theoretical equations and strength from FEA. Also, since the ratios of predicted strength to FE model strength are generally less than 100%, the predicted panel zone shear strength is considered conservative. It is noted, however, that the variation in rafter and column lengths for the MP models used shorter rafters and longer columns. As the ratio of rafter length to column length increases, the axial force in the rafter will increase and the panel zone shear strength will decrease. If the ratio of rafter length to column length increases significantly above the values used in this study, the prediction equation may become unconservative.

Table 6-11 Validation of the Modified Derived Equations – Substudy
(Column and Rafter Lengths, Tapered Section versus Prismatic Section)

Model #	$\frac{\max(h_c, h_r)}{t_w}$	h_r/h_c	$M_{P1}{}^*$	$M_{P2}{}^*$	P.Z. shear strength from FEA V_{FEM} (kips)	K	$C_v{}^*$	C_t	V_{TFA} (kips)	V_{cr} (kips)	P. Z. shear strength from derived eqns V_{PZ} (kips)	$\frac{V_{PZ}}{V_{FEM}/1.08}$
8	144	1.00	0.046	0.046	217	9.34	0.36	0.68	97.3	102	199	99%
8MP	144	1.00	0.046	0.046	221	9.34	0.36	0.68	97.3	102	199	97%
8MT	144	1.00	0.046	0.046	231	9.34	0.36	0.68	97.3	102	199	93%
10	144	1.33	0.005	0.005	126	7.59	0.44	0.61	19.4	94.0	113	97%
10MP	144	1.33	0.005	0.005	125	7.59	0.44	0.61	19.4	94.0	113	98%
10MT	144	1.33	0.005	0.005	133	7.59	0.44	0.61	19.4	94.0	113	92%
23	192	1.00	0.094	0.094	331	9.34	0.27	0.75	192	105	297	97%
23MP	192	1.00	0.094	0.094	347	9.34	0.27	0.75	192	105	297	92%
23MT	192	1.00	0.094	0.094	370	9.34	0.27	0.75	192	105	297	87%
28	192	1.50	0.009	0.009	133	7.12	0.35	0.70	30.8	88.7	120	97%
28MP	192	1.50	0.009	0.009	134	7.12	0.35	0.70	30.8	88.7	120	97%
28MT	192	1.50	0.009	0.009	144	7.12	0.35	0.70	30.8	88.7	120	89%

Table 6-11 (Continued) Validation of the Modified Derived Equations – Substudy
(Column and Rafter Lengths, Tapered Section versus Prismatic Section)

Model #	$\frac{\max(h_c, h_r)}{t_w}$	h_r/h_c	$M_{P1}{}^*$	$M_{P2}{}^*$	P.Z. shear strength from FEA V_{FEM} (kips)	K	$C_v{}^*$	C_t	V_{TFA} (kips)	V_{cr} (kips)	P. Z. shear strength from derived eqns V_{PZ} (kips)	$\frac{V_{PZ}}{V_{FEM}/1.08}$
29	256	1.50	0.011	0.011	146	16.0	0.27	0.77	60.1	77.4	138	102%
29MP	256	1.50	0.011	0.011	145	16.0	0.27	0.77	60.1	77.4	138	102%
29MT	256	1.50	0.011	0.011	160	16.0	0.27	0.77	60.1	77.4	138	93%
											Average:	96%
											Standard deviation:	4%
											Percentage of models with 20% difference or less:	100%
											Percentage of models with 10% difference or less:	87%

6.2.2.2 Sub-study on Flange Flexural Strength Parameter

Table 6-12 shows the results for the 24 models of the substudy calculated with the modified theoretical equations. It is observed that the predicted strength agrees well with the strength from the FEA, and the difference between the two values is less than 10% for almost all cases considered. It is also noted that switching the flange strength from strong flange on the panel zone side and weak flange on the panel zone top to strong flange on top and weak flange on the side had negligible effect on the panel zone shear strength and negligible effect on the predicted strength. This implies that simpler equations using a flange strength equal to the average of the two flange strengths can be used with equal accuracy.

Table 6-12 Validation of the Modified Derived Equations – Substudy
(Flange Flexural Strength Parameter)

Model #	$\frac{\max(h_c, h_r)}{t_w}$	h_r/h_c	$M_{P1}{}^*$	$M_{P2}{}^*$	P.Z. shear strength from FEA V_{FEM} (kips)	K	$C_v{}^*$	C_t	V_{TFA} (kips)	V_{cr} (kips)	P. Z. shear strength from derived eqns V_{PZ} (kips)	$\frac{V_{PZ}}{V_{FEM}/1.08}$
1A	144	0.75	0.005	0.009	174	13.5	0.44	0.61	38.5	125	164	101%
1B	144	0.75	0.009	0.005	173	13.5	0.44	0.61	39.4	125	165	103%
2A	144	1.00	0.005	0.009	157	9.34	0.36	0.68	36.2	102	138	95%
2B	144	1.00	0.009	0.005	156	9.34	0.36	0.68	36.8	102	139	96%

Table 6-12 (Continued) Validation of the Modified Derived Equations – Substudy
(Flange Flexural Strength Parameter)

Model #	$\frac{\max(h_c, h_r)}{t_w}$	h_r/h_c	$M_{P1}{}^*$	$M_{P2}{}^*$	P.Z. shear strength from FEA V_{FEM} (kips)	K	$C_v{}^*$	C_t	V_{TFA} (kips)	V_{cr} (kips)	P. Z. shear strength from derived eqns V_{PZ} (kips)	$\frac{V_{PZ}}{V_{FEM}/1.08}$
3A	144	1.33	0.005	0.012	128	7.59	0.44	0.61	22.4	94.0	116	98%
3B	144	1.33	0.012	0.005	127	7.59	0.44	0.61	23.1	94.0	117	99%
4A	192	0.75	0.005	0.012	199	13.5	0.32	0.72	58.2	122	181	98%
4B	192	0.75	0.012	0.005	197	13.5	0.32	0.72	60.1	122	182	100%
5A	192	1.00	0.005	0.012	176	9.34	0.27	0.75	53.0	105	158	97%
5B	192	1.00	0.012	0.005	175	9.34	0.27	0.75	54.4	105	159	98%
6A	192	1.33	0.005	0.009	141	7.59	0.32	0.72	31.7	91.8	123	95%
6B	192	1.33	0.009	0.005	143	7.59	0.32	0.72	32.2	91.8	124	94%
7A	256	0.75	0.005	0.012	127	13.5	0.25	0.78	45.5	72.9	118	100%
7B	256	0.75	0.012	0.005	126	13.5	0.25	0.78	47.0	72.9	120	102%
8A	256	1.00	0.005	0.012	112	9.34	0.23	0.80	40.9	65.4	106	103%
8B	256	1.00	0.012	0.005	111	9.34	0.23	0.80	42.0	65.4	107	105%
9A	256	1.33	0.005	0.009	89.0	7.59	0.25	0.78	24.8	54.7	79.4	96%
9B	256	1.33	0.009	0.005	88.9	7.59	0.25	0.78	25.2	54.7	79.8	97%
10A	292	0.75	0.006	0.010	104	13.5	0.24	0.80	40.2	59.0	99.1	103%
10B	292	0.75	0.010	0.006	105	13.5	0.24	0.80	41.0	59.0	100	103%
11A	292	1.00	0.006	0.010	91.3	9.34	0.22	0.81	35.9	53.9	89.8	106%
11B	292	1.00	0.010	0.006	92.2	9.34	0.22	0.81	36.5	53.9	90.5	106%
12A	292	1.33	0.004	0.010	69.8	7.59	0.24	0.80	21.1	44.2	65.3	101%
12B	292	1.33	0.010	0.004	70.3	7.59	0.24	0.80	21.5	44.2	65.7	101%
											Average:	100%
											Standard deviation:	4%
											Percentage of models with 20% difference or less:	100%
											Percentage of models with 10% difference or less:	100%

6.2.2.3 Sub-study on Orientation of End-Plate Connection

Table 6-13 shows the results for the 6 models of the specific sub-study calculated with the modified theoretical model. The agreement with the results of the FEA is satisfactory, and the error is less than 10% for all cases considered. That being said, there is a trend that the prediction equations produced panel zone shear strengths that were an average of 6% unconservative as compared to the FEA results for horizontal end-plates and an average of 4% unconservative as compared to the FEA results for sloped end-plates. Based on this limited sub-study, a reduction in panel zone shear strength

may be appropriate for knee joint configurations with horizontal and sloped end-plates. As described above in section 6.1.2.3, it is hypothesized that the variation in panel zone shear strength may be related to rafter axial force and therefore rafter axial forces that are significantly different from those assumed in this study may produce different results.

Table 6-13 Validation of the Calibrated Derived Equations – Substudy
(Orientation of End-Plate Connection)

Model #	$\frac{\max(h_c, h_r)}{t_w}$	h_r/h_c	$M_{P1}{}^*$	$M_{P2}{}^*$	P.Z. shear strength from FEA V_{FEM} (kips)	K	$C_v{}^*$	C_t	V_{TFA} (kips)	V_{cr} (kips)	P. Z. shear strength from derived eqns V_{PZ} (kips)	$\frac{V_{PZ}}{V_{FEM}/1.08}$
6	144	1.00	0.005	0.005	156	9.34	0.36	0.68	33.5	102	135	94%
6H	144	1.00	0.005	0.005	141	9.34	0.36	0.68	33.5	102	135	103%
6S	144	1.00	0.005	0.005	144	9.34	0.36	0.68	33.5	102	135	101%
25	192	1.33	0.011	0.011	146	7.59	0.32	0.72	42.1	91.8	134	99%
25H	192	1.33	0.011	0.011	133	7.59	0.32	0.72	42.1	91.8	134	109%
25S	192	1.33	0.011	0.011	135	7.59	0.32	0.72	42.1	91.8	134	107%
											Average:	105%
											Standard deviation:	4%
											Percentage of models with 20% difference or less:	100%
											Percentage of models with 10% difference or less:	100%

6.2.2.4 Sub-study on Roof Slope

The modified theoretical model gives very good estimates of the panel strength as compared to FEA results for the six models of this sub-study, as presented in Table 6-14. For roof slopes equal to 4:12, the prediction equation was unconservative by an average of 4% as compared to the FEA results. For roof slopes greater than 4:12, the prediction equation may not be appropriate.

Table 6-14 Validation of the Calibrated Derived Equations – Substudy (Roof Slope)

Model #	$\frac{\max(h_c, h_r)}{t_w}$	h_r/h_c	$M_{P1}{}^*$	$M_{P2}{}^*$	P.Z. shear strength from FEA V_{FEM} (kips)	K	$C_v{}^*$	C_t	V_{TFA} (kips)	V_{cr} (kips)	P. Z. shear strength from derived eqns V_{PZ} (kips)	$\frac{V_{PZ}}{V_{FEM}/1.08}$
6	144	1.00	0.005	0.005	156	9.34	0.36	0.68	33.5	102	135	94%
6C	144	1.00	0.005	0.005	171	9.34	0.36	0.68	33.5	102	135	85%
6D	144	1.00	0.005	0.005	142	9.34	0.36	0.68	33.5	102	135	103%
25	192	1.33	0.011	0.011	146	7.59	0.32	0.72	42.1	91.8	134	99%
25C	192	1.33	0.011	0.011	157	7.59	0.32	0.72	42.1	91.8	134	92%
25D	192	1.33	0.011	0.011	138	7.59	0.32	0.72	42.1	91.8	134	105%
											Average:	96%
											Standard deviation:	9%
											Percentage of models with 20% difference or less:	100%
											Percentage of models with 10% difference or less:	75%

6.2.4 Summary

Table 6-15 provides a summary of the results obtained in this chapter for the prototype knee joint configurations. For the range of parameter values considered in this study, the modified prediction equations of the theoretical model can accurately predict the panel zone shear strength.

Table 6-15 Summary of the Computational Study

Total number of models	98
Panel web thickness (in.)	0.164 – 0.250
Panel web height (in.)	24 – 48
Panel web width (in.)	24 – 48
Panel flange width (in.)	5 – 16
Panel flange thickness (in.)	0.25 – 1.5
Panel web slenderness $\max(h_c, h_r)/t_w$	144 – 292
Panel web aspect ratio h_r/h_c	0.67 – 1.50
Panel flange flexural strength parameter $M_{P1}{}^*$	0.005 – 0.1
Panel flange flexural strength parameter $M_{P2}{}^*$	0.005 – 0.1
Colum and rafter sectional property	Prismatic, tapered
Orientation of end-plate connection	Vertical, horizontal, sloped
Roof slope	0:12, 2:12, 4:12
Average of $V_{PZ}/(V_{FEM}/1.08)$	99%
Standard deviation of $V_{PZ}/(V_{FEM}/1.08)$	4%
Percentage of models with 20% difference or less	100%
Percentage of models with 10% difference or less	99%

6.3 Use of Panel Zone for Energy Dissipation

An additional topic that is deemed worthy of a preliminary investigation is the use of the panel zone for dissipating seismic energy in metal building gable frames. The present study pursues a preliminary finite element analysis of a typical knee joint configuration, to examine the feasibility of appropriately detailing the panel zone to ensure a stable hysteretic energy dissipation under cyclic loading. The panel zone thickness is selected to ensure that inelastic deformations will occur in the panel rather than the rafter or column. The selected panel web thickness also corresponds to an adequate relative stiffness of the panel flanges to ensure a hardening force-displacement response, in accordance with the discussion in Section 6.1.1. Furthermore, the panel zone is provided with circular cut-outs to control the yielding behavior, as such cut-outs have been shown (Koppal and Eatherton 2013) to delay the occurrence of extensive buckling-induced deformations and prevent the premature strength degradation under cyclic shear loading.

The dimensions of the knee-joint considered are provided in Table 6-16. The analysis is conducted for the same material properties as those used in the parametric study. The circular cutouts of the panel zone are designed per Section 7a of ANSI/AISC 341-16 (AISC 2016b). The panel zone is subjected to a cyclic displacement loading protocol, which is determined according to ANSI/AISC 341-16 (AISC 2016b) and shown in Figure 6-15.

Table 6-16 Knee Joint Configuration with Panel Zone Cut-outs

Panel web thickness t_w (in.)	Panel height h_r (in.)	Panel width h_c (in.)	Panel flange width b_f (in.)	Panel flange thickness t_f (in.)	End-plate thickness t_p (in.)	Column length l_c (ft)	Rafter length l_r (ft)	Diameter of cut-outs D (in.)	Spacing of cut-outs s (in.)
0.5	36	36	8	0.625	0.75	15	20.5	6	3×4.5*

*: Clear distance of cut-outs is 3 inches parallel to the column and 4.5 inches perpendicular to the column.

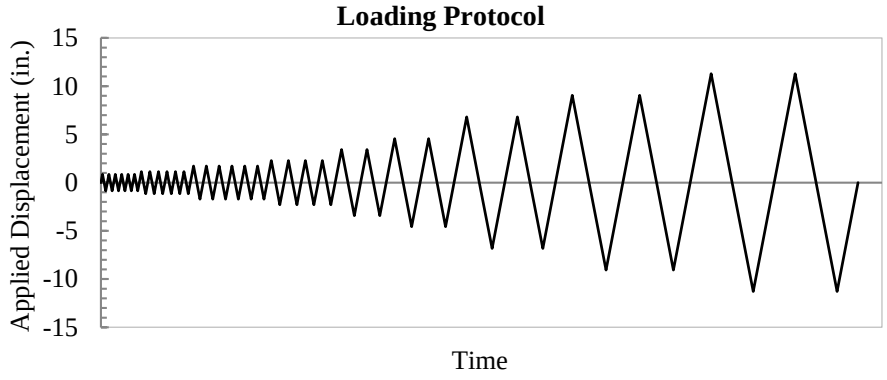

Figure 6-15 Cyclic loading protocol

Figure 6-16 shows the contours of the Von Mises stress and the effective plastic strain of the FE model after the first cycle with a drift ratio of 2%. A major portion of the panel zone yields at this level of story drift, and the relatively large values of effective plastic strain (as obtained from the corresponding contour plot) indicate that fracture due to ultra-low-cycle fatigue is probable. The force-displacement response of the model, shown in Figure 6-17, includes a stable hysteretic loop shape, thus demonstrating the suitability and effectiveness of a panel zone with cut-outs for seismic energy dissipation.

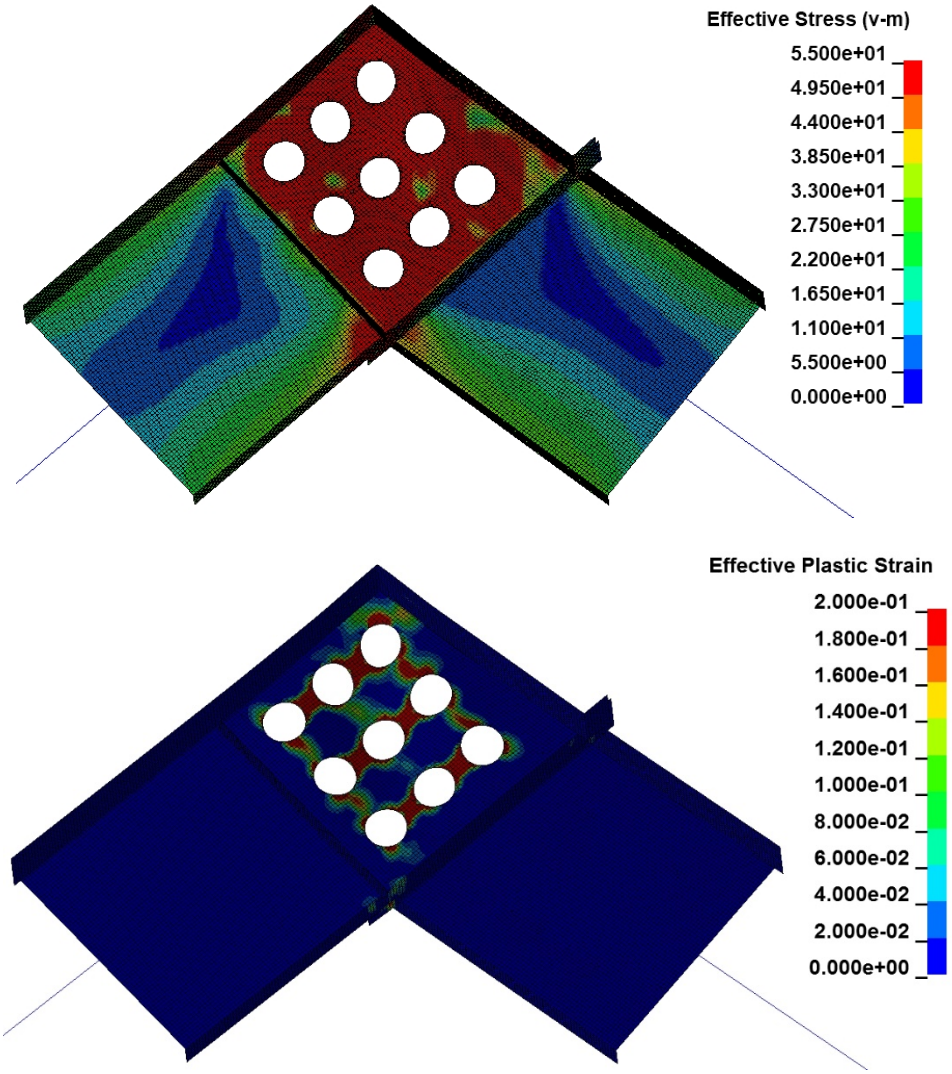

Figure 6-16 Contours of Von Mises stress and effective plastic strain at 2% story drift

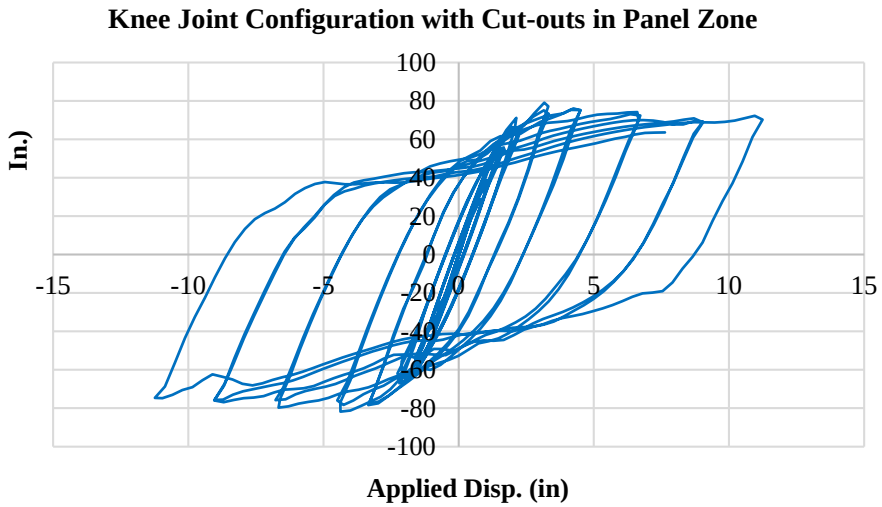

Figure 6-17 Hysteretic response for knee joint configuration with cut-outs in panel zone, subjected to cyclic loading.

6.4 Further Discussion

Several issues which have hitherto not been discussed warrant examination. Specifically, the fact that the analyses of several knee joints have led to a softening post-peak response (i.e., involving strength degradation), may imply that a mechanism depending on the post-buckling resistance of the panel regions may lead to a sudden (brittle) system failure, especially under load-control scenarios (i.e., the structure is subjected to prescribed forces, which do not change with increasing deformations). Furthermore, the analyses of prototype knee-joint configurations have neglected the potential impact of several details which are common in industry practice. The present section briefly touches upon these issues, by means of additional analyses or arguments and suggestions for future work.

6.4.1 Investigate Impact of Softening for Joints under Positive Bending for Frame Response

The parametric FE study has led to the observation that softening occurs in the post yielding response of a knee joint with the panel flange flexural strength parameter, M_p^*, equal to 0.005 or 0.01. Section 6.1.1 identified two reasons to be cautious in the design of a panel zone joint that has softening behavior: 1) the cumulative plastic strains were larger than the models with

hardening behavior and thus softening joints may be more prone to fracture, and 2) the panel zone shear strength is expected to be more sensitive to initial imperfections and residual stresses.

A third concern is examined in this section. For a full building frame, the ultimate failure mode associated with softening behavior in the knee joints could lead to sudden instability if the loading is force-controlled (e.g. constant wind pressure as opposed to earthquake loading which is more like an applied displacement). To elucidate the implications of softening joint response on the system-level failure mode, an FE model for a full frame was analyzed, using the same modeling approach as that employed in the parametric study.

The frame model, shown in Figure 6-18, uses the knee joint configuration of Model #6 in the parametric study. The specific knee joint configuration has a value of M_p^* equal to 0.005 and exhibits softening post-yielding behavior. The total length of two rafters of the frame is taken as four times the rafter length of the knee joint. To obtain the global lateral force-displacement response of the frame, the finite element model is subjected to a monotonically increasing lateral displacement. The corresponding lateral global force is equal to the horizontal reaction of the frame. Horizontal displacements are applied on the panel flange level with the mid-height of the panel zone.

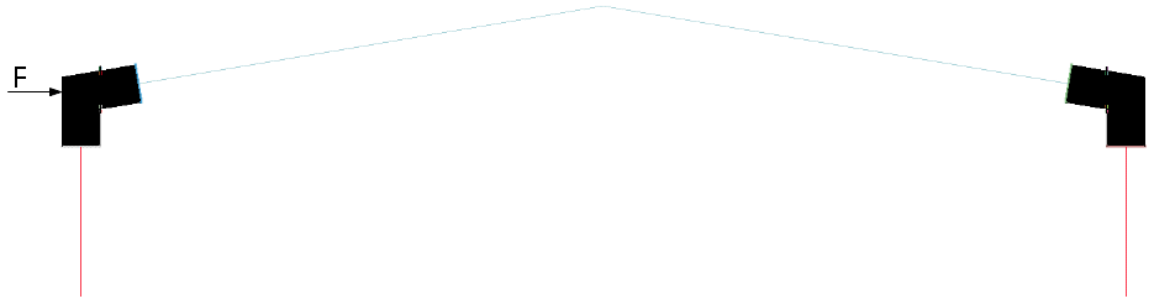

Figure 6-18 FE model for a full frame

Figure 6-19 shows the global lateral force-displacement curve for the full frame analysis. The post-yield global response of the frame is found to be dominated by hardening, rather than softening. This is attributed to the fact that one of the two knee joints is bound to be subjected to negative bending for which tension field action fully develops. It is also demonstrated in Figure 6-20 that softening response occurs at the knee joint under positive bending, while hardening response occurs at the knee joint under negative bending. The analysis indicates that for this

symmetric gable frame, the softening shear-force-versus-deformation behavior of a single knee joint with small values of M_p^* did not lead to softening system-level response. Thus a ductile post-yield response is expected for this symmetric frame.

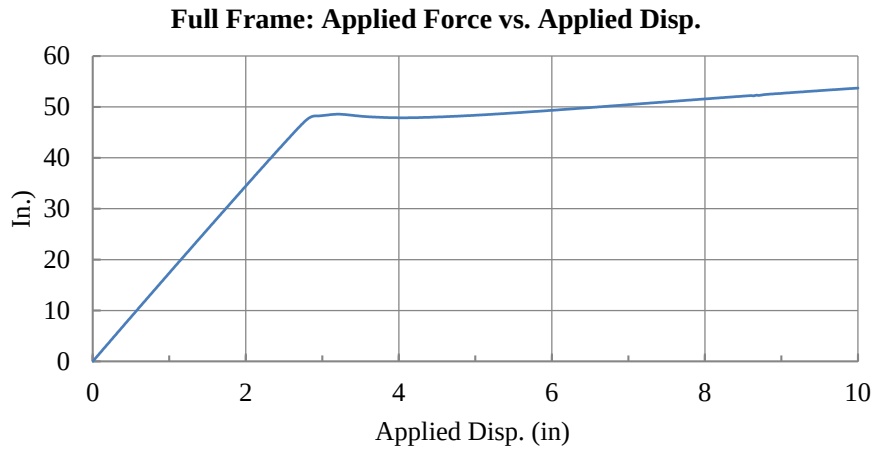

Figure 6-19 Applied force-displacement curve for full frame model

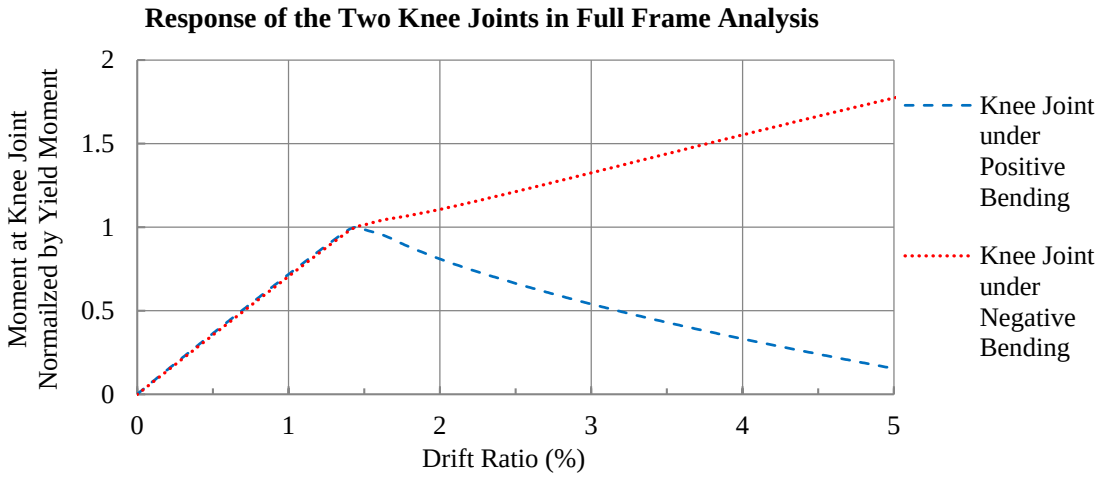

Figure 6-20 Normalized moment-drift ratio curves for the two knee joints of the full frame model

It is concluded that although sudden instability was avoided for this frame, the increased fracture potential and added uncertainty in panel zone shear strength warrant further testing of configurations with softening behavior. With further study, it may be possible to develop an appropriate resistance factor based on experimental tests and reliability analysis that can account for these potential issues.

6.4.2 Effects of Eave Bracket

Eave brackets, as schematically shown in Figure 6-21, are commonly used at the exterior corner of gable frames in practice to support the eave strut. Such brackets have not been included in the computational models of the present study. To investigate the effects of eave brackets, a further FE analysis is conducted for Model #6 of the parametric study, for three different sizes of eave bracket (with leg length of 2", 4", and 8" respectively). The results of the additional analyses are summarized in Table 6-17 and Figure 6-22. The presence of eave brackets is found to very slightly increase the peak strength of the knee joint. However, the difference is negligible, which is also reflected by the nearly identical force-versus displacement curves obtained for the three analyses in Figure 6-22.

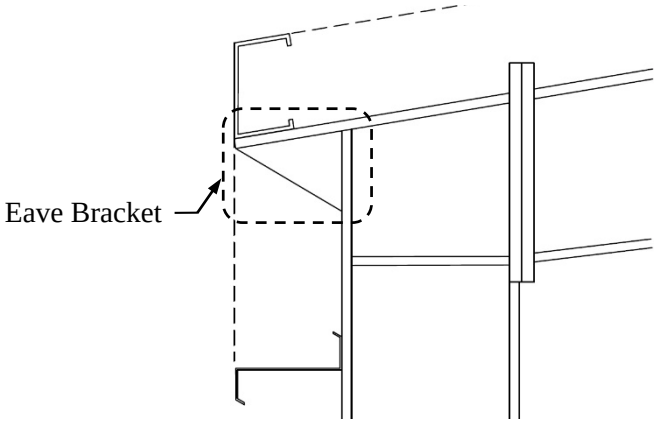

Figure 6-21 Typical configuration of eave bracket

Table 6-17 Maximum Applied Force for Knee Joints with Different Sizes of Eave Bracket

Knee Joint Configuration	F_{max} (kips)	Ratio*
No eave bracket	47.96	100.0%
2" eave bracket	48.01	100.1%
4" eave bracket	48.70	101.5%
8" eave bracket	48.29	100.7%

*: Ratios are relative to the maximum applied force of the knee joint without eave bracket.

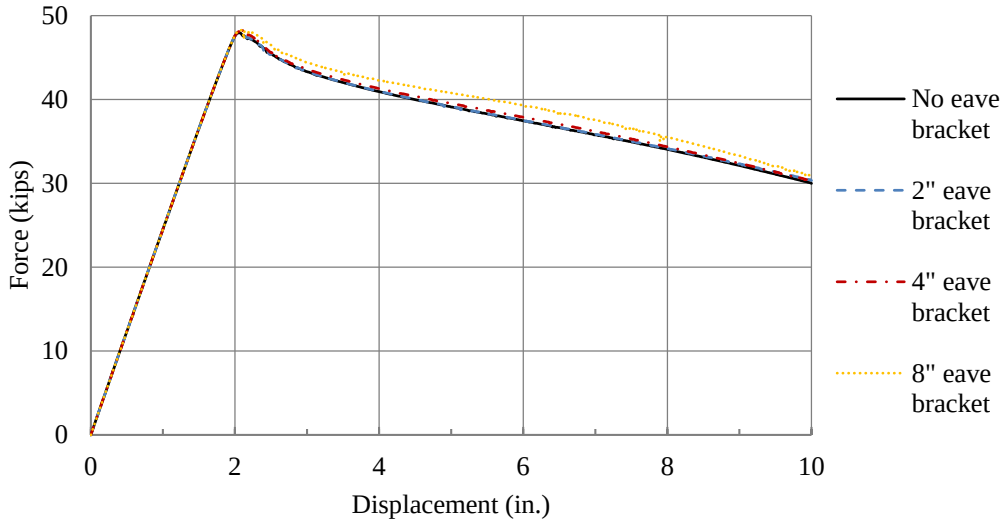

Figure 6-22 Applied force-displacement curves for knee joints with different sizes of eave bracket

6.4.3 Effects of Rod Bracing

Rod bracing is another issue that was not considered in this study. Figure 6-23 shows a typical configuration of rod bracing for metal buildings. Having a bracing rod connected to the panel zone web plate is expected to have two counteracting effects on the behavior of a panel zone. Specifically:

1) Rod bracing can stabilize the panel web by providing lateral support when the web buckles in such a way that the tensile force of the rod increases. In such a case, the rod bracing will increase the buckling strength of the web and the shear strength of the knee joint.
2) Rod bracing can also destabilize the panel web by introducing lateral forces, decreasing the web buckling strength and thus the shear strength of the knee joint. This destabilizing effect will occur when buckling of the web reduces the tensile elongation on the rod, and will be significant when the axial force in the bracing is sufficiently large to affect the buckling shape of the joint panel. Determining the exact conditions under which rod bracing has an effect on the buckling mode and strength is outside the focus of this report.

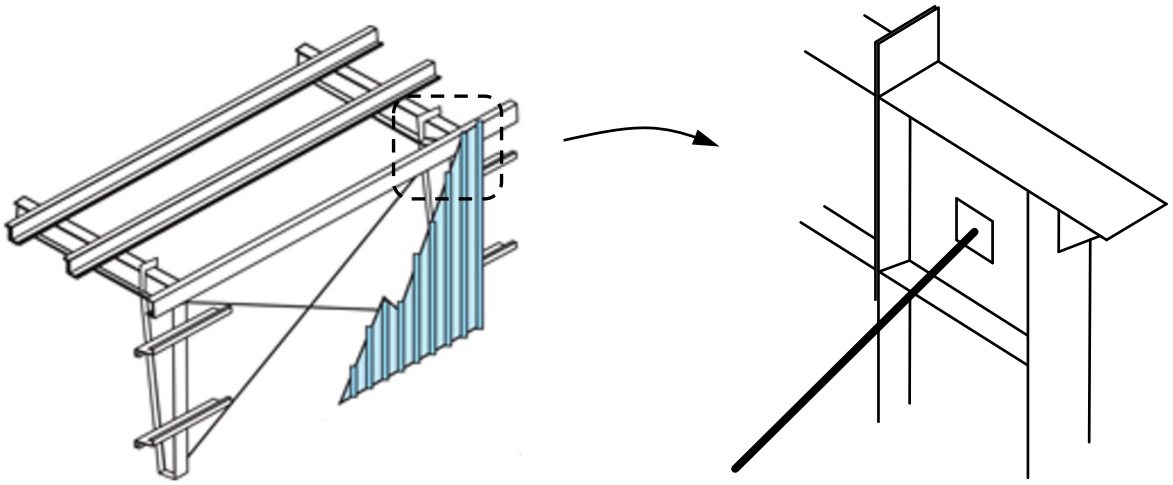

Figure 6-23 Typical configuration of rod bracing

Based on the above, the axial force in the bracing rods will decide whether rod bracing has a beneficial or detrimental effect on the knee joint strength of real-life structures. It is recommended that full-scale tests be conducted to further investigate this issue.

6.4.4 Effects of Welds on Exterior Corner of Panel Zone Flanges

Feedback provided from industry members during the course of this study has made the authors aware of the fact that fillet welds on the exterior corner of the panel zone flanges (see Figure 6-24) may not be stiff or strong enough for the flanges to develop a plastic hinge. The present computational study is calibrated to match the tests by Young and Murray (1997). The specimens in the tests by Young and Murray (1997), which used knee joints produced by a metal building company, led to deformation patterns that indicated fixity (i.e. moment transfer) between the flanges at the exterior corner. However, detailed information on the exterior corner weld of the specific specimens was unavailable.

The theoretical model assumes a plastic hinge in the weaker of the two flanges at the exterior corner of the panel zone and the computational model assumes rotational fixity between the flanges at the exterior corner. These assumptions produce results that match the deformed shape and panel zone shear strength of the models by Young and Murray (1997). Further testing with well-documented welds at the exterior corner are recommended to determine if the tests by

Young and Murray (1997) are representative of metal building knee connections. If not, the assumptions in the theoretical and computational models should be adjusted. Also, whether the welds of the panel zone web to the flanges are only on one side or on both sides would affect the behavior as well, and should be included in any further studies.

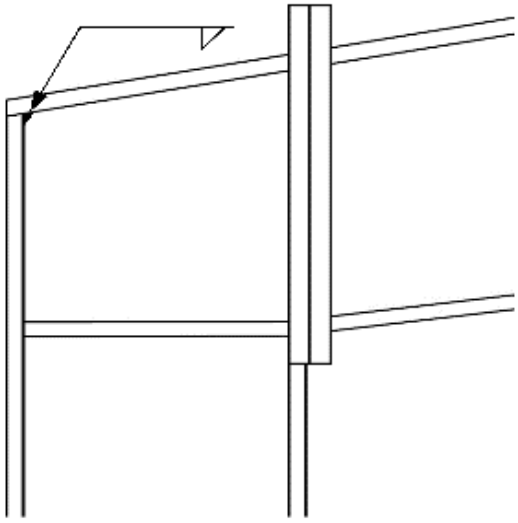

Figure 6-24 Welds on the exterior corner of panel zone flanges

CHAPTER 7 CONCLUSIONS AND RECOMMENDATIONS

7.1 Conclusions

This study formulated a theoretical model based on plastic analysis to predict the post-buckling shear strength of knee joint panel zones subjected to positive bending (bottom flange of rafter in tension) including partially developed tension field action. An equation was derived to estimate the panel zone shear strength associated with the tension field action. The strength value was found to primarily depend on three design parameters, namely, flange flexural strength, panel aspect ratio, and panel slenderness. A parametric computational study involving 56 models corresponding to different values of the three parameters was conducted to validate and modify the proposed equations. Several substudies were also performed to investigate the application of the proposed equations for predicting shear strength of knee joint configurations with different member lengths, section types (prismatic or tapered) of column and rafter, different flexural strength for the panel flanges, different orientations of end-plate connections, and different roof slopes.

Two types of load-displacement response were obtained, some that experienced hardening (i.e. increasing in strength) after the mechanism formed, and others that experienced softening associated with larger flange deformations. It was found that configurations with normalized flange flexural strength less than 0.05 exhibited softening. There are three reasons to be cautious with configurations that produce softening response including: 1) the cumulative plastic strains were larger than the models with hardening behavior and thus softening joints may be more prone to fracture, 2) the panel zone shear strength is expected to be more sensitive to initial imperfections and residual stresses, and 3) the consequences of reaching this limit state are worse because it is a brittle failure mode. For these reasons, the use of TFA in positive bending is not recommended for configurations that will produce softening (normalized flange flexural strength less than 0.05), until further testing is conducted.

The results of the computational study show that, for the range of parameters considered in this study (as provided in Table 6-15), the modified prediction equations below can predict the panel zone shear strength with an average error of 1% and standard deviation of the error equal to 4%.

One of the sub-studies suggests that the prediction equations may produce unconservative results if the ratio of rafter length to column length is larger than the values considered in this study. Another substudy found that the panel zone shear strength from the prediction equation was approximately 6% unconservative when the end-plate was oriented horizontally. Based on that limited sub-study, a reduction in panel zone shear strength of 6% may be appropriate for knee joints with horizontal end-plates and 4% for knee joints with sloped end-plates. A limited sub-study on roof slope showed that the prediction equations were an average of 4% unconservative for roof slopes of 4:12. The provided prediction equations may not be appropriate for roof slopes larger than 4:12.

The final proposed equations for panel zone shear strength, V_{PZ}, in knee joints subjected to positive bending including consideration of tension field action when M_P^* is greater than or equal to 0.05 are given as follows:

$$V_{PZ} = V_{cr} + V_{TFA} \tag{7-1}$$

where

$$V_{cr} = A_v \tau_{cr} = d_c t_w C_v^* \sigma_{yw} \Big/ \sqrt{3} \tag{7-2}$$

$$V_{TFA} = \left[\frac{M_{P1}^* - M_{P2}^* - M_{P,min}^*}{6 \tan\theta} + \cos\theta \sqrt{\frac{C_t}{3}} \left(\sqrt{M_{P1}^* + M_{P,min}^*} + \sqrt{M_{P2}^* + M_{P,min}^*} \right) \right] h_c t_w \sigma_{yw} \tag{7-3}$$

$$C_v^* = \frac{\sqrt{3}}{2} K \left[\frac{\pi^2 E \Big/ \sigma_{yw}}{12\left(1-\mu^2\right)} \right] \left(\frac{t_w}{h_c} \right)^2 + 0.17 \tag{7-4}$$

$$K = \begin{cases} 5.34 + 4\left(\dfrac{h_c}{h_r} \right)^2 & \text{for } \dfrac{h_c}{h_r} < 1.0 \\ 5.34\left(\dfrac{h_c}{h_r} \right)^2 + 4 & \text{for } \dfrac{h_c}{h_r} > 1.0 \end{cases} \tag{7-5}$$

$$C_t = -\frac{\sqrt{3} C_v^* \sin 2\theta}{2} + \sqrt{1 + \frac{\left(C_v^*\right)^2}{3} \left(\left(\frac{3 \sin 2\theta}{2} \right)^2 - 3 \right)} \tag{7-6}$$

$$\theta = arctan\frac{h_r}{h_c} \tag{7-7}$$

$$M_{P1}^{*} = \frac{M_{P1}}{M_y} = \frac{3b_{f1}t_{f1}^{2}\sigma_{yf}}{2t_w h_c{}^{2}\sigma_{yw}} \tag{7-8}$$

$$M_{P2}^{*} = \frac{M_{P2}}{M_y} = \frac{3b_{f2}t_{f2}^{2}\sigma_{yf}}{2t_w h_c{}^{2}\sigma_{yw}} \tag{7-9}$$

$$M_{P,min}^{*} = min\left(M_{P1}^{*}, M_{P2}^{*}\right) \tag{7-10}$$

where

V_{PZ} = shear strength of panel zone considering tension field action

V_{cr} = shear strength of panel zone at shear buckling of the web plate

V_{TFA} = shear strength of panel zone developed by tension field action

M_{P1} = plastic bending moment of panel zone flange along the top of column

M_{P2} = plastic bending moment of panel zone flange along the exterior side of column

M_y = yield moment of the panel web cross section along the top of the column

σ_{yw} = yield stress of the panel web plate material

σ_{yf} = yield stress of the panel flange material

τ_{cr} = critical shear stress at buckling

K = shear buckling coefficient

C_v^{*} = modified web shear coefficient

C_t = tensile stress coefficient

M_{P1}^{*} = normalized flexural strength parameter for panel zone flange along the top of column

M_{P2}^{*} = normalized flexural strength parameter for panel flange along the exterior side of column

A_v = overall area of the panel web plate cross section along the top of column = $d_c \times t_w$

d_c = full depth of the panel zone along the top of column

h_c = height of the panel web plate along the top of column

h_r = height of the panel web plate along the rafter face

t_w = thickness of panel zone web plate

b_{f1} = width of the panel flange along the top of column

b_{f2} = width of the panel flange along the exterior flange of column

t_{f1} = thickness of the panel flange along the top of column

t_{f2} = thickness of the panel flange along the exterior flange of column

θ = angle between the panel web diagonal and the column face of panel zone

7.2 Recommendations for Future Work

The authors strongly recommend additional large-scale experimental tests to further validate the refined computational models and design-oriented equations. The work described in this report is based on using finite element analyses to extrapolate from the results of four experimental tests (Young and Murray 1997). The FE models are not capable of capturing fracture and it is possible that fracture could limit the panel zone shear strength or that special detailing (e.g. stronger welds around the panel zone) would be needed to reach the panel zone shear strengths given by the proposed equations. Also, the fracture resistance and variability in strength should be experimentally evaluated for configurations expected to produce softening load-deformation response (configurations with M_P^* less than 0.05).

REFERENCES

American Institute of Steel Construction. (2016a). *Steel construction manual* (15th ed.). Chicago, Illinois: American Institute of Steel Construction.

American Institute of Steel Construction. (2016b). *Seismic Provisions for Structural Steel Buildings*. Chicago, Illinois: American Institute of Steel Construction.

Baumberger , A. M. (2005). *Finite Element Analysis of Shear in the Panel Zone of Steel Gable Frames* (Master's thesis, Virginia Tech, 2005). Blacksburg, Virginia: Virginia Tech.

Cristutiu, I. M., & Dubina, D. (2010). Influence of Member Components on the Structural Performance of Beam-to-Column Joints of Pitched Roof Portal Frames with Class 3 and 4 Sections. In *International Colloquium on Stability and Ductility of Steel Structures*. Red Hook, New York: Curran Associates, Inc.

Forest, R., & Murray, T. M. (1982). *Rigid Frame Studies Final Report - Full Scale Frame Tests* (Rep. No. FSEL/STAR 82-01). Norman, Oklahoma: University of Oklahoma.

Gillman, C. L. (2004). *Finite Element Analysis of Shear in the Panel Zone of a Steel Gable Frame* (Master's thesis, Virginia Tech, 2004). Blacksburg, Virginia: Virginia Tech.

Hong, J. K., & Uang, C. M. (2012). Cyclic testing of a metal building moment frame system with web-tapered members. *Journal of Constructional Steel Research*, *70*, 248-255.

Hongwei, L., & Jun, L. (2012). Initial Stiffness Analysis of Steel Portal Frame End-plate Connections Based on Finite Element Method. *Advanced Materials Research, 446-449*, 867-870.

Hughes, T. J., & Liu, W. K. (1981a). Nonlinear finite element analysis of shells: Part I. Three-dimensional shells. *Computer methods in applied mechanics and engineering*, *26*(3), 331-362.

Hughes, T. J., & Liu, W. K. (1981b). Nonlinear finite element analysis of shells-part II. two-dimensional shells. *Computer Methods in Applied Mechanics and Engineering*, *27*(2), 167-181.

Jenner, R. K., Densford, T. A., Astaneh-Asl, A., & Murray, T. M. (1985). *Experimental Investigation of Rigid Frames Including Knee Connection Studies* - (Rep. No. FSEL/MESCO 85-01). Norman, Oklahoma: University of Oklahoma.

Kim, D. W., & Uang, C. M. (2015). *Shear Resistance of End Panels in Steel and Steel-concrete Composite Girders* (Rep. No. SSRP-15/02). La Jolla, California: Universit of California, Sandiago

Krawinkler, H. (1978). Shear in beam-column joints in seismic design of steel frames. *Engineering Journal*, *15*(3).

Koppal, M., & Eatherton, M. R. (2013). Perforated Steel Plate Shear Walls for Tunable Seismic Resistance. In *Structures Congress 2013: Bridging Your Passion with Your Profession*(pp. 2884-2894).

Lasdon, L. S., Waren, A. D., Jain, A., & Ratner, M. (1978). Design and testing of a generalized reduced gradient code for nonlinear programming. *ACM Transactions on Mathematical Software (TOMS)*, *4*(1), 34-50.

Liu, H. W., & Li, J. (2012). Initial Stiffness Analysis of Steel Portal Frame End-Plate Connections Based on Finite Element Method. In *Advanced Materials Research* (Vol. 446, pp. 867-870). Trans Tech Publications.

Livermore Software Technology Corporation. (2016a). *LS-DYNA Keyword User's Manual: Volumn I* (Version R9.0). Livermore, CA.: Livermore Software Technology Corporation.

Livermore Software Technology Corporation. (2016b). *LS-DYNA Keyword User's Manual: Volumn II* (Version R9.0). Livermore, CA.: Livermore Software Technology Corporation.

Metal Building Manufacturers Association. (2012). *Metal Building Systems Manual.* Cleveland, Ohio: Metal Building Manufacturers Association.

Murray, T. M., & Shoemaker, W. L. (2002). *Flush and extended multiple-row moment end-plate Connections*. American Institute of Steel Construction.

Porter, D. M., Rockey, K. C., & Evans, H. R. (1975). COLLAPSE BEHAVIOUR OF PLATE GIRDERS LOADED IN SHEAR. *Structural Engineer, 53*(8), 313-325.

Rockey, K. C., & Skaloud, M. (1972). Ultimate load behaviour of plate girders loaded in shear. *Structural Engineer, 50*(1), 29-47.

Scheer, J., Pasternak, H., & Schween, T. (1991). Structural behavior of stiffened knee joints with thin webs. *Journal of structural engineering New York, N.Y., 117*(9), 2600-2619.

Spangler, D. D., Jr., & Murray, T. M. (1989). *Experimental Investigation of Rigid Frame Knee Connections* (Rep. No. CE/VPI-ST 89/01). Blacksburg, Virginia: Virginia Tech.

Sullivan, S. V., Charney, F. A., & Murray, T. M. (2006). *Performance of Diagonal Knee Connections with and without Stiffeners* (Master's thesis, Virginia Tech, 2006). Blacksburg, Virginia: Virginia Tech.

Uang, C. M., Smith, M. D., & Shoemaker, W. L. (2011). Earthquake simulator testing of metal building systems. In *Structures Congress 2011* (pp. 693-704).

Young, J., & Murray, T. M. (1997). *Experimental Investigation of Positive Bending Moment Strength of Rigid Knee Connections* (Rep. No. CE/VPI-ST 97/08). Blacksburg, Virginia: Virginia Tech.

APPENDIX A INDUSTRY SURVEY

A1 Questionnaire

RETURN TO:

MBMA

ATTN: Eva Brunk

1300 Sumner Avenue

Cleveland, OH 44115

E-MAIL: ebrunk@mbma.com

FAX: 216-241-0105

SUBJECT: Panel Zone Project - Industry Survey

MBMA BULLETIN NO. 010-17 (E)

The panel zone project scope includes Phase 2, Developing Study Parameters. In this phase, the researchers will determine the parameters to be investigated in the computational study, relying on their literature review and on input from MBMA. This survey will provide the MBMA input.

Please provide the information requested below. In addition, provide drawings of panel zone details. Any company identification on the information provided will be removed prior to sending it to the researchers.

Panel Zone:

- Material, such as ASTM Specification, and grade, if applicable
- Panel web thickness:
  - Minimum inches
  - Maximum inches
  - Typical inches (provide a range if applicable)

- Panel dimensions:
    - Height:
        - Minimum inches
        - Maximum inches
        - Typical inches (provide a range if applicable)
    - Width:
        - Minimum inches
        - Maximum inches
        - Typical inches (provide a range if applicable)
- Panel aspect ratios (height-to-width):
    - Minimum
    - Maximum
    - Typical
- Panel zone flange dimensions:
    - Width
        - Minimum inches
        - Maximum inches
        - Typical inches (provide a range if applicable)
    - Thickness
        - Minimum inches
        - Maximum inches
        - Typical inches (provide a range if applicable)
- Additional information:

<u>Panel Zone Web Options:</u>

- Part of one of the connected frame members, same thickness: ☐ Yes ☐ No
- Inserted plate, thickness can differ from connected frame members: ☐ Yes ☐ No
- Doubler plate is permitted, when needed: ☐ Yes ☐ No

- Additional information:

Panel Zone Flange Options:

- Part of one of the connected frame members, same dimensions: ☐ Yes ☐ No
- Both flanges, vertical and top, same dimensions: ☐ Yes ☐ No

- Additional information:

Panel Zone Stiffeners (stiffeners that cross the panel zone):

For continuity plates on the perimeter of the panel zone, see the following section.

- Material, such as ASTM Specification, and grade, if applicable
- Used in approximately what percent of your buildings: %
- Orientation:
    - Horizontal ☐
    - Vertical ☐
    - Diagonal ☐
- Stiffener location:
    - One side ☐
    - Both sides ☐
- Stiffener welding:
    - Long edge fillet welds:

        - Continuous ☐
        - Intermittent ☐
    - Short edges welded:
        - One edge ☐
        - Both edges ☐
    - Other ☐
- Standard details of panel zone stiffeners attached: ☐ Yes ☐ No

- Additional information:

<u>Continuity Plates (stiffeners in the column at the level of the rafter bottom flange or stiffeners in the rafter aligned with the interior column flange):</u>

- Material, such as ASTM Specification, and grade, if applicable
- Aligned with beam bottom flange or horizontal? ☐ Aligned ☐ Horizontal
- Aligned with column flange or vertical? ☐ Aligned ☐ Vertical
- How often are they partial depth?
- How often are they full depth?
- Standard details of continuity plates attached: ☐ Yes ☐ No

- Additional information:

<u>Column-Rafter Bolted End-Plate Connection Orientation</u>:

- Orientation varies? ☐ Yes ☐ No
- Orientations used:
    - Horizontal ☐ %
    - Vertical ☐ %
    - Sloped (perpendicular to roof slope) ☐ %

- Other ☐ %

- Additional information:

Columns Adjacent to the Panel Zone:

- Material, such as ASTM Specification, and grade, if applicable
- Depth:
  - Minimum inches
  - Maximum inches
  - Typical inches
- Web thickness:
  - Minimum inches
  - Maximum inches
  - Typical inches
- Flange width:
  - Minimum inches
  - Maximum inches
  - Typical inches
- Flange thickness:
  - Minimum inches
  - Maximum inches
  - Typical inches

- Additional information:

Rafters Adjacent to the Panel Zone:

- Material, such as ASTM Specification, and grade, if applicable
- Depth:
    - Minimum inches
    - Maximum inches
    - Typical inches
- Web thickness:
    - Minimum inches
    - Maximum inches
    - Typical inches
- Flange width:
    - Minimum inches
    - Maximum inches
    - Typical inches
- Flange thickness:
    - Minimum inches
    - Maximum inches
    - Typical inches

- Additional information:

<u>Roof Slope</u>:

Roof slope, from the horizontal. For the typical values, provide a range of slopes that are used in 90% of your buildings.

- Minimum degrees
- Typical minimum degrees
- Maximum degrees
- Typical maximum degrees

- Additional information:

Additional Information:

- Standard details of panel zone attached: ☐ Yes ☐ No
- Additional information:

Name:

Company:

PLEASE RETURN TO ebrunk@mbma.com AT THE MBMA OFFICE

BY NO LATER THAN WEDNESDAY, JANUARY 18, 2017

A2 Responses

Table A-1 Industry Survey Responses

			Company A		Company B	Company C	Company D	Company E	Company F	Company G	Company H
			Person 1	Person 2							
Panel Zone	Material		A1011 SS (or HSLAS Cl 1) Gr.55 <= 3/16" thick, A572 Gr.55 3/16" to 3/8", A572 Gr.50 > 3/8"	A572 Gr. 55, A1011 Gr. 55	NA	Gr. 55 SS	A1011, A572, A529, Gr.55	A572, A529, A1011, Gr.55	NA	A1011 Gr.55, A529 Gr.55, A572 Gr.55 and Gr.50	A1011, A572, A529, A1018, Gr.55
	Panel web thickness	Min (in.)	0.134	0.134	0.1345	0.1345	0.125	0.1345	0.1345	0.125	0.125
		Max (in.)	0.625	1	0.625	0.75	0.625	0.625	0.75	0.5	0.5
		Typical (in.)	0.134-0.3125	0.156-0.875	0.25	0.1345-0.5	0.1875-0.3125	0.1345-0.25	0.1345-0.375	0.1345-0.3125	0.15-0.3125
	Panel height	Min (in.)	10	10	7	12	10	6	8	7	12
		Max (in.)	70	62	120	72	60	72	72	60	60
		Typical (in.)	24-48	18	12-48	18, 24, 36, 48	20-40	12-60	8-50	12-48	20-48
	Panel width	Min (in.)	10	10	7	12	8	6	8	7	8
		Max (in.)	70	62	120	60	60	72	72	60	60
		Typical (in.)	24-48	18	12-72	18, 24, 36, 48	20-40	8-60	8-50	12-36	12-48
	Panel aspect ratios	Min	no spec. limit	0.5	dependent	0.5	0.75	None	0.5	0.25	NA
		Max	no spec. limit	1.5	on loading	2	2.5	None	5	3	NA
		Typical	~1.0	1	and span	0.8-1.25	1	0.8-1.2	1.0-2.0	0.75-1.5 (~1.0)	0.5-3.0 (~1)
	Panel zone flange width	Min (in.)	5	5	5	5	6	5	5	5	5
		Max (in.)	12	20	22	16	14	20	15	14	12
		Typical (in.)	6-10	6-18	5-8	6, 8, 10	6-10	5-10	5-8	6-12	6-10
	Panel zone flange thickness	Min (in.)	0.25	0.25	0.25	0.1345	0.25	0.25	0.1875	0.1875	0.1875
		Max (in.)	1	2	1.5	1.5	1.25	1.5	1.5	1.5	1
		Typical (in.)	0.25-0.75	0.375-1.50	0.375	0.25-1.0	0.25-0.5	0.25-0.75	0.1875-0.75	0.25-1	0.25-0.625
Panel Zone Web Options	Part of one of the connected frame members, same thickness.		Yes	Yes	Yes	Yes	Yes	No	Yes	Yes	Yes
	Inserted plate, thickness can differ from connected frame members.		Yes	Yes	Yes	Yes	Yes	Yes	Yes	Yes	Yes
	Doubler plate is permitted, when needed.		No	No	No	No	No	No	No	Yes	No
Panel Zone Flange Options	Part of one of the connected frame members, same thickness.		No	Yes	Yes	Yes	Yes	Yes	Yes	Yes	Yes
	Both flanges, vertical and top, same dimensions		No	No	No	No	No	No	No	No	No

Table A-1 (Continued) Industry Survey Responses

			Company A		Company B	Company C	Company D	Company E	Company F	Company G	Company H
			Person 1	Person 2							
Panel Zone Stiffeners (stiffeners that cross the panel zone)	Material		NA	A572 Gr. 55	NA	Same as standard	NA	A572, A529, A1011, Gr.55	A572 Gr.55	A572 Gr.50 and Gr.55, A529 Gr.50 and Gr.55	A36, A529 Gr.55
	Used in approx. what percent of your buildings?		0%	10%	75%	50%	0%	1%	10%	Low	25%
	Orientation	Horizontal		√	√	√		√	√	√	√
		Vertical			√	√					√
		Diagnal		√	√			√		√	√
	Stiffener location			One side	Both sides	One/both side(s)		One/both side(s)	One side	One/both side(s)	One/both side(s)
	Stiffener welding	Long edge		Continuous	Continuous	Intermittent			Intermittent	Continuous Intermittent	Continuous
		Short edges			Both edges	One/both edge(s)		Both edges	Both edges	One edge	One/both edge(s)
		Other									
Continuity Plates	Material		ASTM A572 Gr.50 or 55	ASTM A572 Gr.55	NA	Same as frame material	Same as panel zone	A572, A529, A1011, Gr. 55	A572 Gr. 55	A572 Gr.50 and Gr.55, A529 Gr.50 and Gr.55	A36, A529 Gr.55
	Aligned with beam bottom flange or horizontal?		Horizontal	Aligned, Horizontal	Aligned, Horizontal	Aligned, Horizontal	Horizontal	Horizontal	Horizontal	Horizontal	Horizontal
	Aligned with column flange or vertical?		Vertical	Vertical	Aligned, Vertical	Aligned	Vertical	Aligned, Vertical	Vertical	NA	NA
	How often are they partial depth?		Rarely	Never	Sometimes, needed to minimize	Never	Never	At rafters with interior columns, always partial	10%	Never	Never
	How often are they full depth?		Almost always	Always	Always when using tension field	Always	Always	At rafter bottom flange, always full	90%	Always	Always
Column-Rafter Bolted End-Plate Connection Orientation	Orientation varies?		No	Yes	Yes	Yes	Yes	Yes	Yes	No	Yes
	Orientation used	Horizontal	0%	0%	0%	50%	0%	1%	0%	0%	90%
		Vertical	100%	98%	15%	25%	30%	19%	50%	100%	0%
		Sloping (Perp. to roof slope)	0%	1%	85%	25%	70%	80%	50%	0%	10%
		Other	0%	1% (diagnal)	0%	0%	0%	0%	0%	0%	0%
Columns Adjacent to the Panel Zone	Material		similar to PZ	A572 Gr.55	NA	Same as frame material	Same as PZ	A572, A529, A1011, Gr.55	A572 Gr. 55	For webs see PZ. For flanges see Continuity Plates.	A529 Gr.55
	Depth	Min (in.)	10	8	7	12	8	6	8	7	8
		Max (in.)	70	60	120	60	60	72	72	60	60
		Typical (in.)	24-48	24	12-36	18, 24, 36, 48	20-40	8-48	8-50	12-36	NA
	Web thickness	Min (in.)	0.134	0.134	0.1345	0.1345	0.125	0.1345	0.1345	0.125	0.125
		Max (in.)	0.625	1	1.5	0.75	0.375	0.625	0.75	0.5	0.375
		Typical (in.)	0.134-0.315	0.156- 0.875	0.25	0.1345-0.5	0.156-0.25	0.1345-0.25	0.1345-0.375	0.1345-0.3125	NA
	Flange width	Min (in.)	5	5	5	5	6	5	5	5	5
		Max (in.)	12	20	22	16	14	20	15	14	12
		Typical (in.)	6-10	6-18	6-8	6, 8, 10	6-10	5-10	5-10	6-12	NA
	Flange thickness	Min (in.)	0.25	0.25	0.25	0.1345	0.25	0.25	0.1875	0.1875	0.1875
		Max (in.)	1	2	1.5	1.5	1.5	1.5	1.5	1.5	1
		Typical (in.)	0.25-0.75	0.375-1.50	0.375	0.25-1.0	0.25-0.5	0.25-0.75	0.1875-0.75	0.25-1.0	NA

Table A-1 (Continued) Industry Survey Responses

			Company A		Company B	Company C	Company D	Company E	Company F	Company G	Company H
			Person 1	Person 2							
Rafters Adjacent to the Panel Zone	Material		similar to PZ	same as PZ	NA	Same as frame material	Same as PZ	A572, A529, A1011, Gr.55	A572 Gr. 55	For webs see PZ. For flanges see Continuity Plates.	A529 Gr.55
	Depth	Min (in.)	10	10	7	12	10	6	8	7	8
		Max (in.)	70	62	120	72	60	72	72	60	60
		Typical (in.)	24-48	18	12-36	18, 24, 36, 48	20-40	12-60	8-50	12-48	NA
	Web thickness	Min (in.)	0.134	0.134	0.1345	0.1345	0.125	0.1345	0.1375	0.125	0.125
		Max (in.)	0.625	1	0.5	0.75	0.375	0.625	0.75	0.5	0.375
		Typical (in.)	0.134-0.315	0.156-0.875	0.25	0.1345-0.5	0.1875-0.3125	0.1345-0.25	0.1345-0.375	0.1345-0.3125	NA
	Flange width	Min (in.)	5	5	5	5	6	5	5	5	5
		Max (in.)	12	20	22	16	14	20	15	14	12
		Typical (in.)	6-10	6, 8, 10, 12, 14, 16, 18	6-8	6, 8, 10	6-10	5-10	5-10	6-12	NA
	Flange thickness	Min (in.)	0.25	0.25	0.25	0.1345	0.25	0.25	0.1875	0.1875	0.1875
		Max (in.)	1	2	1.5	1.5	1.5	1.5	1.5	1.5	1
		Typical (in.)	0.25-0.75	0.375-1.50	0.375	0.25-1.0	0.25-0.5	0.25-0.75	0.1875-0.75	0.25-1.0	NA
Roof Slope	Min (deg.)		1.19	1.19	1.19	0	1.2	1.19	1.19	0	0
	Typical min (90%) (deg.)		1.19	4.76	4.76	1.1	2.4	1.19-9.46	2.386	1.2	2.4
	Max (deg.)		26.565	26.565	45	45	45	None	36.87	26.6	20
	Typical max (90%) (deg.)		14.036	18.435	18.435	10	20	None	26.565	18.4	18
Standard details of panel zone attached?			Yes	No	No	Yes	Yes	Yes	No	Yes	No

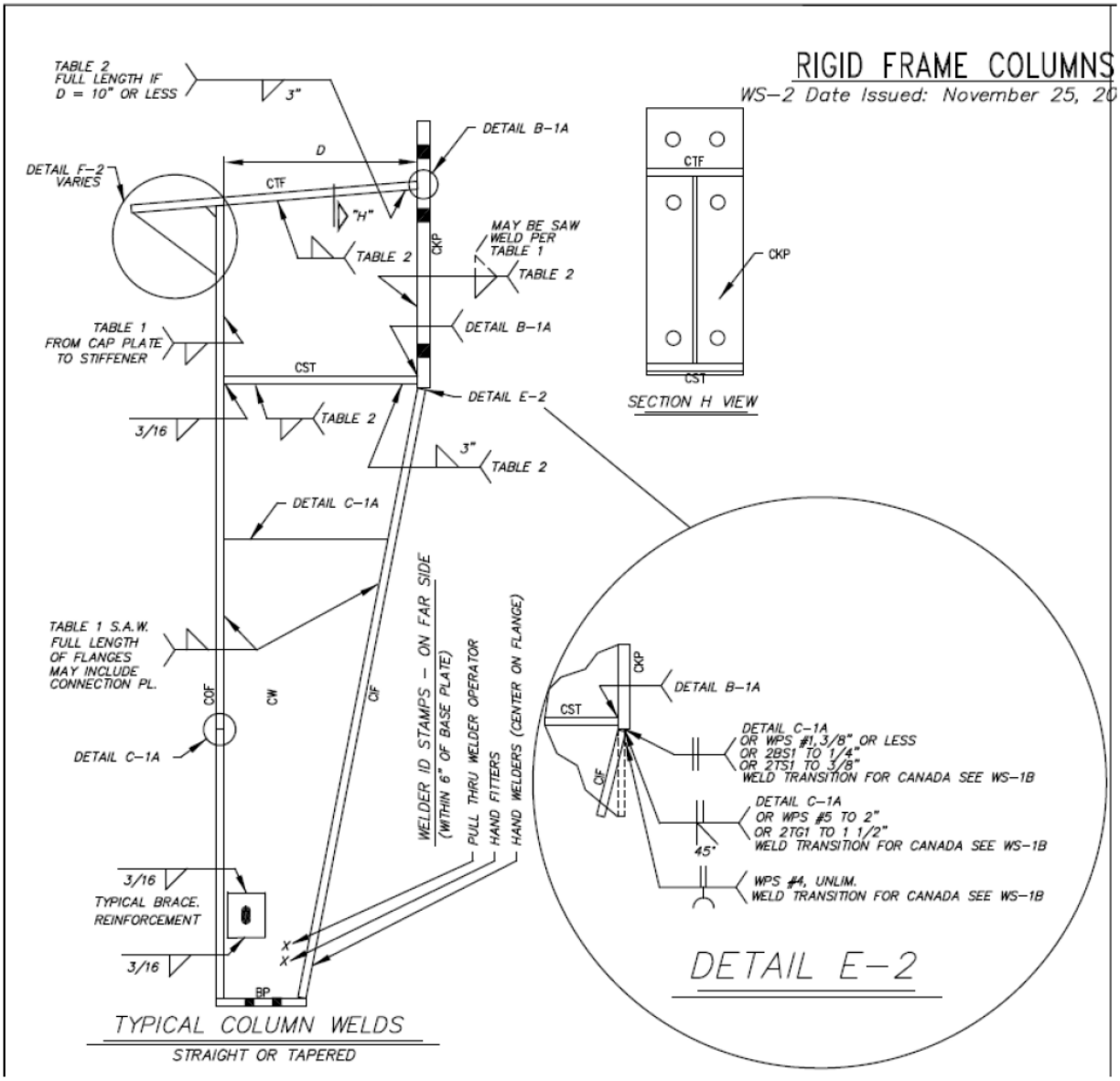

Figure A-1 Drawings of panel zone details from Company A

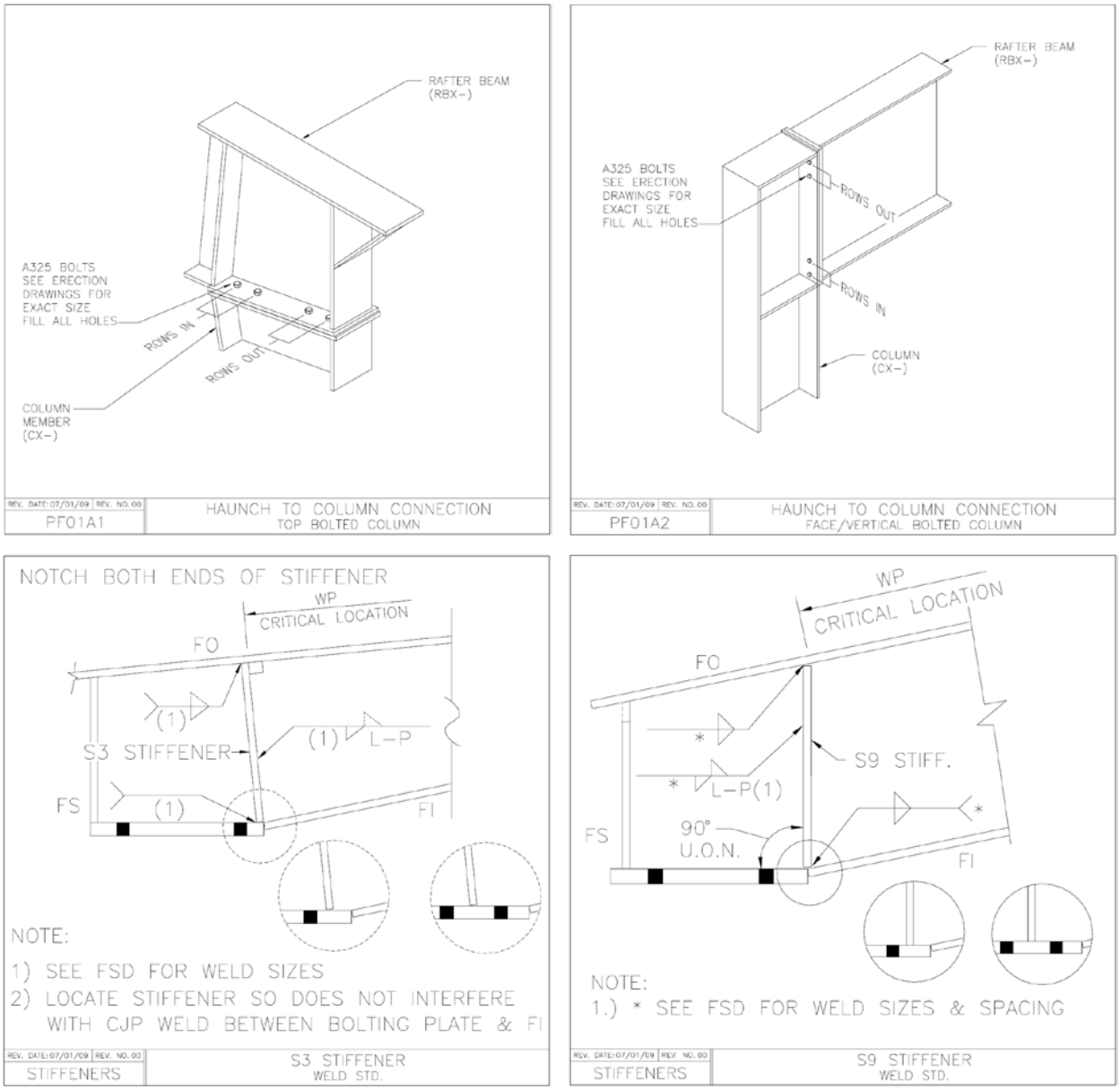

Figure A-2 Drawings of panel zone details from Company C

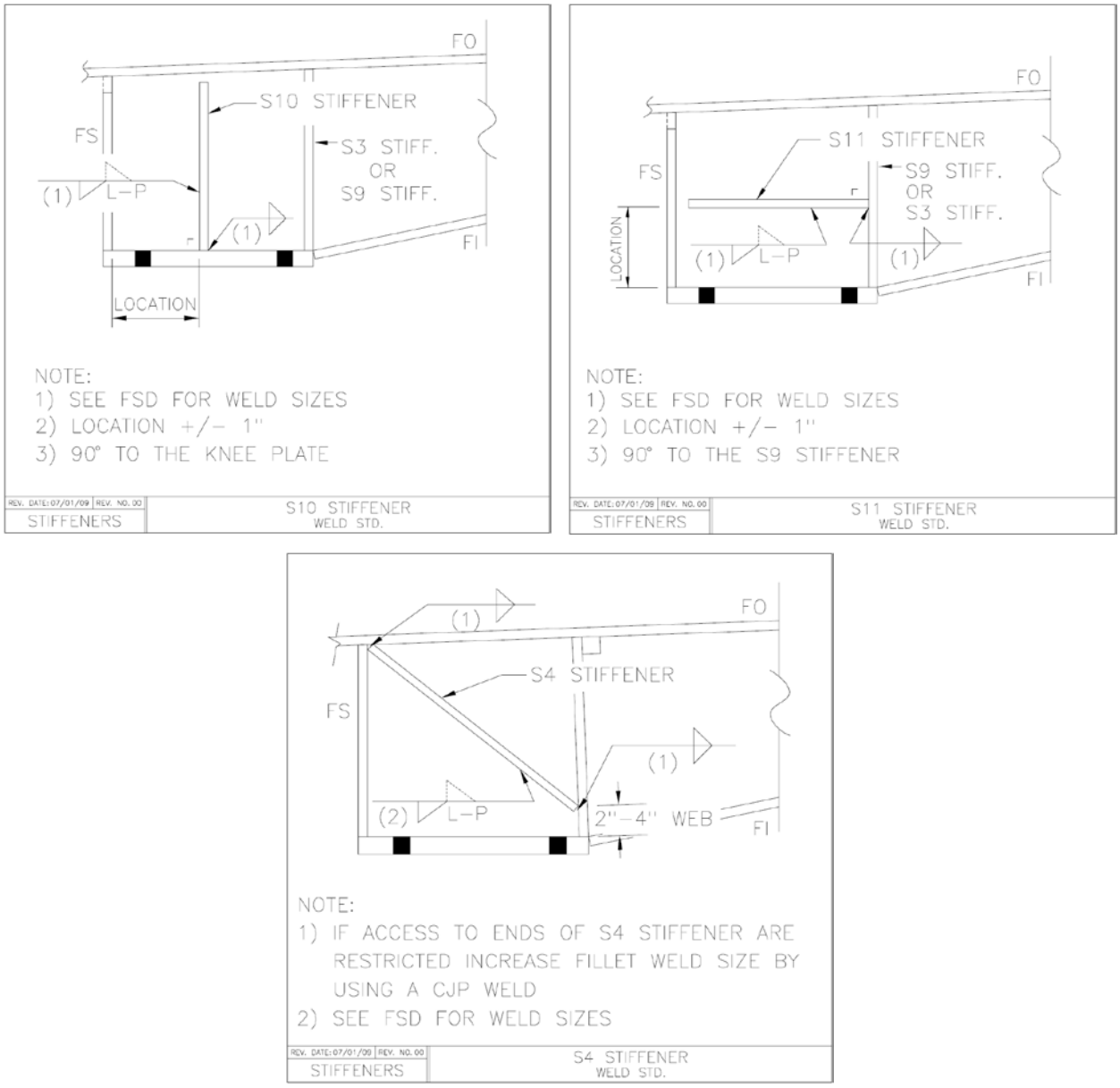

Figure A-2 (Continued) Drawings of panel zone details from Company C

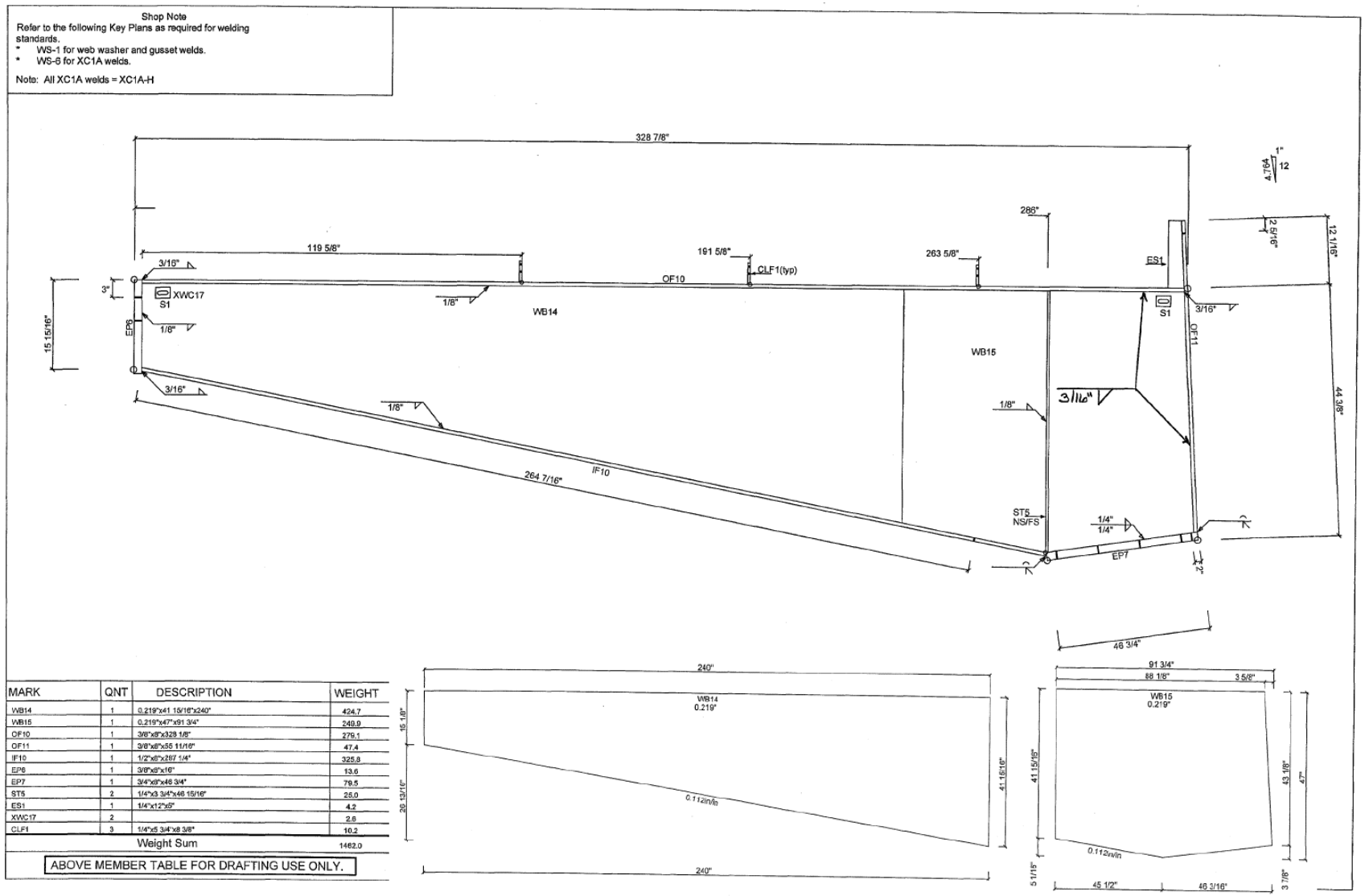

MARK	QNT	DESCRIPTION	WEIGHT
WB14	1	0.219"x41 15/16"x240"	424.7
WB15	1	0.219"x47"x91 3/4"	249.9
OF10	1	3/8"x8"x328 1/8"	279.1
OF11	1	3/8"x8"x55 11/16"	47.4
IF10	1	1/2"x8"x267 1/4"	325.8
EP6	1	3/8"x8"x16"	13.6
EP7	1	3/4"x8"x46 3/4"	79.5
ST5	2	1/4"x3 3/4"x46 15/16"	25.0
ES1	1	1/4"x12"x8"	4.2
XWC17	2		2.6
CLF1	3	1/4"x5 3/4"x8 3/8"	10.2
		Weight Sum	1462.0

ABOVE MEMBER TABLE FOR DRAFTING USE ONLY.

Figure A-3 Drawings of panel zone details from Company D

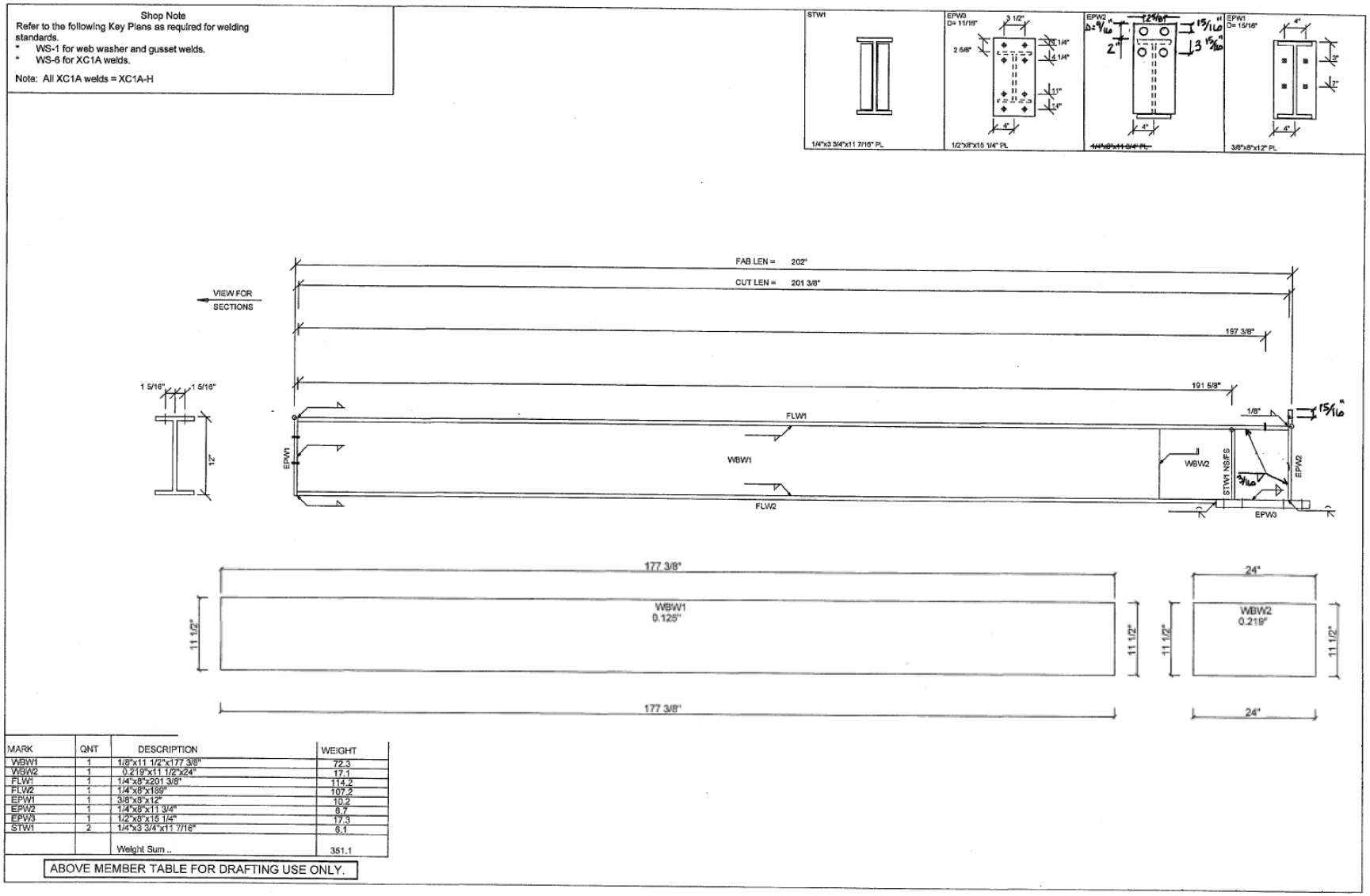

MARK	QNT	DESCRIPTION	WEIGHT
WBW1	1	1/8"x11 1/2"x177 3/8"	72.3
WBW2	1	0.219"x11 1/2"x24"	17.1
FLW1	1	1/4"x8"x201 3/8"	114.2
FLW2	1	1/4"x8"x189"	107.2
EPW1	1	3/8"x8"x12"	10.2
EPW2	1	1/4"x8"x11 3/4"	6.7
EPW3	1	1/2"x8"x15 1/4"	17.3
STW1	2	1/4"x3 3/4"x11 7/16"	6.1
		Weight Sum ..	351.1

ABOVE MEMBER TABLE FOR DRAFTING USE ONLY.

Figure A-3 (Continued) Drawings of panel zone details from Company D

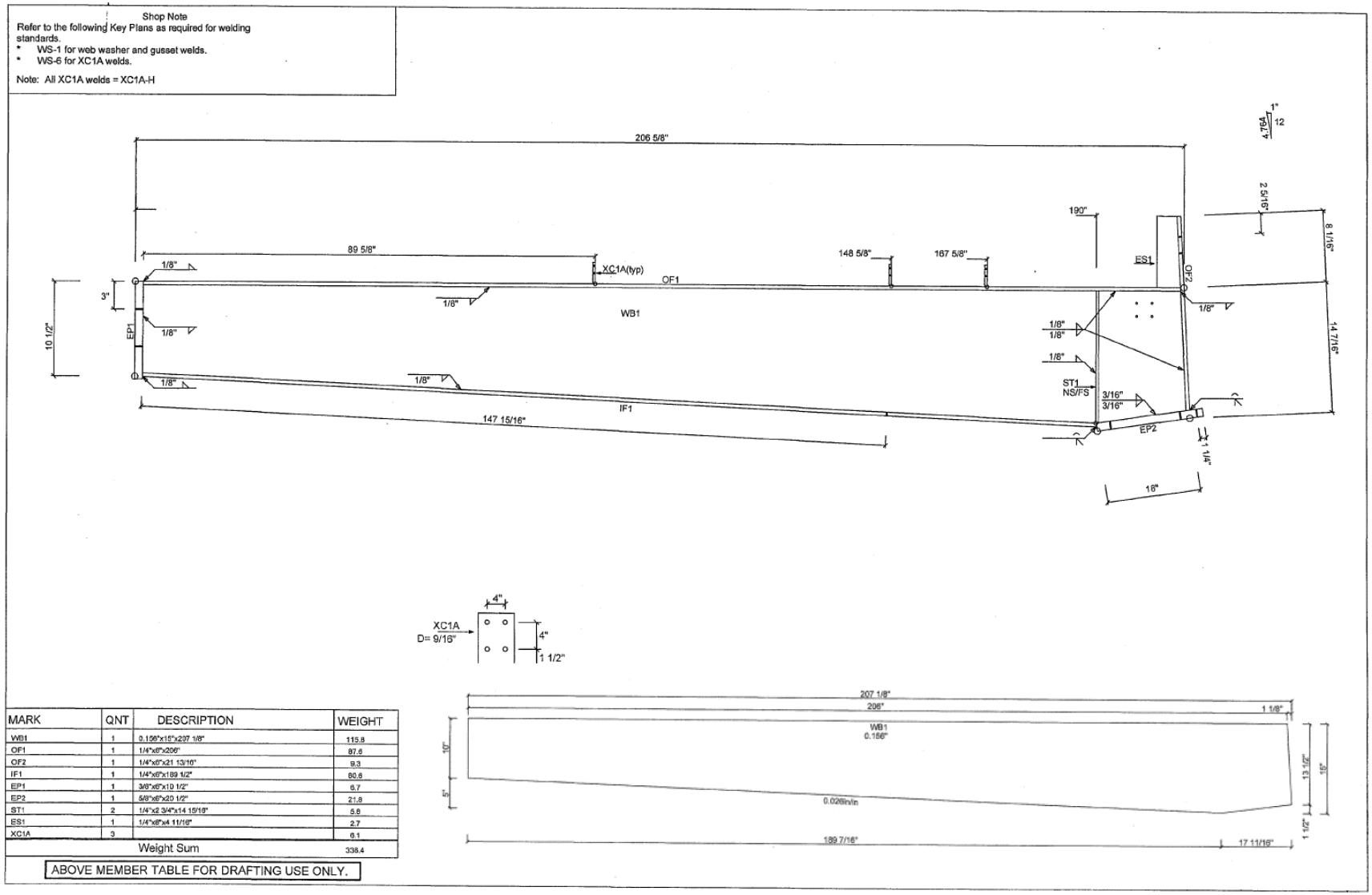

MARK	QNT	DESCRIPTION	WEIGHT
WB1	1	0.156"x15"x207 1/8"	115.8
OF1	1	1/4"x6"x206"	87.6
OF2	1	1/4"x6"x21 13/16"	9.3
IF1	1	1/4"x6"x189 1/2"	80.6
EP1	1	3/8"x6"x10 1/2"	6.7
EP2	1	5/8"x6"x20 1/2"	21.8
ST1	2	1/4"x2 3/4"x14 15/16"	5.8
ES1	1	1/4"x8"x4 11/16"	2.7
XC1A	3		6.1
Weight Sum			338.4

ABOVE MEMBER TABLE FOR DRAFTING USE ONLY.

Figure A-3 (Continued) Drawings of panel zone details from Company D

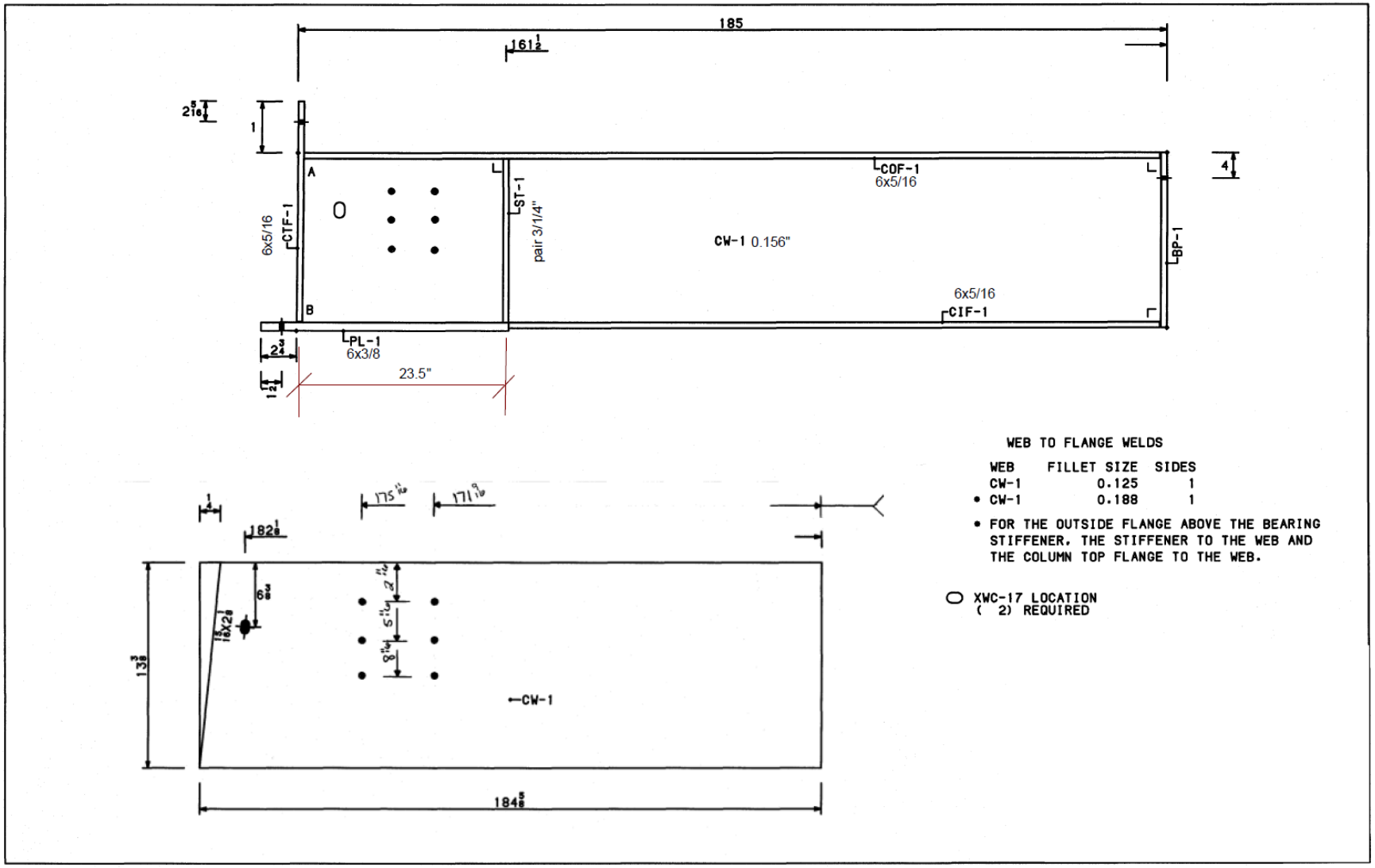

Figure A-3 (Continued) Drawings of panel zone details from Company D

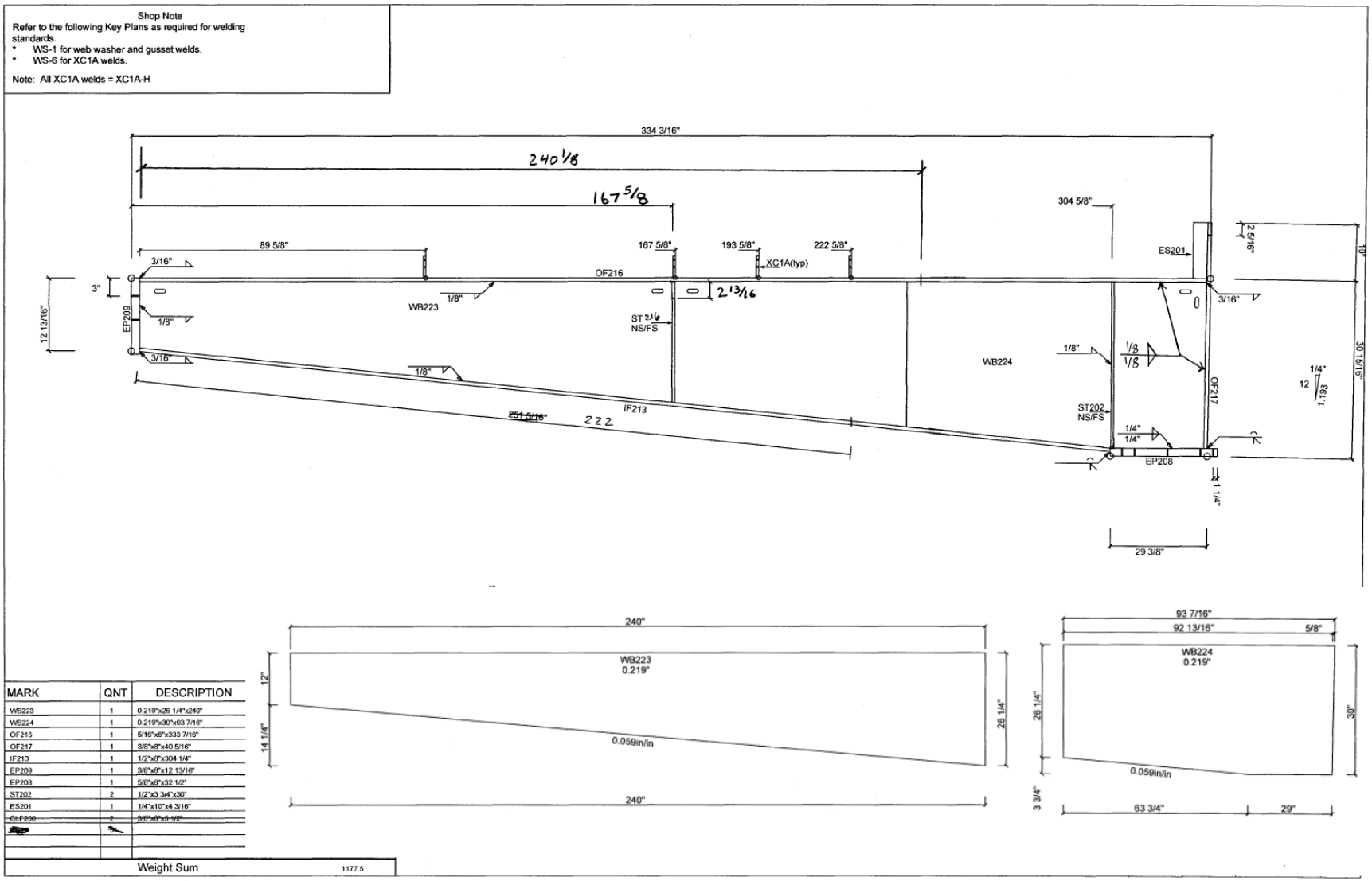

MARK	QNT	DESCRIPTION
WB223	1	0.219"x26 1/4"x240"
WB224	1	0.219"x30"x93 7/16"
OF216	1	5/16"x8"x333 7/16"
OF217	1	3/8"x8"x40 5/16"
IF213	1	1/2"x8"x304 1/4"
EP209	1	3/8"x8"x12 13/16"
EP208	1	5/8"x8"x32 1/2"
ST202	2	1/2"x3 3/4"x30"
ES201	1	1/4"x10"x4 3/16"
~~OLF200~~	~~2~~	~~3/8"x8"x5 1/2"~~
~~WB~~	~~3~~	
Weight Sum		1177.5

Figure A-3 (Continued) Drawings of panel zone details from Company D

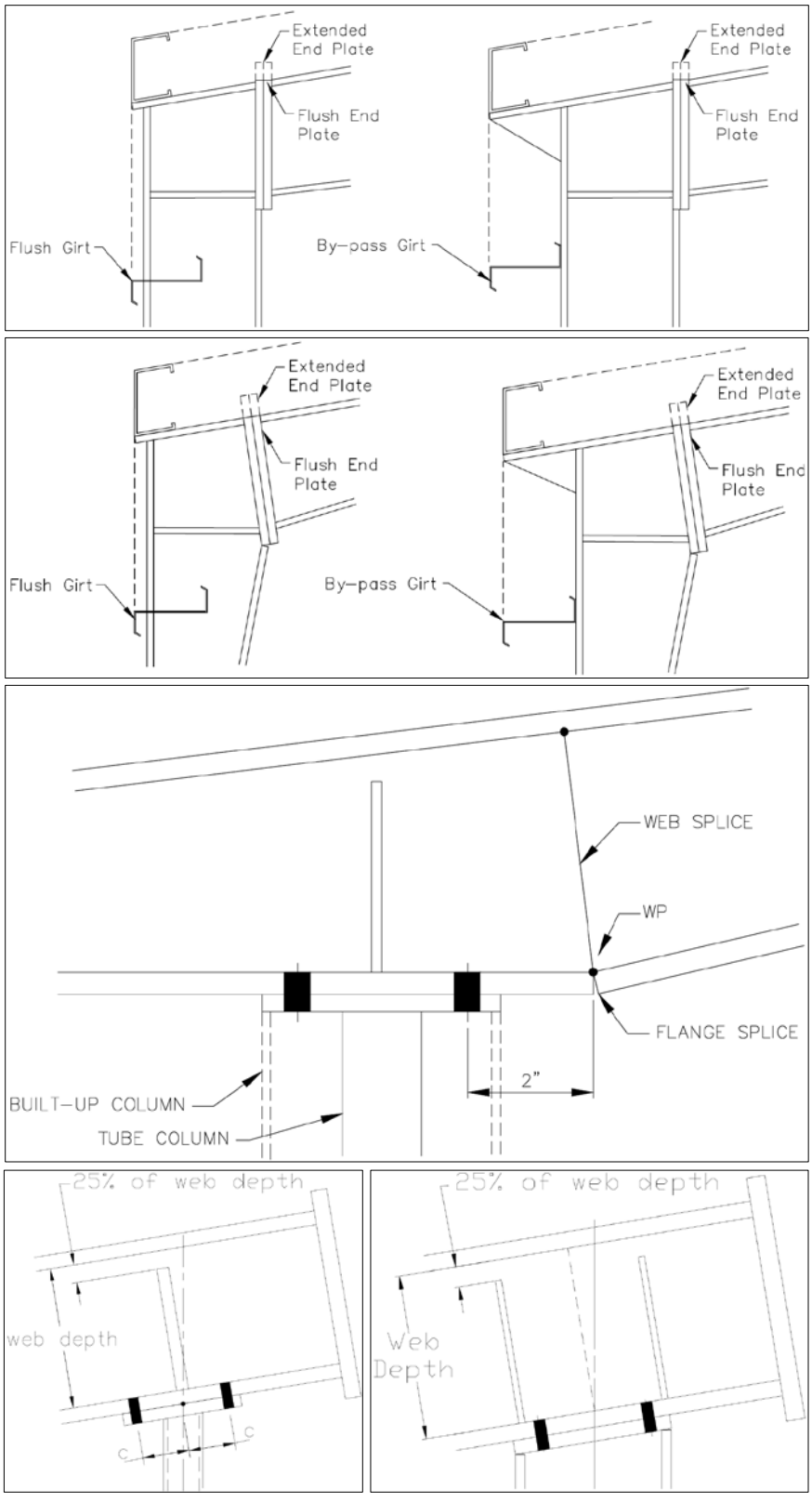

Figure A-4 Drawings of panel zone details from Company E

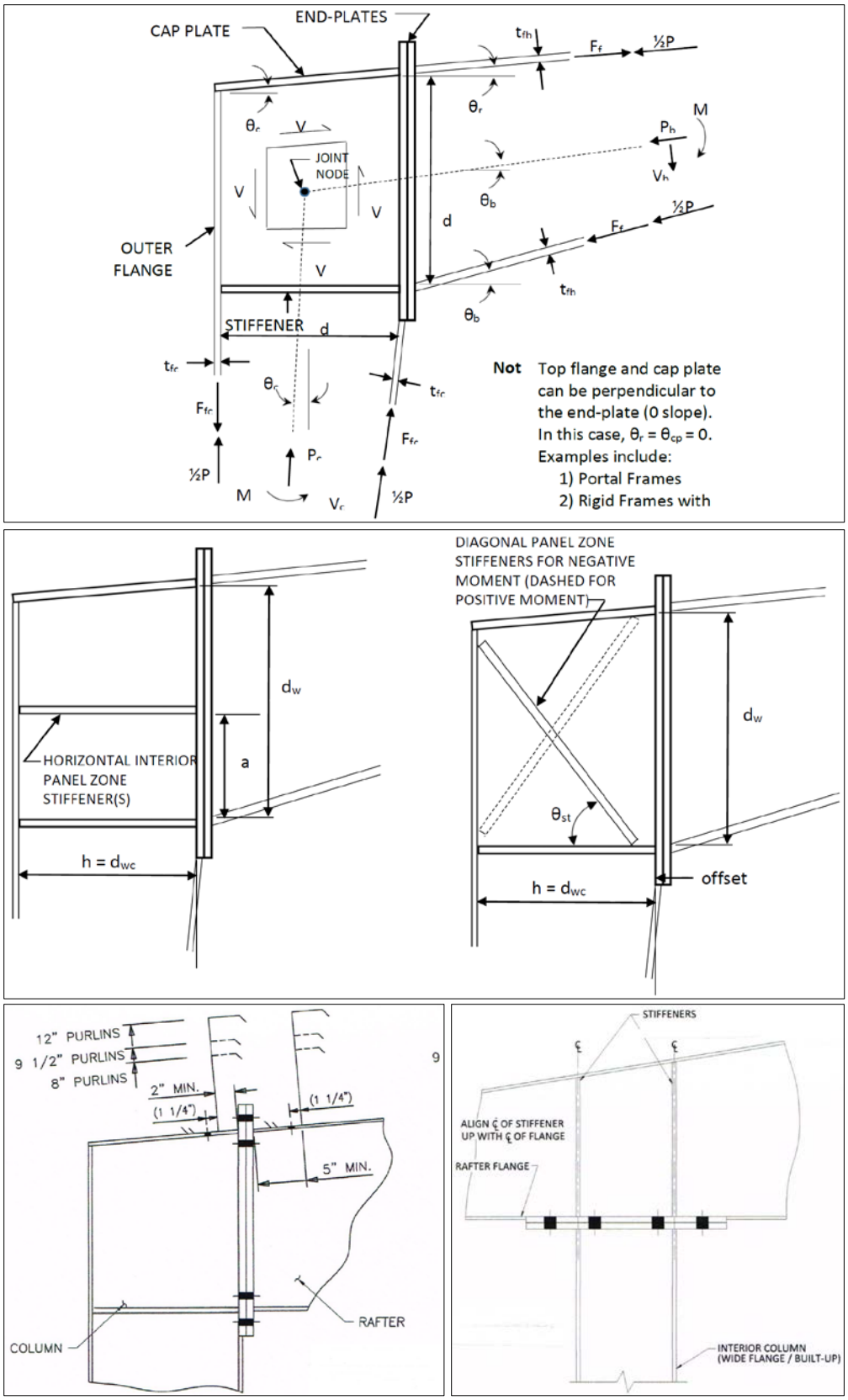

Figure A-5 Drawings of panel zone details from Company G

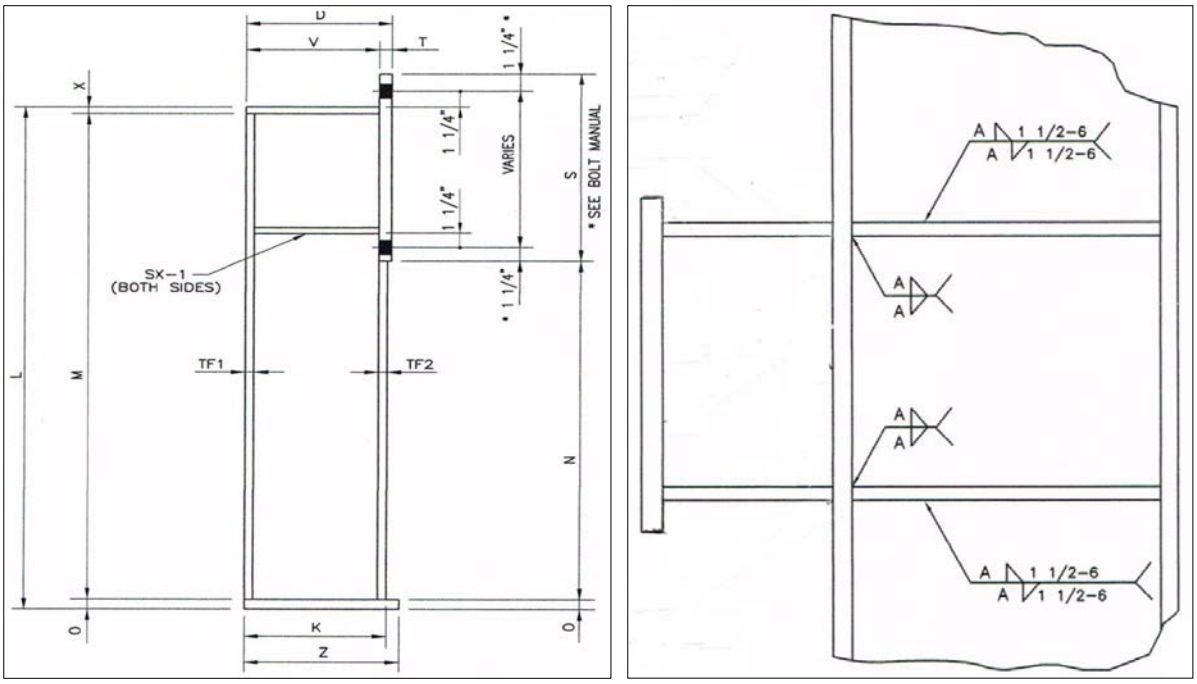

Figure A-5 (Continued) Drawings of panel zone details from Company G

APPENDIX B DESIGNS FROM METAL BUILDING SOFTWARE, INC.

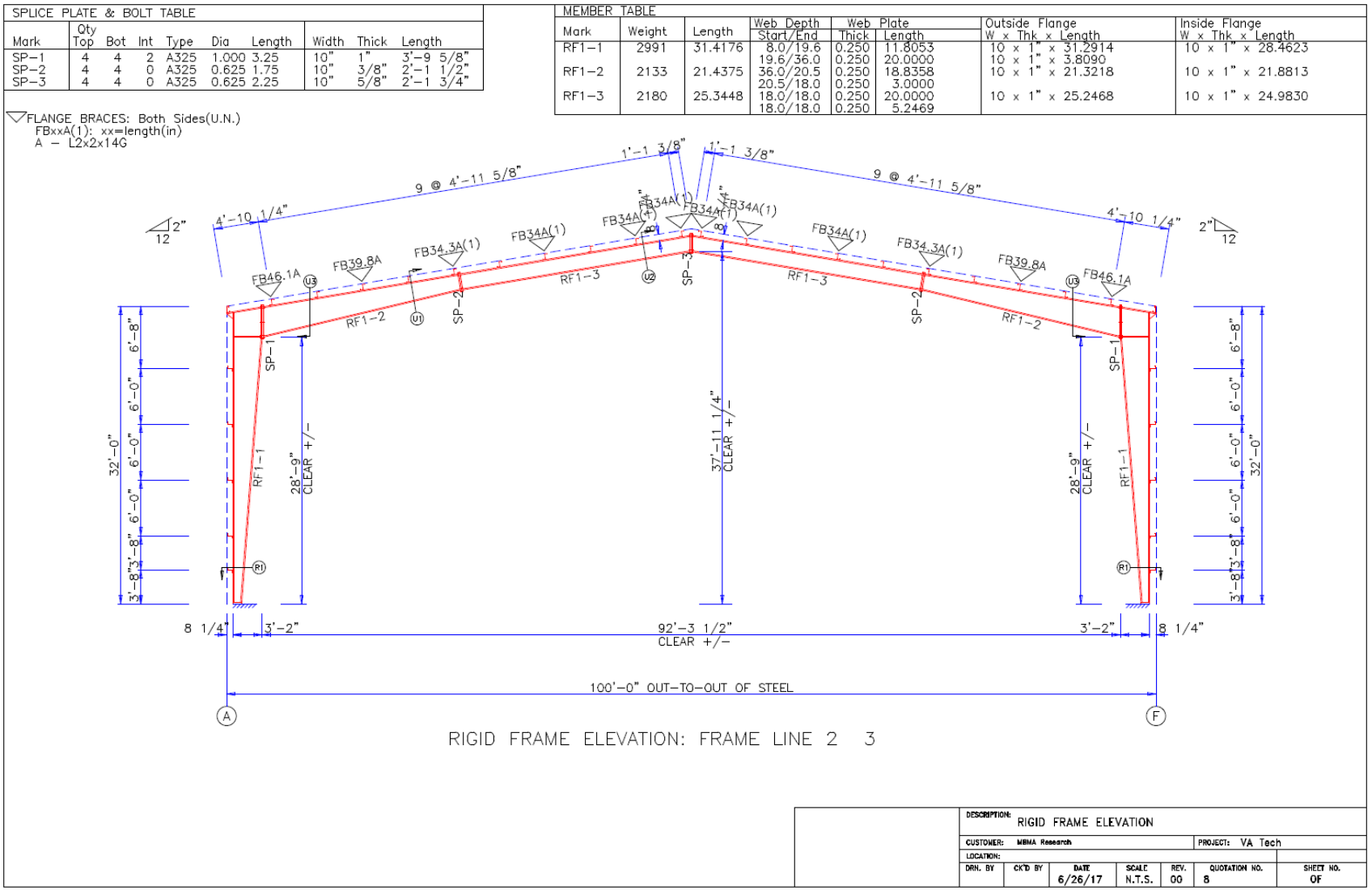

SPLICE PLATE & BOLT TABLE

Mark	Qty Top	Bot	Int	Type	Dia	Length	Width	Thick	Length
SP-1	4	4	2	A325	1.000	3.25	10"	1"	3'-9 5/8"
SP-2	4	4	0	A325	0.625	1.75	10"	3/8"	2'-1 1/2"
SP-3	4	4	0	A325	0.625	2.25	10"	5/8"	2'-1 3/4"

MEMBER TABLE

Mark	Weight	Length	Web Depth Start/End	Web Plate Thick	Web Plate Length	Outside Flange W x Thk x Length	Inside Flange W x Thk x Length
RF1-1	2991	31.4176	8.0/19.6	0.250	11.8053	10 x 1" x 31.2914	10 x 1" x 28.4623
			19.6/36.0	0.250	20.0000	10 x 1" x 3.8090	
RF1-2	2133	21.4375	36.0/20.5	0.250	18.8358	10 x 1" x 21.3218	10 x 1" x 21.8813
			20.5/18.0	0.250	3.0000		
RF1-3	2180	25.3448	18.0/18.0	0.250	20.0000	10 x 1" x 25.2468	10 x 1" x 24.9830
			18.0/18.0	0.250	5.2469		

FLANGE BRACES: Both Sides(U.N.)
FBxxA(1): xx=length(in)
A - L2x2x14G

RIGID FRAME ELEVATION: FRAME LINE 2 3

DESCRIPTION: RIGID FRAME ELEVATION						
CUSTOMER: MBMA Research					PROJECT: VA Tech	
LOCATION:						
DRN. BY	CK'D BY	DATE 6/26/17	SCALE N.T.S.	REV. 00	QUOTATION NO. 8	SHEET NO. OF

Figure B-1 Design drawings for Model #8

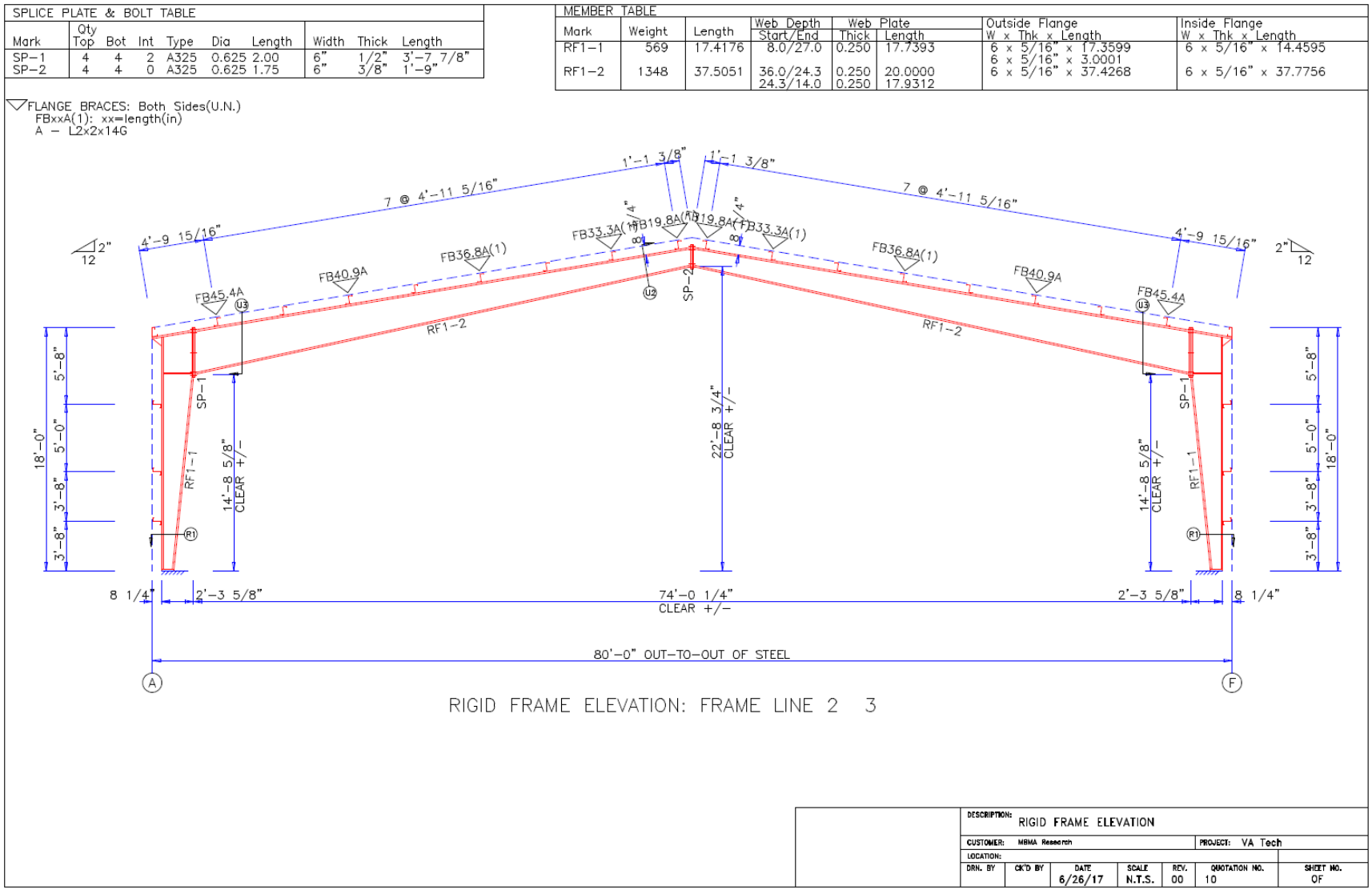

Figure B-2 Design drawings for Model #10

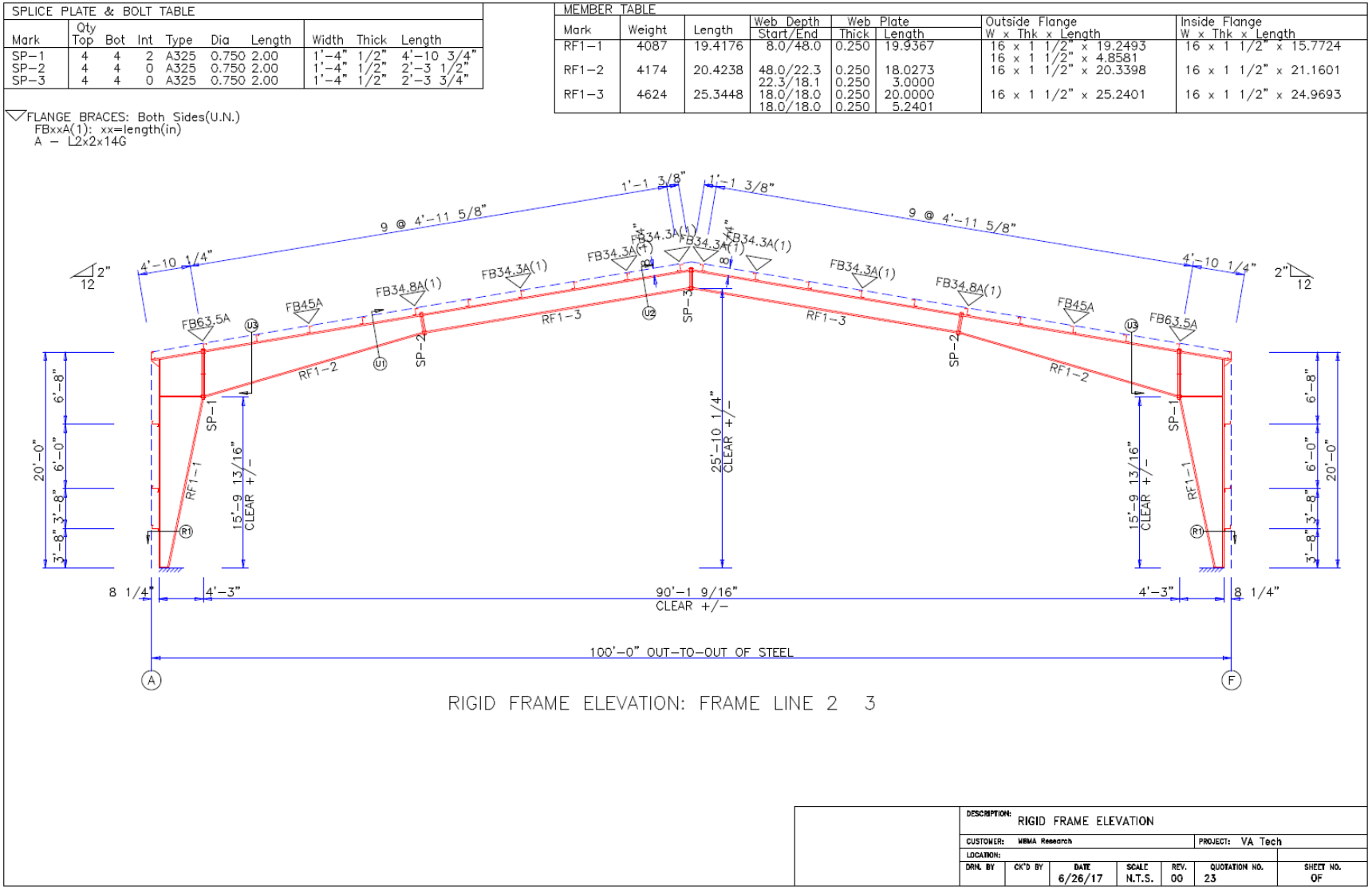

Figure B-3 Design drawings for Model #23

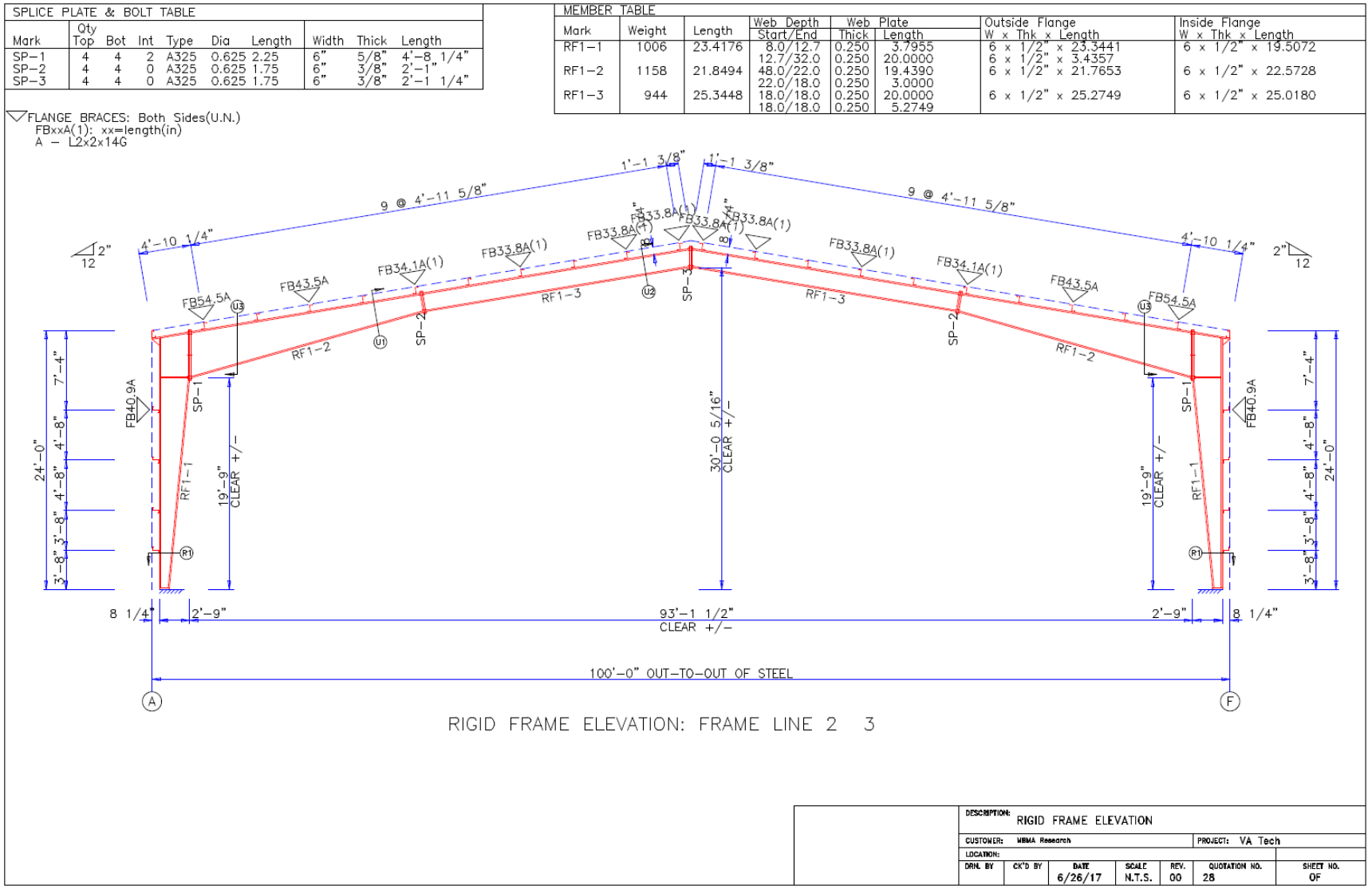

Figure B-4 Design drawings for Model #28

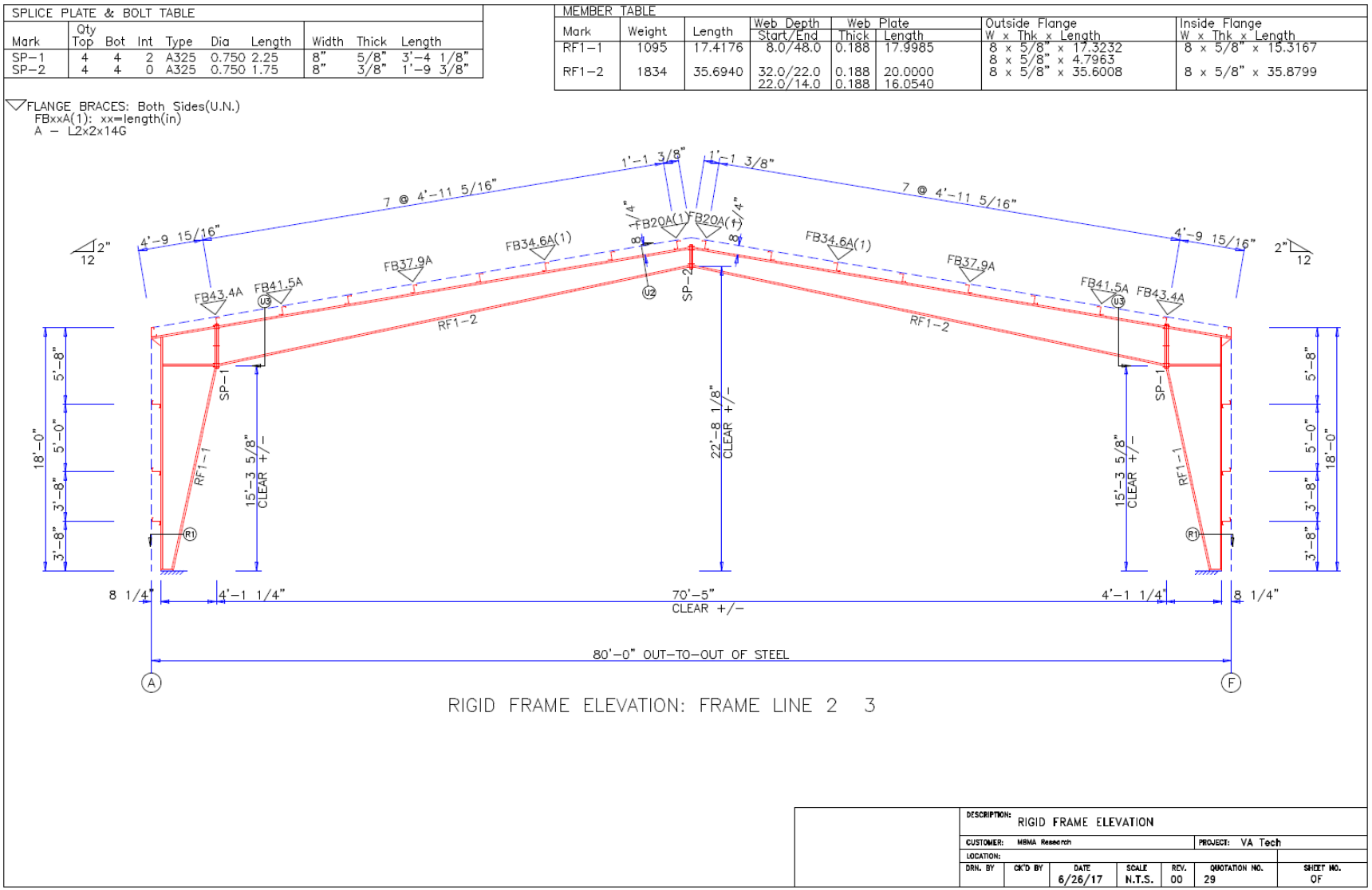

Figure B-5 Design drawings for Model #29

APPENDIX C DETAILED RESULTS OF FE STUDY

C1 Parametric Study

Maximum applied force: 40.42 kips
Story drift at maximum applied force: 1.16%
Yield displacement δy: 2.14 in.
Maximum out-of-plane displacement of panel zone: 2.15 in.

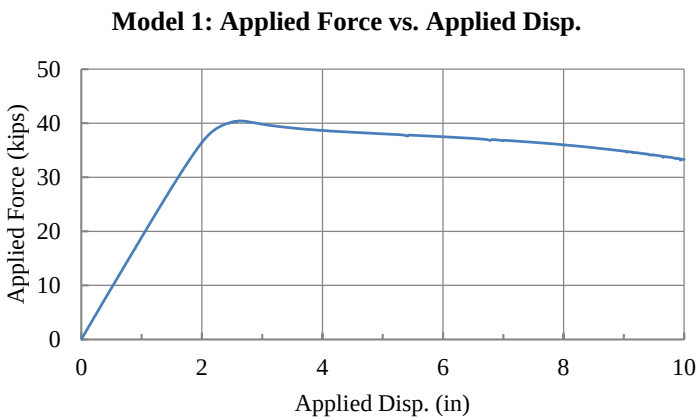

Maximum applied force: 42.83 kips
Story drift at maximum applied force: 0.95%
Yield displacement δy: 2.00 in.
Maximum out-of-plane displacement of panel zone: 2.22 in.

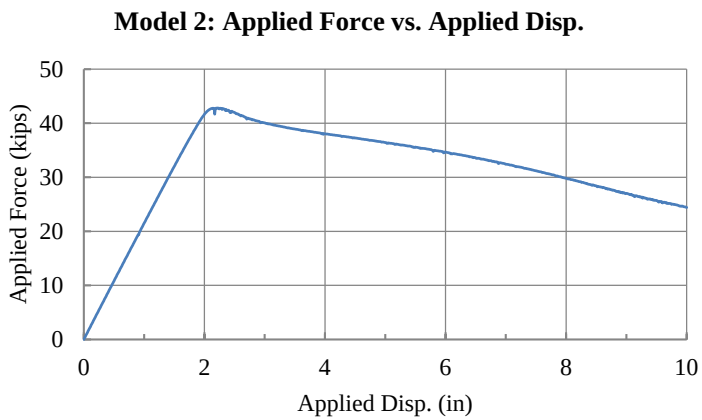

Maximum applied force: 42.38 kips
Story drift at maximum applied force: 1.11%
Yield displacement δy: 2.04 in.
Maximum out-of-plane displacement of panel zone: 2.23 in.

Model 3: Applied Force vs. Applied Disp.

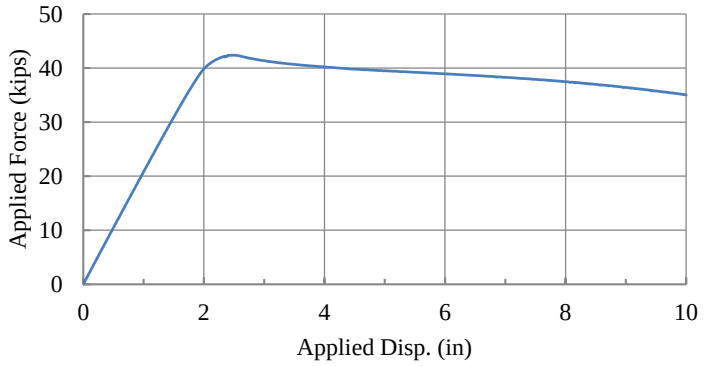

Maximum applied force: 51.22 kips
Story drift at maximum applied force: 3.57%
Yield displacement δy: 1.84 in.
Maximum out-of-plane displacement of panel zone: 1.82 in.

Model 4: Applied Force vs. Applied Disp.

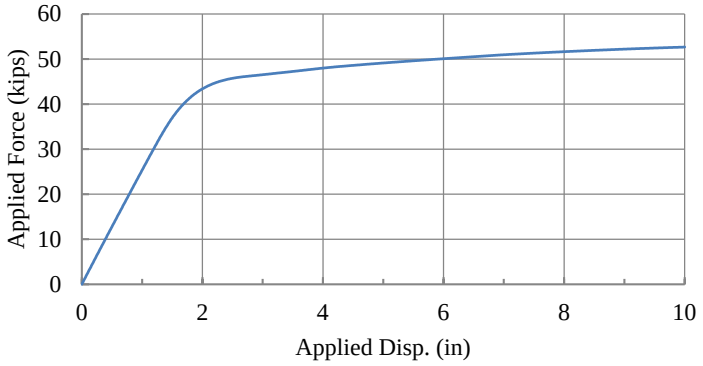

Maximum applied force: 61.78 kips
Story drift at maximum applied force: 3.64%
Yield displacement δy: 1.82 in.
Maximum out-of-plane displacement of panel zone: 1.50 in.

Model 5: Applied Force vs. Applied Disp.

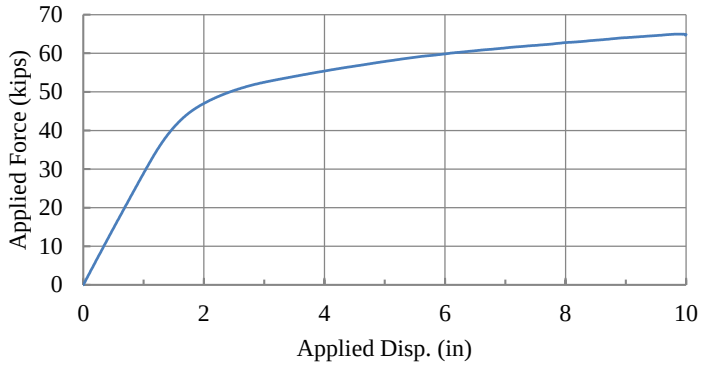

Maximum applied force: 47.96 kips
Story drift at maximum applied force: 0.90%
Yield displacement δy: 1.96 in.
Maximum out-of-plane displacement of panel zone: 2.50 in.

Model 6: Applied Force vs. Applied Disp.

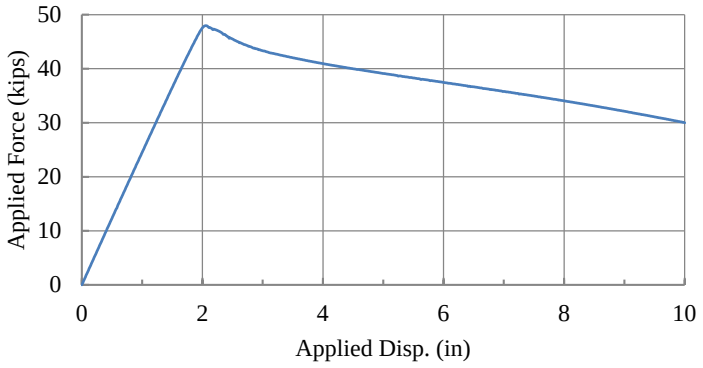

Maximum applied force: 47.78 kips
Story drift at maximum applied force: 1.02%
Yield displacement δy: 1.94 in.
Maximum out-of-plane displacement of panel zone: 2.51 in.

Model 7: Applied Force vs. Applied Disp.

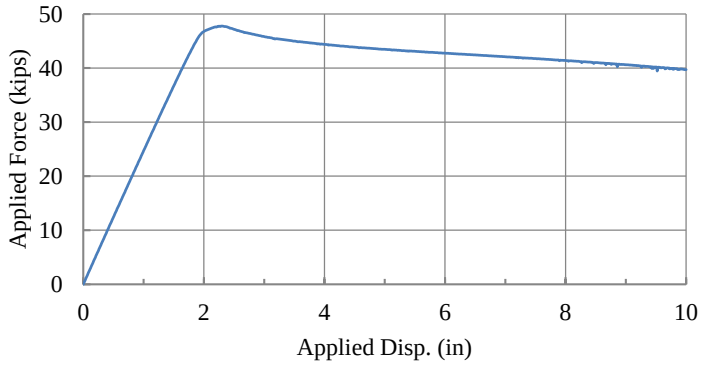

Maximum applied force: 56.92 kips
Story drift at maximum applied force: 3.30%
Yield displacement δy: 1.71 in.
Maximum out-of-plane displacement of panel zone: 2.09 in.

Model 8: Applied Force vs. Applied Disp.

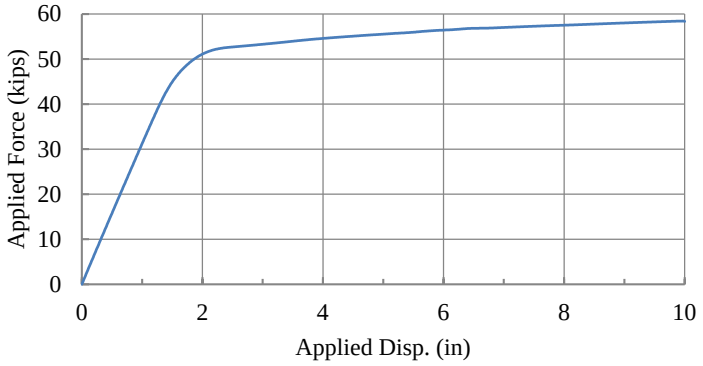

Maximum applied force: 68.71 kips
Story drift at maximum applied force: 3.25%
Yield displacement δy: 1.65 in.
Maximum out-of-plane displacement of panel zone: 1.96 in.

Model 9: Applied Force vs. Applied Disp.

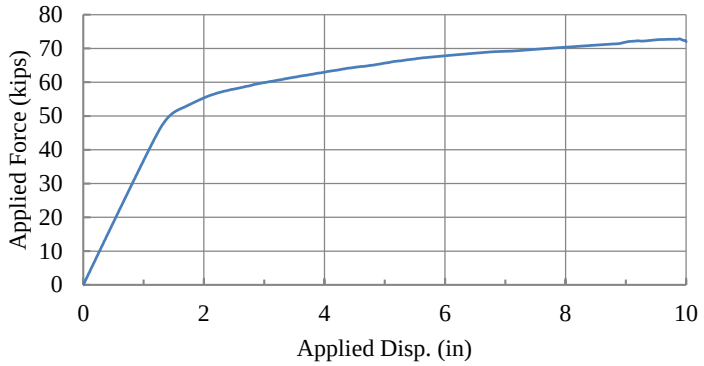

Maximum applied force: 39.86 kips
Story drift at maximum applied force: 1.19%
Yield displacement δy: 2.55 in.
Maximum out-of-plane displacement of panel zone: 2.53 in.

Model 10: Applied Force vs. Applied Disp.

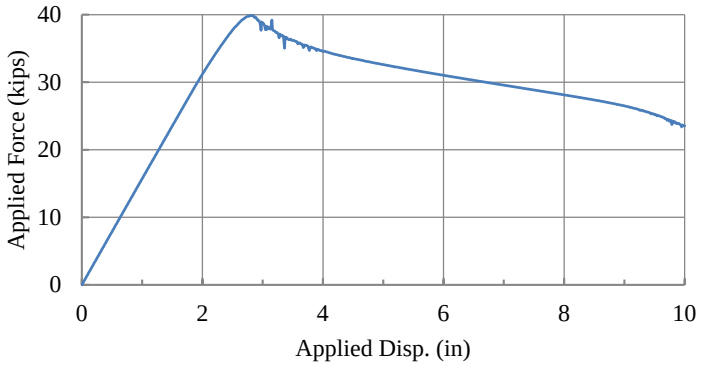

Maximum applied force: 38.33 kips
Story drift at maximum applied force: 0.96%
Yield displacement δy: 2.07 in.
Maximum out-of-plane displacement of panel zone: 2.42 in.

Model 11: Applied Force vs. Applied Disp.

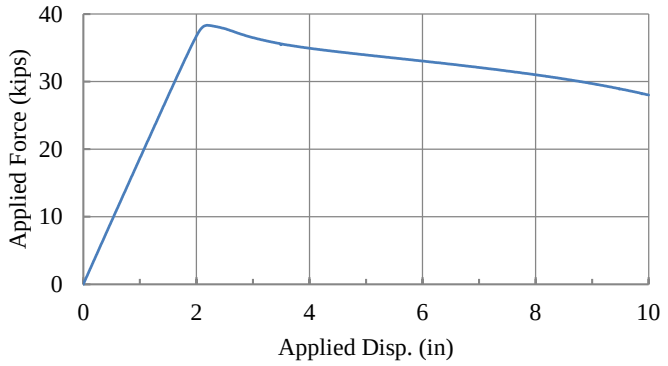

Maximum applied force: 41.85 kips
Story drift at maximum applied force: 3.39%
Yield displacement δy: 1.79 in.
Maximum out-of-plane displacement of panel zone: 1.96 in.

Model 12: Applied Force vs. Applied Disp.

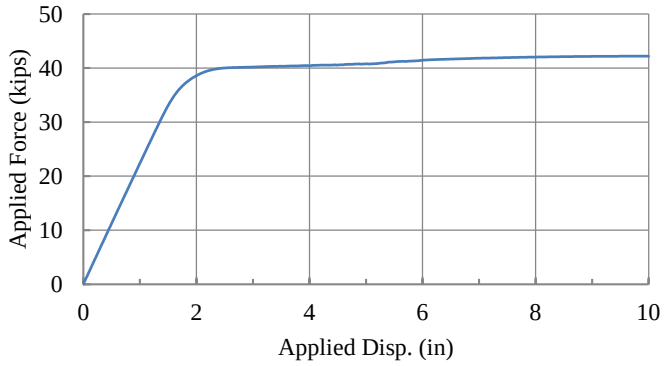

Maximum applied force: 49.28 kips
Story drift at maximum applied force: 3.28%
Yield displacement δy: 1.69 in.
Maximum out-of-plane displacement of panel zone: 1.72 in.

Model 13: Applied Force vs. Applied Disp.

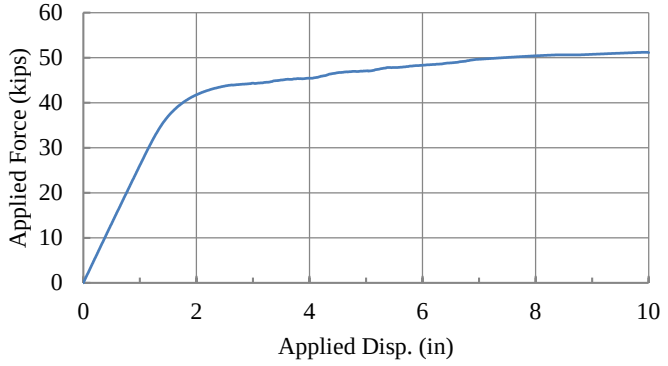

Maximum applied force: 36.04 kips
Story drift at maximum applied force: 1.27%
Yield displacement δy: 2.72 in.
Maximum out-of-plane displacement of panel zone: 2.45 in.

Model 14: Applied Force vs. Applied Disp.

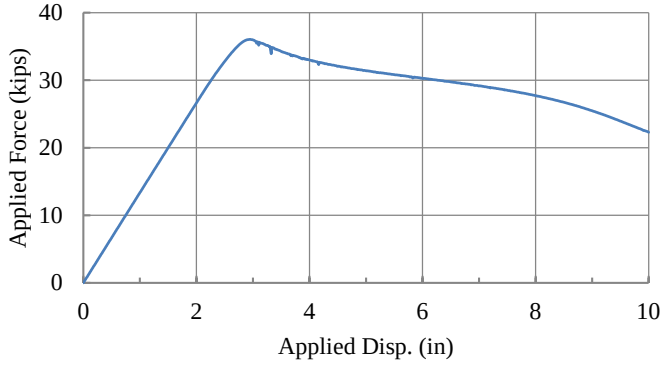

Maximum applied force: 55.66 kips
Story drift at maximum applied force: 1.11%
Yield displacement δy: 1.86 in.
Maximum out-of-plane displacement of panel zone: 2.58 in.

Model 15: Applied Force vs. Applied Disp.

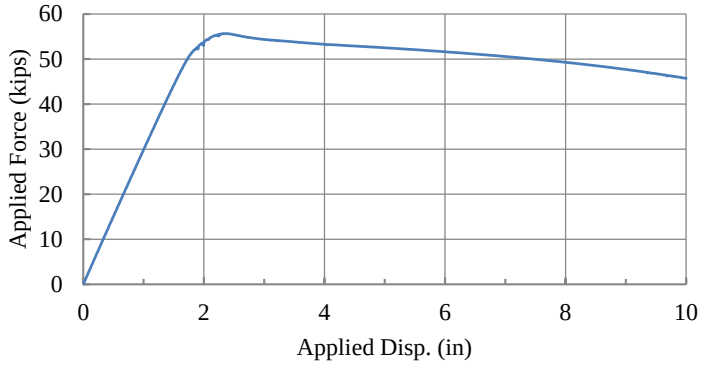

Maximum applied force: 58.37 kips
Story drift at maximum applied force: 1.01%
Yield displacement δy: 1.88 in.
Maximum out-of-plane displacement of panel zone: 2.49 in.

Model 16: Applied Force vs. Applied Disp.

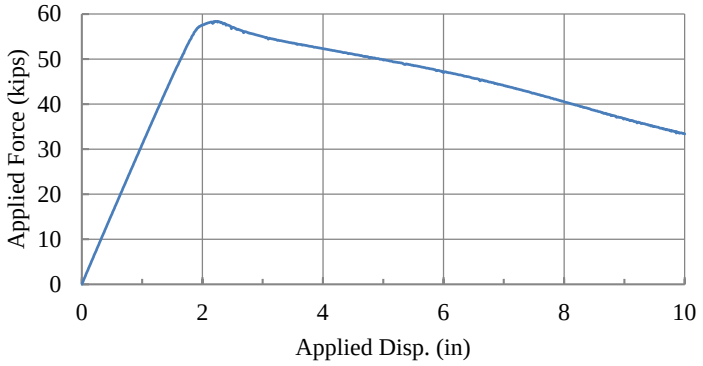

Maximum applied force: 58.37 kips
Story drift at maximum applied force: 1.03%
Yield displacement δy: 1.76 in.
Maximum out-of-plane displacement of panel zone: 2.65 in.

Model 17: Applied Force vs. Applied Disp.

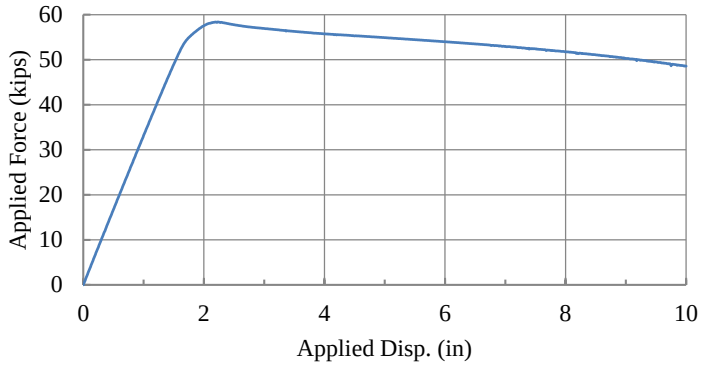

Maximum applied force: 79.58 kips
Story drift at maximum applied force: 3.52%
Yield displacement δy: 1.78 in.
Maximum out-of-plane displacement of panel zone: 2.14 in.

Model 18: Applied Force vs. Applied Disp.

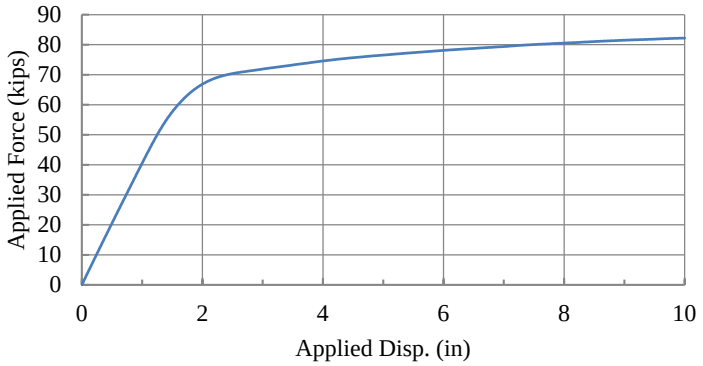

Maximum applied force: 94.93 kips
Story drift at maximum applied force: 3.54%
Yield displacement δy: 1.76 in.
Maximum out-of-plane displacement of panel zone: 2.07 in.

Model 19: Applied Force vs. Applied Disp.

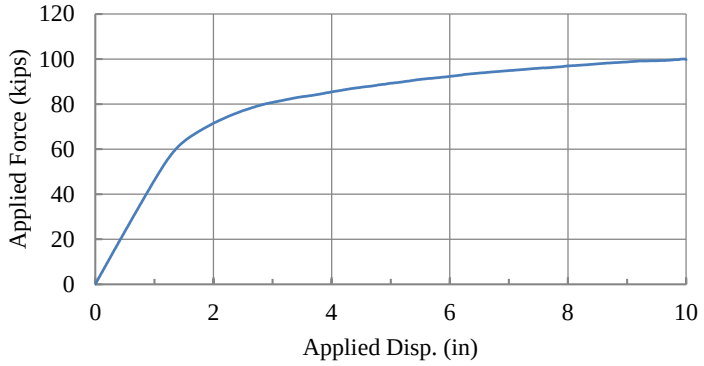

Maximum applied force: 65.29 kips
Story drift at maximum applied force: 0.82%
Yield displacement δy: 1.75 in.
Maximum out-of-plane displacement of panel zone: 2.96 in.

Model 20: Applied Force vs. Applied Disp.

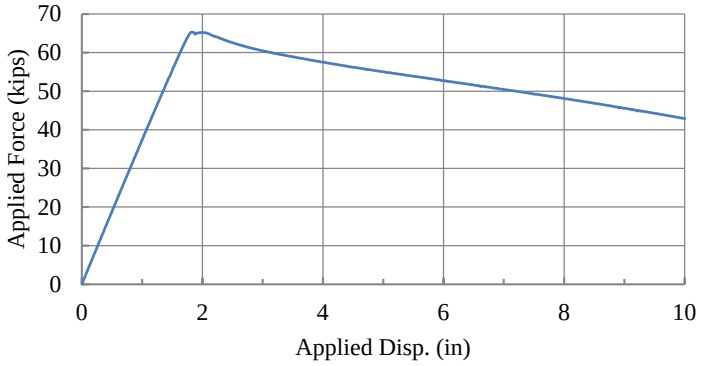

Maximum applied force: 65.72 kips
Story drift at maximum applied force: 0.94%
Yield displacement δy: 1.63 in.
Maximum out-of-plane displacement of panel zone: 2.99 in.

Model 21: Applied Force vs. Applied Disp.

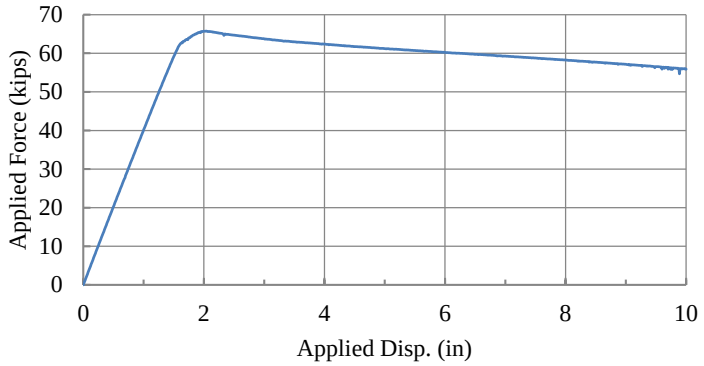

Maximum applied force: 89.37 kips
Story drift at maximum applied force: 3.18%
Yield displacement δy: 1.64 in.
Maximum out-of-plane displacement of panel zone: 2.45 in.

Model 22: Applied Force vs. Applied Disp.

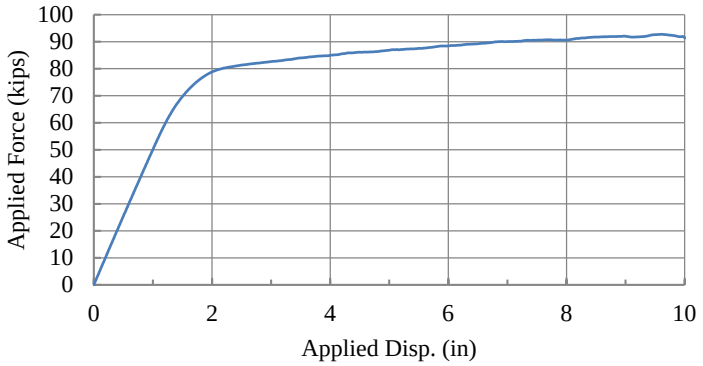

Maximum applied force: 106.10 kips
Story drift at maximum applied force: 3.16%
Yield displacement δy: 1.61 in.
Maximum out-of-plane displacement of panel zone: 2.40 in.

Model 23: Applied Force vs. Applied Disp.

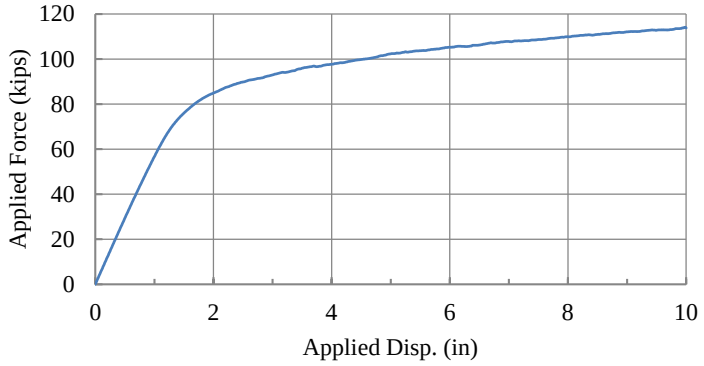

Maximum applied force: 54.61 kips
Story drift at maximum applied force: 0.93%
Yield displacement δy: 2.01 in.
Maximum out-of-plane displacement of panel zone: 2.83 in.

Model 24: Applied Force vs. Applied Disp.

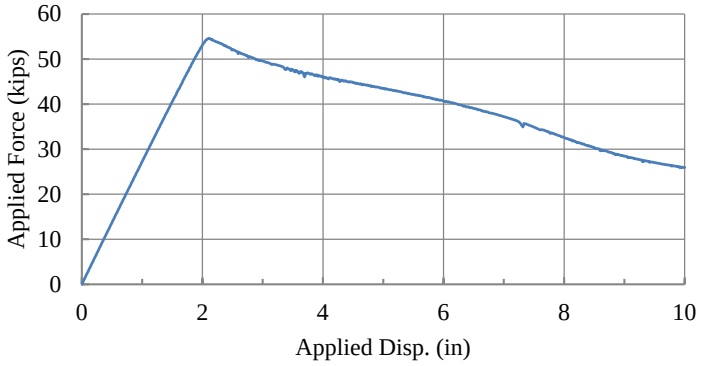

Maximum applied force: 54.56 kips
Story drift at maximum applied force: 1.03%
Yield displacement δy: 1.97 in.
Maximum out-of-plane displacement of panel zone: 2.51 in.

Model 25: Applied Force vs. Applied Disp.

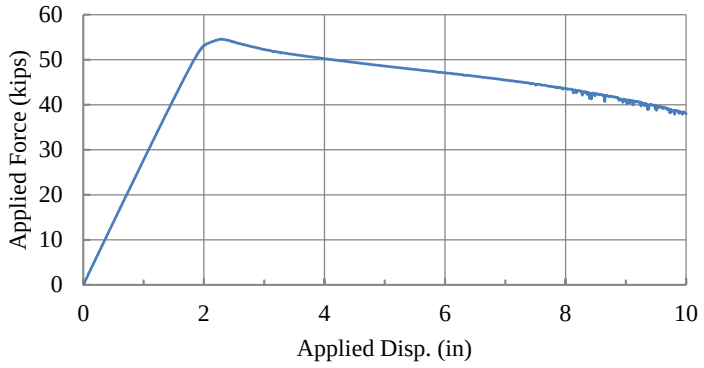

Maximum applied force: 63.14 kips
Story drift at maximum applied force: 3.17%
Yield displacement δy: 1.67 in.
Maximum out-of-plane displacement of panel zone: 2.30 in.

Model 26: Applied Force vs. Applied Disp.

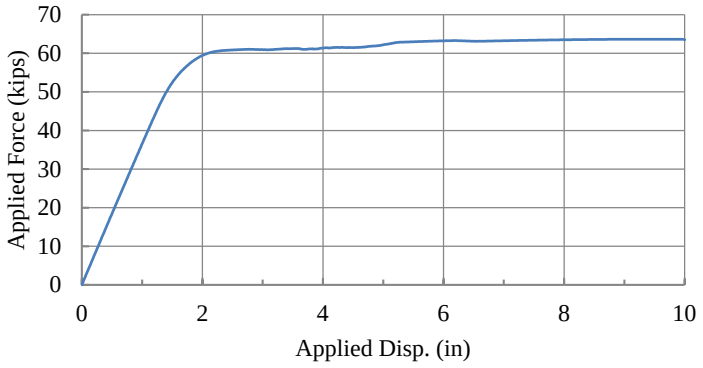

Maximum applied force: 74.92 kips
Story drift at maximum applied force: 3.01%
Yield displacement δy: 1.55 in.
Maximum out-of-plane displacement of panel zone: 2.28 in.

Model 27: Applied Force vs. Applied Disp.

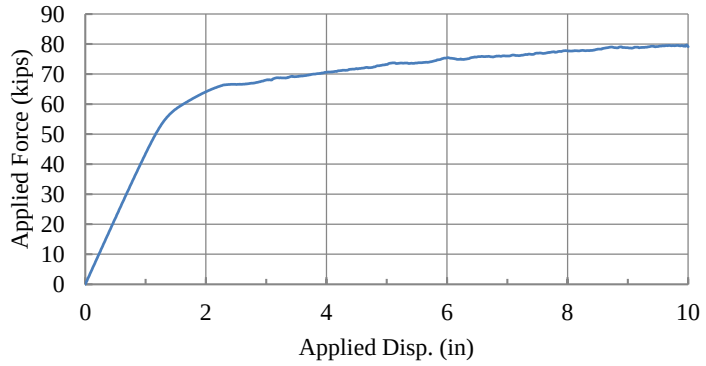

Maximum applied force: 50.21 kips
Story drift at maximum applied force: 1.08%
Yield displacement δy: 2.22 in.
Maximum out-of-plane displacement of panel zone: 2.21 in.

Model 28: Applied Force vs. Applied Disp.

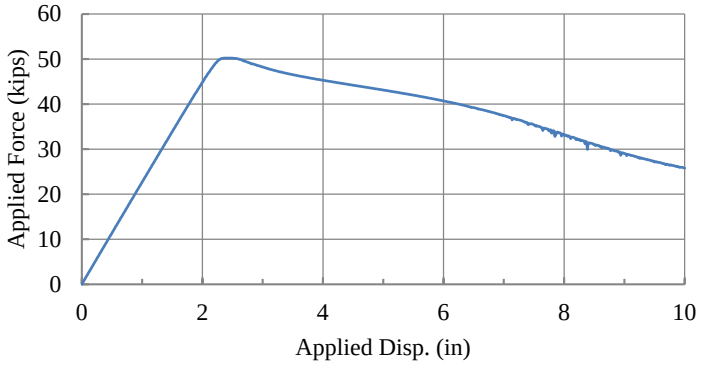

Maximum applied force: 39.37 kips
Story drift at maximum applied force: 0.85%
Yield displacement δy: 1.43 in.
Maximum out-of-plane displacement of panel zone: 2.14 in.

Model 29: Applied Force vs. Applied Disp.

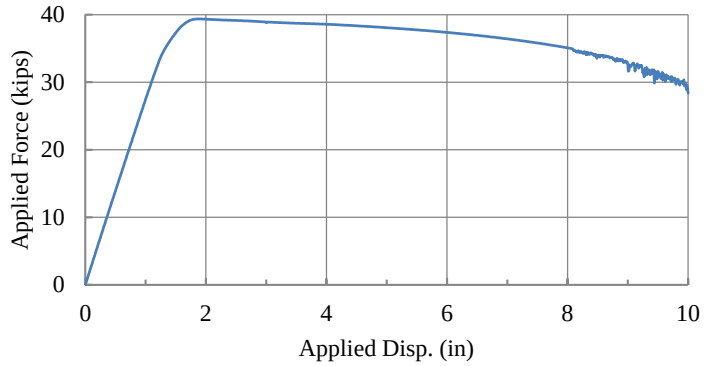

Maximum applied force: 40.12 kips
Story drift at maximum applied force: 0.75%
Yield displacement δy: 1.43 in.
Maximum out-of-plane displacement of panel zone: 2.59 in.

Model 30: Applied Force vs. Applied Disp.

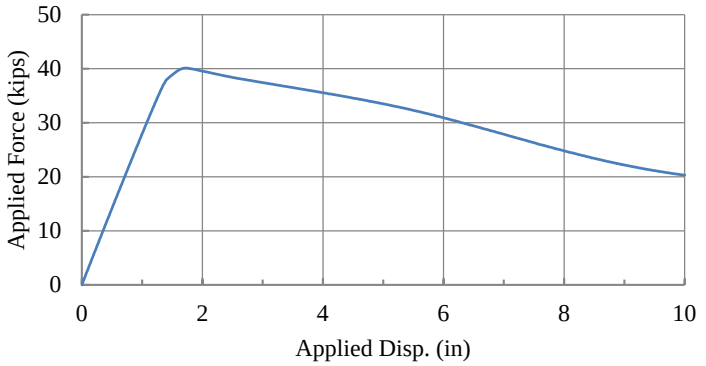

Maximum applied force: 40.99 kips
Story drift at maximum applied force: 0.84%
Yield displacement δy: 1.36 in.
Maximum out-of-plane displacement of panel zone: 2.26 in.

Model 31: Applied Force vs. Applied Disp.

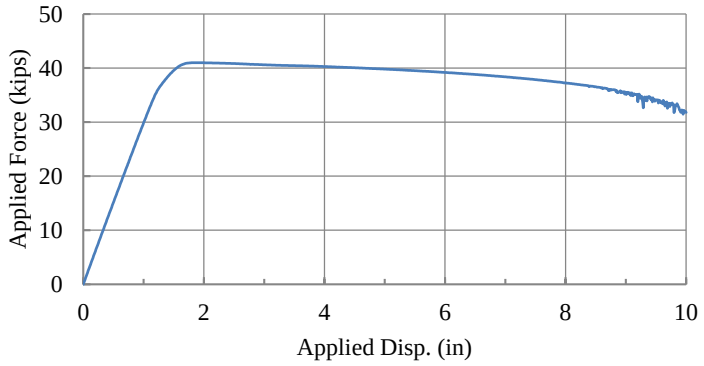

Maximum applied force: 57.19 kips
Story drift at maximum applied force: 2.93%
Yield displacement δy: 1.49 in.
Maximum out-of-plane displacement of panel zone: 2.02 in.

Model 32: Applied Force vs. Applied Disp.

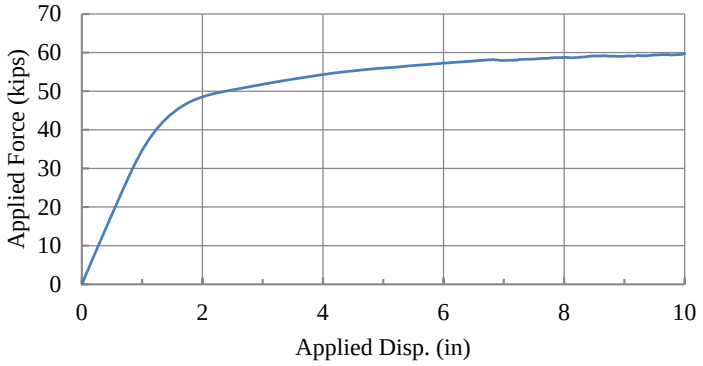

Maximum applied force: 74.76 kips
Story drift at maximum applied force: 3.24%
Yield displacement δy: 1.62 in.
Maximum out-of-plane displacement of panel zone: 1.96 in.

Model 33: Applied Force vs. Applied Disp.

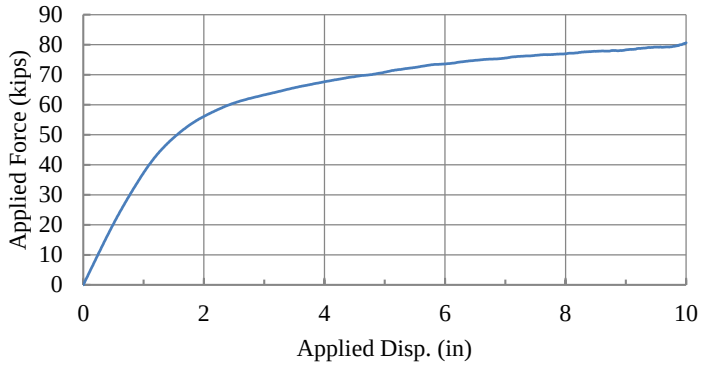

Maximum applied force: 44.60 kips
Story drift at maximum applied force: 0.68%
Yield displacement δy: 1.31 in.
Maximum out-of-plane displacement of panel zone: 2.72 in.

Model 34: Applied Force vs. Applied Disp.

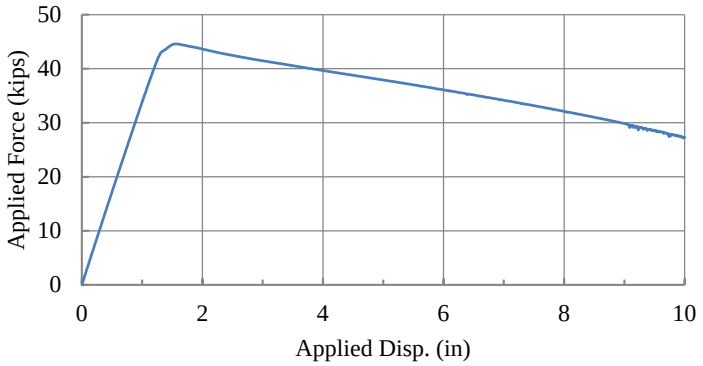

Maximum applied force: 45.97 kips
Story drift at maximum applied force: 0.85%
Yield displacement δy: 1.26 in.
Maximum out-of-plane displacement of panel zone: 2.72 in.

Model 35: Applied Force vs. Applied Disp.

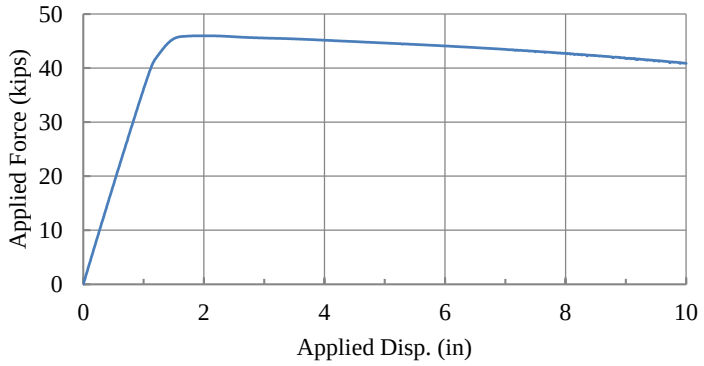

Maximum applied force: 64.08 kips
Story drift at maximum applied force: 2.67%
Yield displacement δy: 1.38 in.
Maximum out-of-plane displacement of panel zone: 2.51 in.

Model 36: Applied Force vs. Applied Disp.

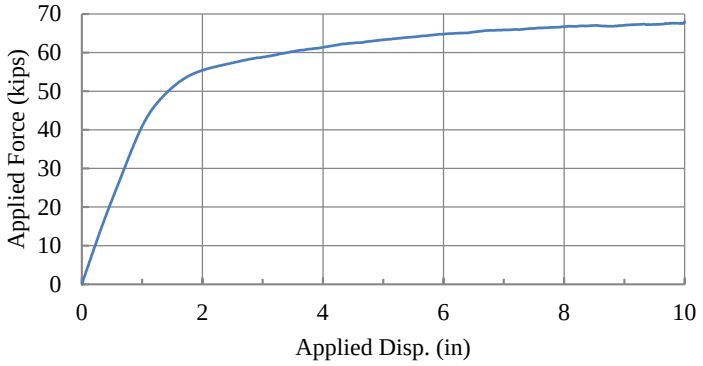

Maximum applied force: 82.87 kips
Story drift at maximum applied force: 2.95%
Yield displacement δy: 1.51 in.
Maximum out-of-plane displacement of panel zone: 2.23 in.

Model 37: Applied Force vs. Applied Disp.

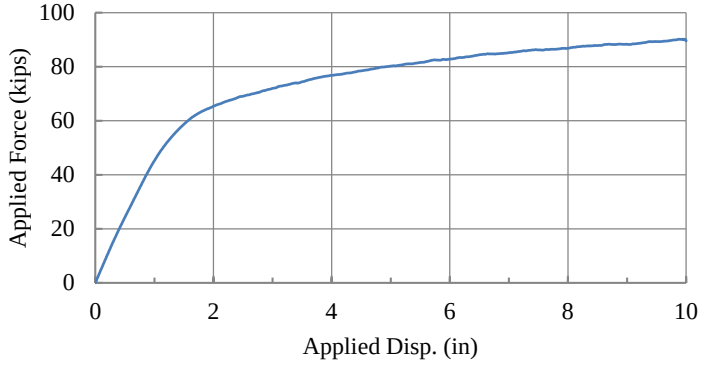

Maximum applied force: 36.08 kips
Story drift at maximum applied force: 0.74%
Yield displacement δy: 1.53 in.
Maximum out-of-plane displacement of panel zone: 2.74 in.

Model 38: Applied Force vs. Applied Disp.

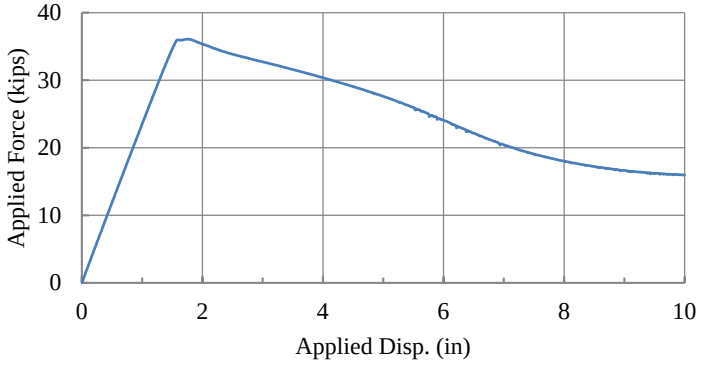

Maximum applied force: 36.82 kips
Story drift at maximum applied force: 0.75%
Yield displacement δy: 1.46 in.
Maximum out-of-plane displacement of panel zone: 2.37 in.

Model 39: Applied Force vs. Applied Disp.

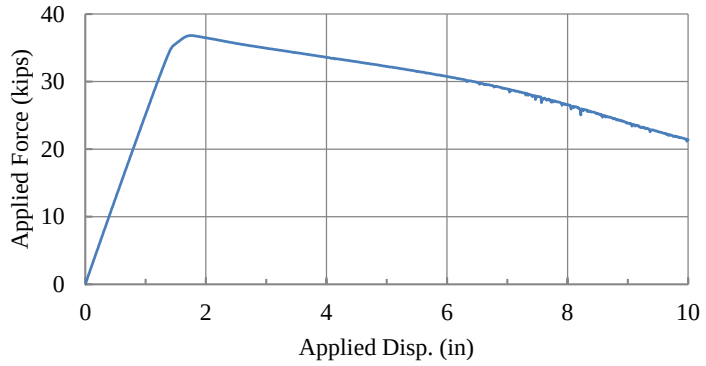

Maximum applied force: 46.13 kips
Story drift at maximum applied force: 2.63%
Yield displacement δy: 1.41 in.
Maximum out-of-plane displacement of panel zone: 2.10 in.

Model 40: Applied Force vs. Applied Disp.

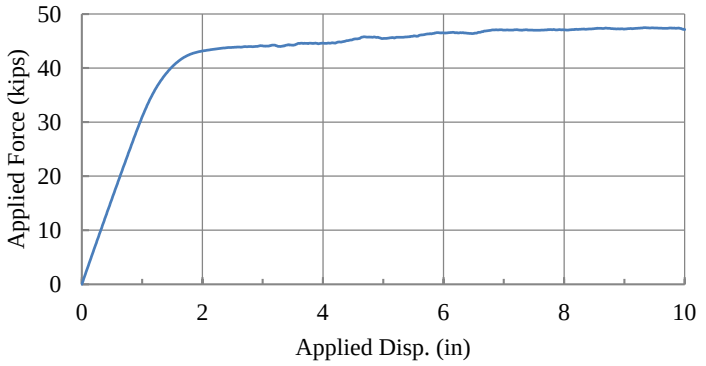

Maximum applied force: 53.94 kips
Story drift at maximum applied force: 2.70%
Yield displacement δy: 1.42 in.
Maximum out-of-plane displacement of panel zone: 2.18 in.

Model 41: Applied Force vs. Applied Disp.

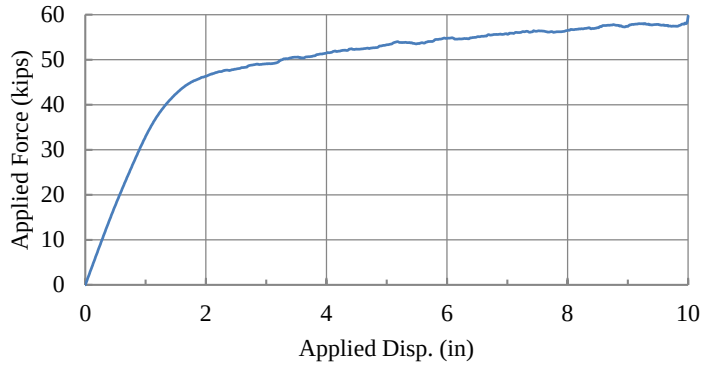

Maximum applied force: 33.18 kips
Story drift at maximum applied force: 0.77%
Yield displacement δy: 1.43 in.
Maximum out-of-plane displacement of panel zone: 2.21 in.

Model 42: Applied Force vs. Applied Disp.

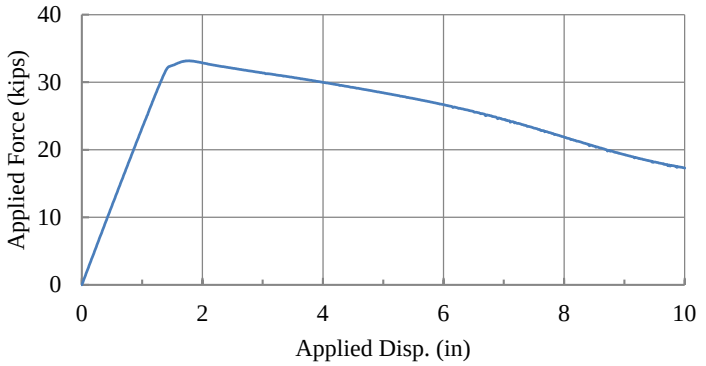

Maximum applied force: 32.37 kips
Story drift at maximum applied force: 0.80%
Yield displacement δy: 1.19 in.
Maximum out-of-plane displacement of panel zone: 2.38 in.

Model 43: Applied Force vs. Applied Disp.

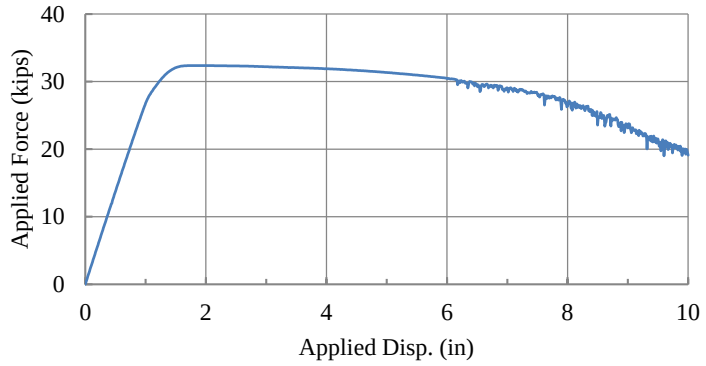

Maximum applied force: 32.94 kips
Story drift at maximum applied force: 0.63%
Yield displacement δy: 1.11 in.
Maximum out-of-plane displacement of panel zone: 2.59 in.

Model 44: Applied Force vs. Applied Disp.

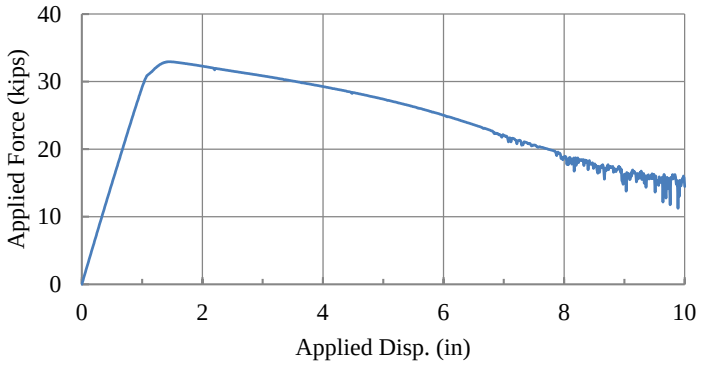

Maximum applied force: 33.67 kips
Story drift at maximum applied force: 0.87%
Yield displacement δy: 1.15 in.
Maximum out-of-plane displacement of panel zone: 2.42 in.

Model 45: Applied Force vs. Applied Disp.

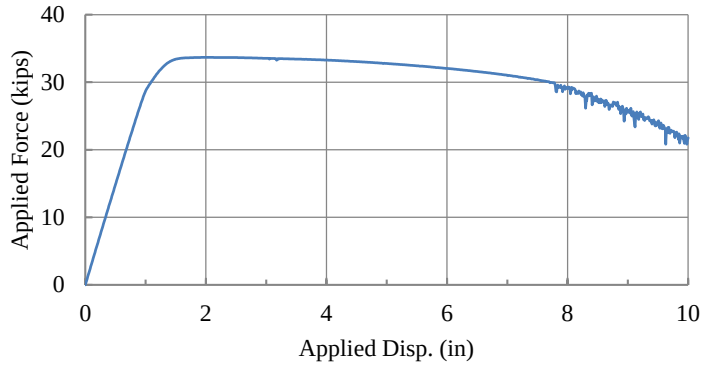

Maximum applied force: 50.05 kips
Story drift at maximum applied force: 2.75%
Yield displacement δy: 1.41 in.
Maximum out-of-plane displacement of panel zone: 1.98 in.

Model 46: Applied Force vs. Applied Disp.

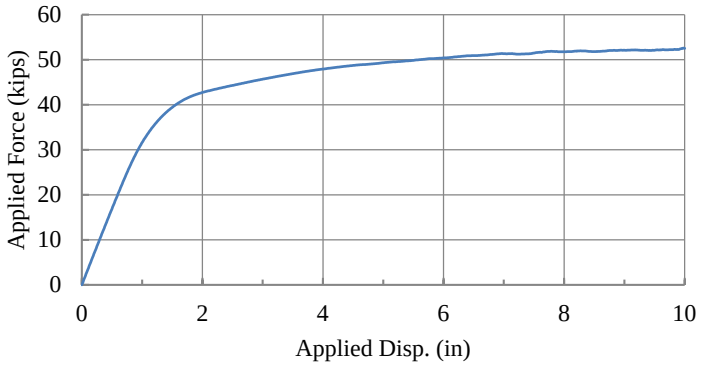

Maximum applied force: 61.76 kips
Story drift at maximum applied force: 3.03%
Yield displacement δy: 1.52 in.
Maximum out-of-plane displacement of panel zone: 1.93 in.

Model 47: Applied Force vs. Applied Disp.

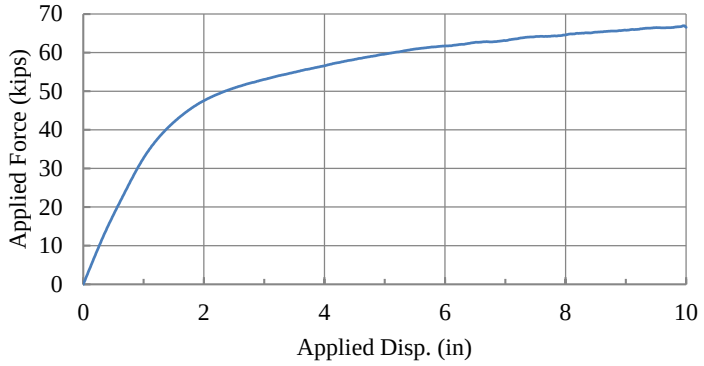

Maximum applied force: 36.33 kips
Story drift at maximum applied force: 0.71%
Yield displacement δy: 1.01 in.
Maximum out-of-plane displacement of panel zone: 3.03 in.

Model 48: Applied Force vs. Applied Disp.

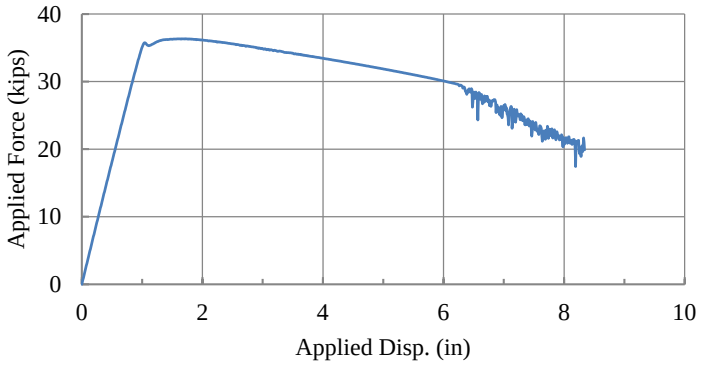

Maximum applied force: 37.50 kips
Story drift at maximum applied force: 1.02%
Yield displacement δy: 1.07 in.
Maximum out-of-plane displacement of panel zone: 3.03 in.

Model 49: Applied Force vs. Applied Disp.

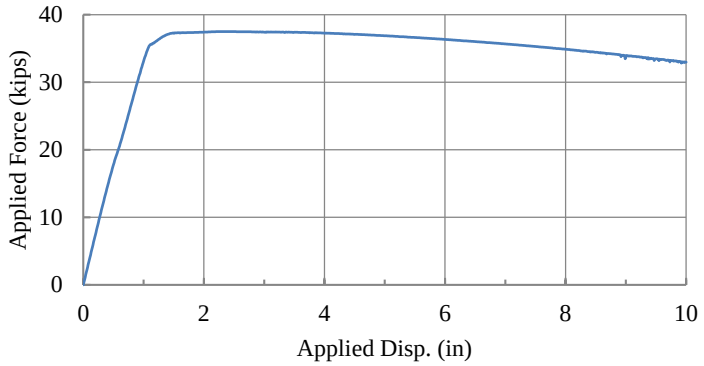

Maximum applied force: 56.13 kips
Story drift at maximum applied force: 2.62%
Yield displacement δy: 1.37 in.
Maximum out-of-plane displacement of panel zone: 3.46 in.

Model 50: Applied Force vs. Applied Disp.

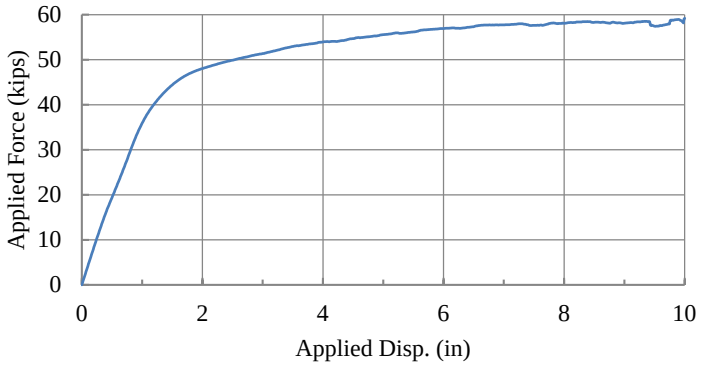

Maximum applied force: 68.97 kips
Story drift at maximum applied force: 2.75%
Yield displacement δy: 1.41 in.
Maximum out-of-plane displacement of panel zone: 3.07 in.

Model 51: Applied Force vs. Applied Disp.

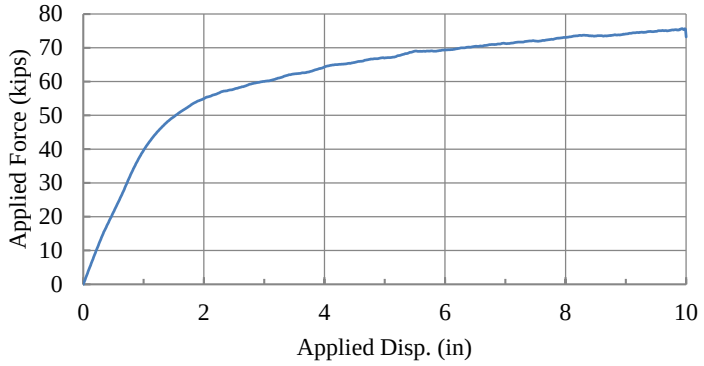

Maximum applied force: 30.63 kips
Story drift at maximum applied force: 0.64%
Yield displacement δy: 1.36 in.
Maximum out-of-plane displacement of panel zone: 3.07 in.

Model 52: Applied Force vs. Applied Disp.

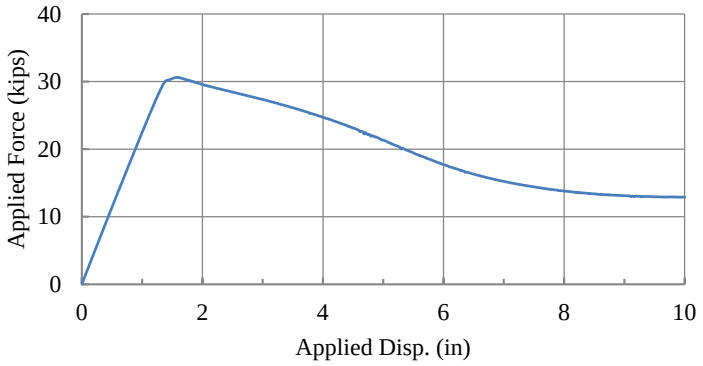

Maximum applied force: 30.26 kips
Story drift at maximum applied force: 0.65%
Yield displacement δy: 1.09 in.
Maximum out-of-plane displacement of panel zone: 2.52 in.

Model 53: Applied Force vs. Applied Disp.

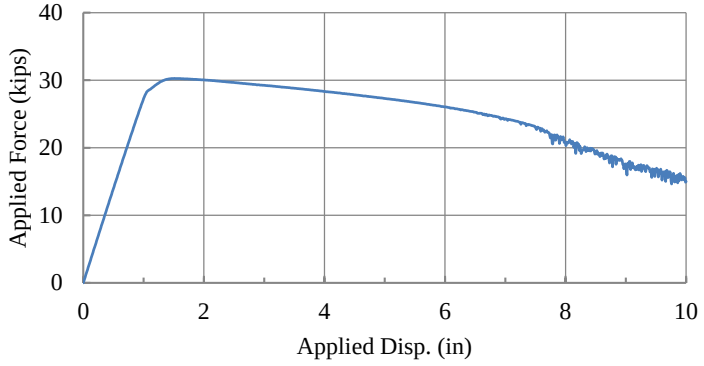

Maximum applied force: 39.19 kips
Story drift at maximum applied force: 2.37%
Yield displacement δy: 1.26 in.
Maximum out-of-plane displacement of panel zone: 2.03 in.

Model 54: Applied Force vs. Applied Disp.

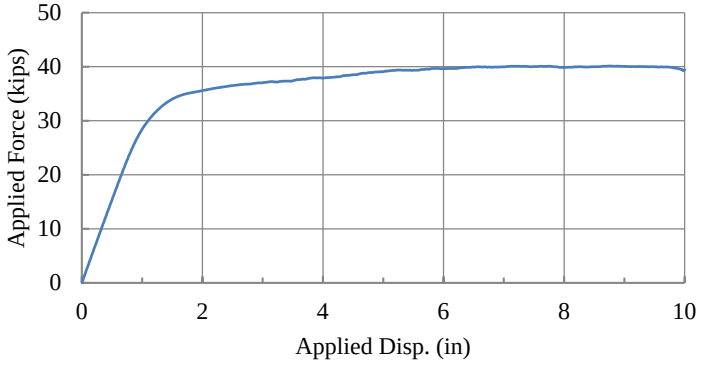

Maximum applied force: 46.45 kips
Story drift at maximum applied force: 2.52%
Yield displacement δy: 1.32 in.
Maximum out-of-plane displacement of panel zone: 2.12 in.

Model 55: Applied Force vs. Applied Disp.

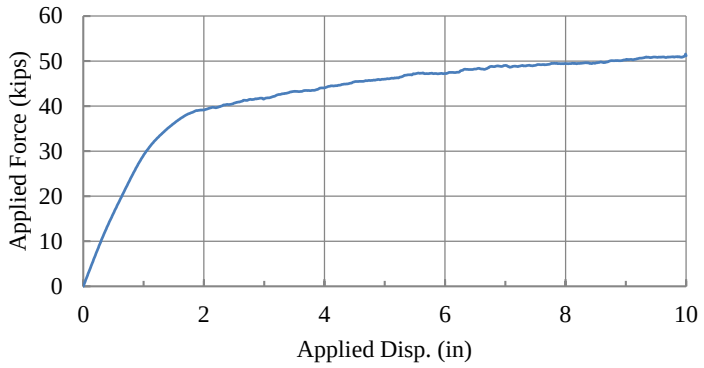

Maximum applied force: 28.03 kips
Story drift at maximum applied force: 0.68%
Yield displacement δy: 1.29 in.
Maximum out-of-plane displacement of panel zone: 2.55 in.

Model 56: Applied Force vs. Applied Disp.

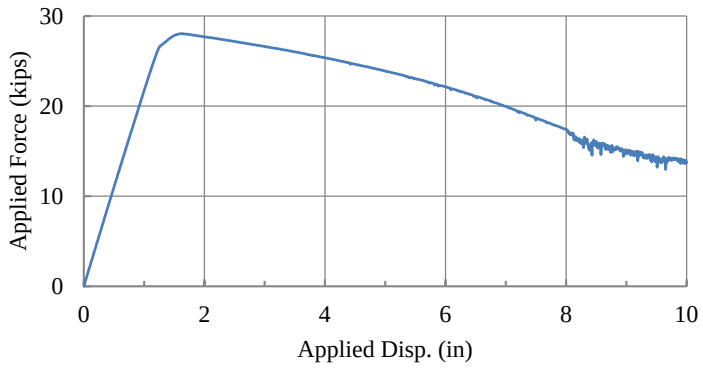

C2 Sub-studies

C2.1 Sub-study on Column and Rafter Lengths, Tapered Section versus Prismatic Section

Maximum applied force: 43.94 kips
Story drift at maximum applied force: 3.84%
Yield displacement δy: 2.14 in.
Maximum out-of-plane displacement of panel zone: 1.81 in.

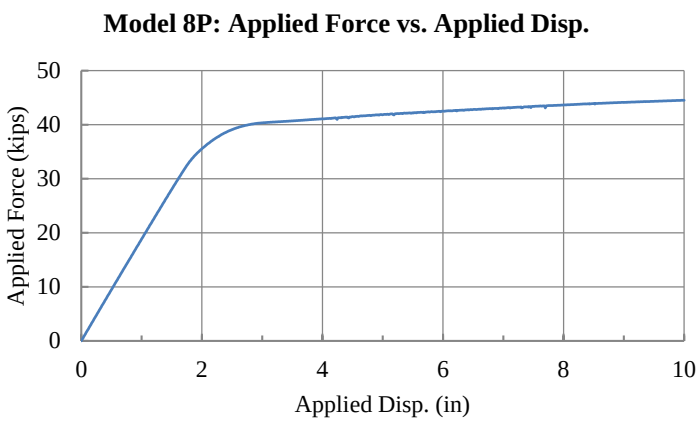

Maximum applied force: 42.35 kips
Story drift at maximum applied force: 1.11%
Yield displacement δy: 2.33 in.
Maximum out-of-plane displacement of panel zone: 2.66 in.

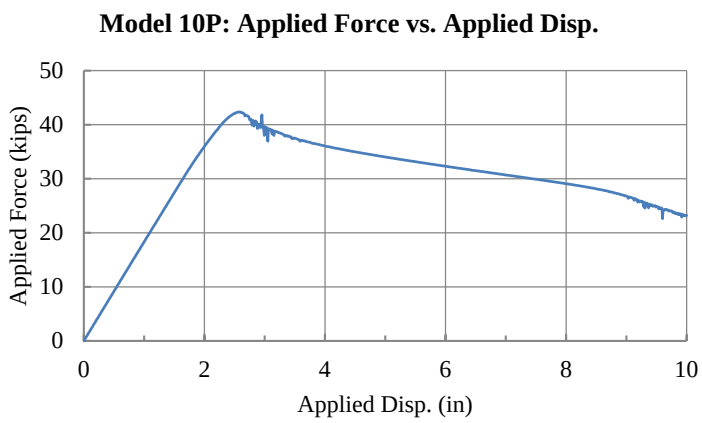

Maximum applied force: 79.80 kips
Story drift at maximum applied force: 2.82%
Yield displacement δy: 1.58 in.
Maximum out-of-plane displacement of panel zone: 2.19 in.

Model 23P: Applied Force vs. Applied Disp.

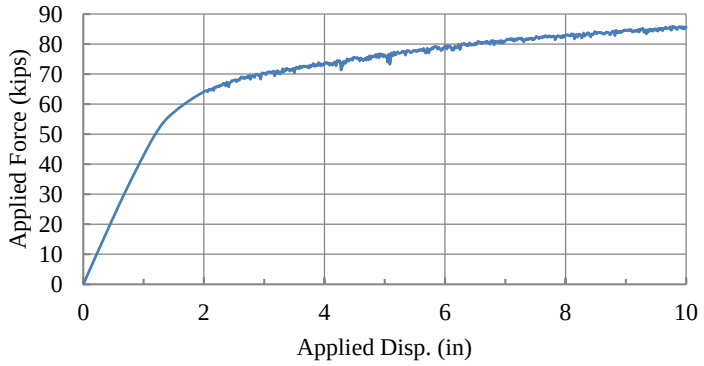

Maximum applied force: 44.38 kips
Story drift at maximum applied force: 1.38%
Yield displacement δy: 2.70 in.
Maximum out-of-plane displacement of panel zone: 2.23 in.

Model 28P: Applied Force vs. Applied Disp.

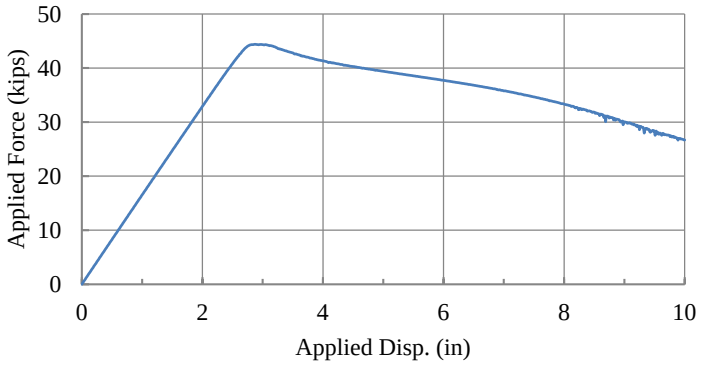

Maximum applied force: 45.70 kips
Story drift at maximum applied force: 0.72%
Yield displacement δy: 1.08 in.
Maximum out-of-plane displacement of panel zone: 2.52 in.

Model 29P: Applied Force vs. Applied Disp.

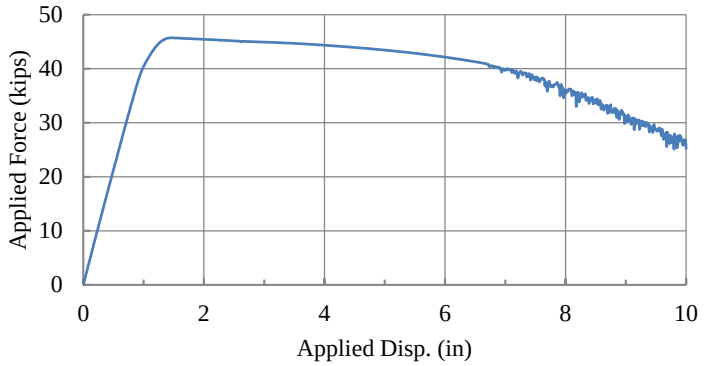

Maximum applied force: 46.63 kips
Story drift at maximum applied force: 4.47%
Yield displacement δy: 2.01 in.
Maximum out-of-plane displacement of panel zone: 1.75 in.

Model 8T: Applied Force vs. Applied Disp.

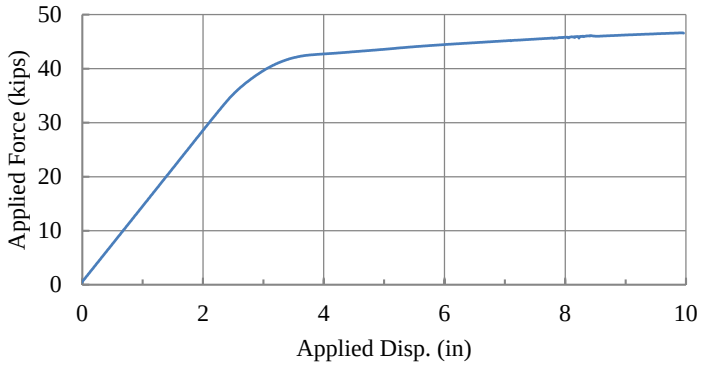

Maximum applied force: 44.89 kips
Story drift at maximum applied force: 1.63%
Yield displacement δy: 2.98 in.
Maximum out-of-plane displacement of panel zone: 2.52 in.

Model 10T: Applied Force vs. Applied Disp.

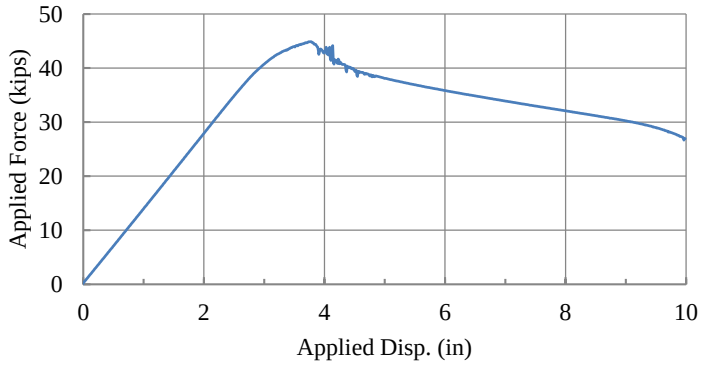

Maximum applied force: 87.34 kips
Story drift at maximum applied force: 3.51%
Yield displacement δy: 1.96 in.
Maximum out-of-plane displacement of panel zone: 2.16 in.

Model 23T: Applied Force vs. Applied Disp.

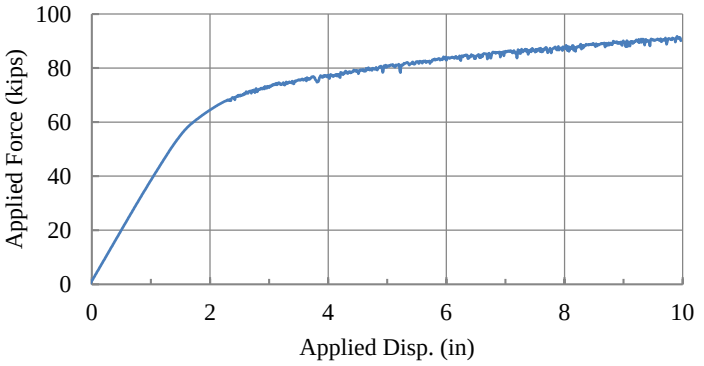

Maximum applied force: 47.98 kips
Story drift at maximum applied force: 1.99%
Yield displacement δy: 3.93 in.
Maximum out-of-plane displacement of panel zone: 2.10 in.

Model 28T: Applied Force vs. Applied Disp.

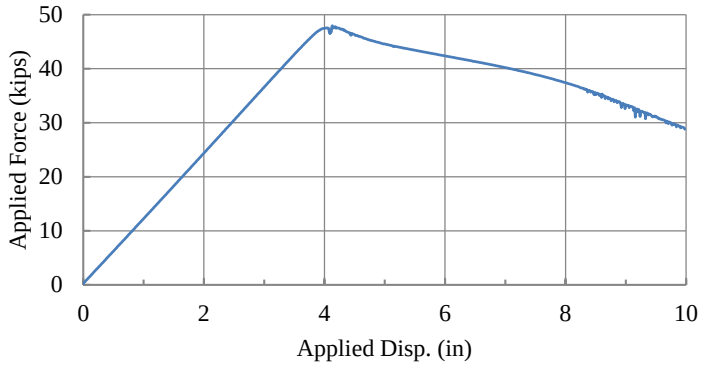

Maximum applied force: 50.24 kips
Story drift at maximum applied force: 0.82%
Yield displacement δy: 1.18 in.
Maximum out-of-plane displacement of panel zone: 2.69 in.

Model 29T: Applied Force vs. Applied Disp.

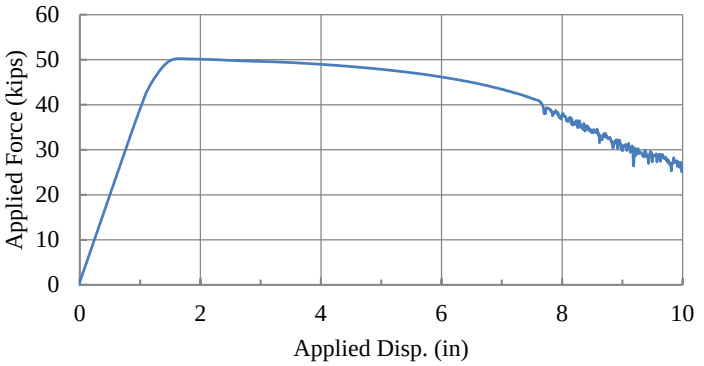

C2.2 Sub-study on Flange Flexural Strength Parameter

Maximum applied force: 43.39 kips
Story drift at maximum applied force: 0.93%
Yield displacement δy: 1.93 in.
Maximum out-of-plane displacement of panel zone: 2.30 in.

Model 1A: Applied Force vs. Applied Disp.

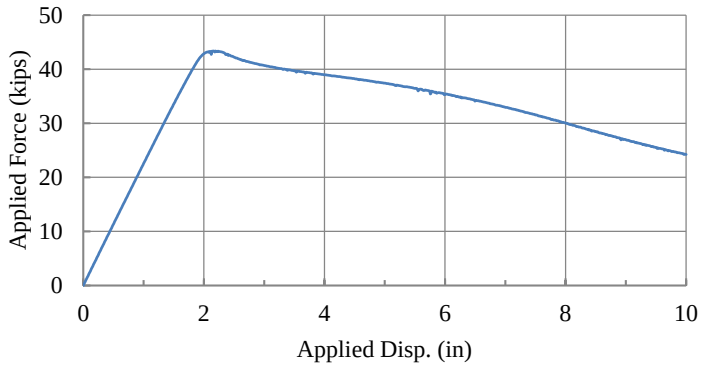

Maximum applied force: 43.29 kips
Story drift at maximum applied force: 0.86%
Yield displacement δy: 1.78 in.
Maximum out-of-plane displacement of panel zone: 2.42 in.

Model 1B: Applied Force vs. Applied Disp.

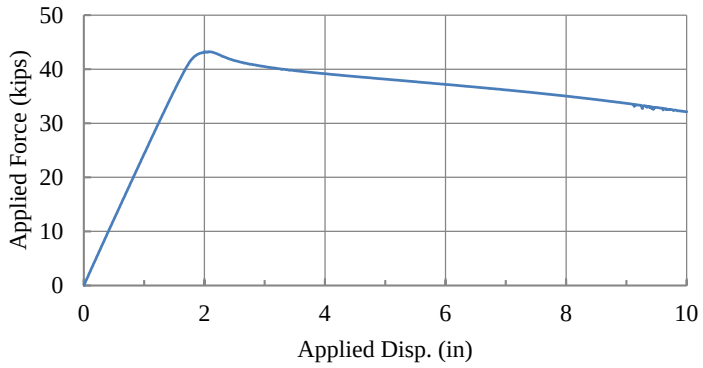

Maximum applied force: 48.19 kips
Story drift at maximum applied force: 0.85%
Yield displacement δy: 1.85 in.
Maximum out-of-plane displacement of panel zone: 2.50 in.

Model 2A: Applied Force vs. Applied Disp.

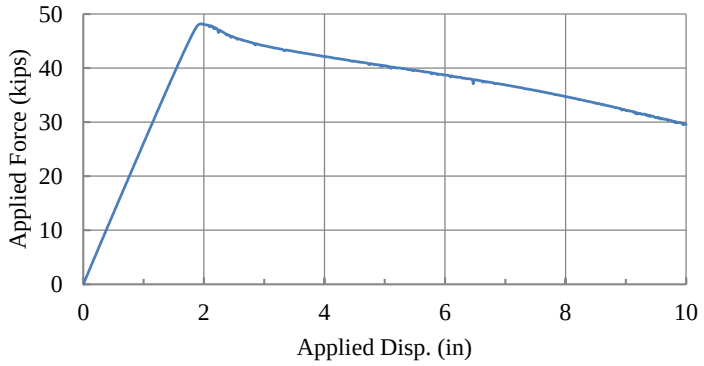

Maximum applied force: 48.19 kips
Story drift at maximum applied force: 0.83%
Yield displacement δy: 1.78 in.
Maximum out-of-plane displacement of panel zone: 2.67 in.

Model 2B: Applied Force vs. Applied Disp.

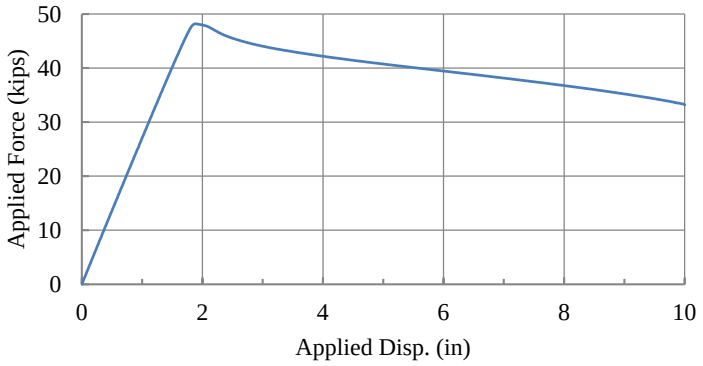

Maximum applied force: 40.43 kips
Story drift at maximum applied force: 0.99%
Yield displacement δy: 2.21 in.
Maximum out-of-plane displacement of panel zone: 2.88 in.

Model 3A: Applied Force vs. Applied Disp.

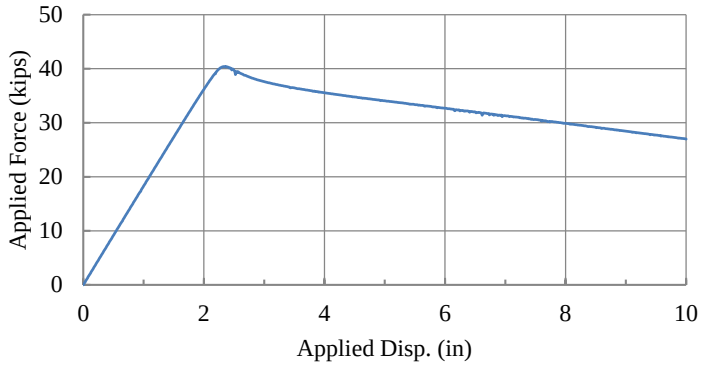

Maximum applied force: 40.53 kips
Story drift at maximum applied force: 1.11%
Yield displacement δy: 2.34 in.
Maximum out-of-plane displacement of panel zone: 3.00 in.

Model 3B: Applied Force vs. Applied Disp.

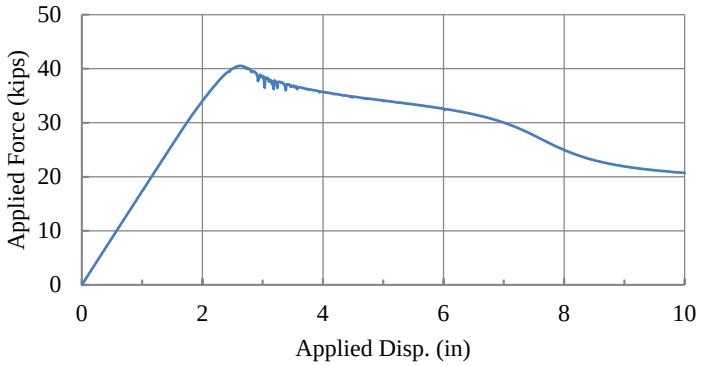

Maximum applied force: 59.82 kips
Story drift at maximum applied force: 0.96%
Yield displacement δy: 1.82 in.
Maximum out-of-plane displacement of panel zone: 2.62 in.

Model 4A: Applied Force vs. Applied Disp.

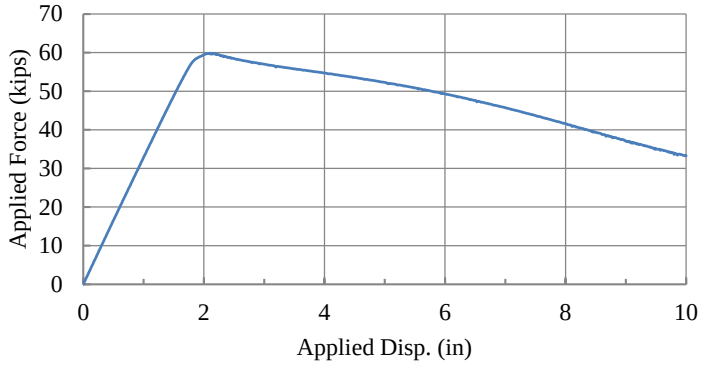

Maximum applied force: 59.64 kips
Story drift at maximum applied force: 0.86%
Yield displacement δy: 1.61 in.
Maximum out-of-plane displacement of panel zone: 2.78 in.

Model 4B: Applied Force vs. Applied Disp.

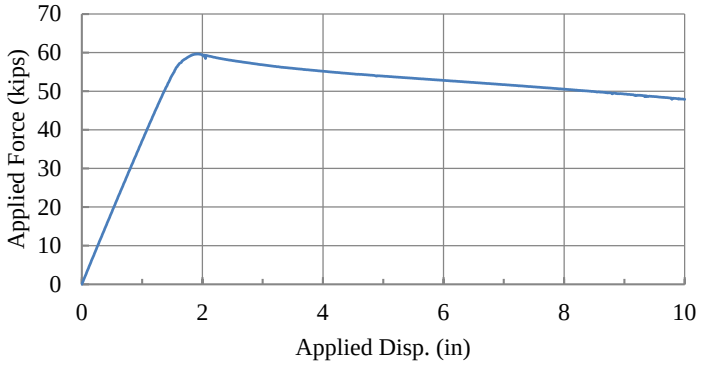

Maximum applied force: 66.83 kips
Story drift at maximum applied force: 0.86%
Yield displacement δy: 1.66 in.
Maximum out-of-plane displacement of panel zone: 2.92 in.

Model 5A: Applied Force vs. Applied Disp.

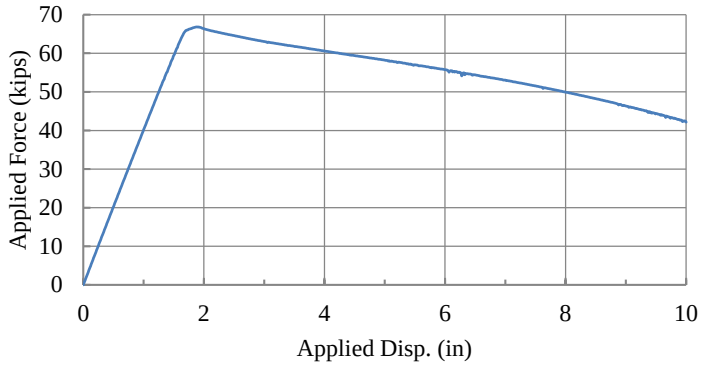

Maximum applied force: 66.69 kips
Story drift at maximum applied force: 0.80%
Yield displacement δy: 1.55 in.
Maximum out-of-plane displacement of panel zone: 3.07 in.

Model 5B: Applied Force vs. Applied Disp.

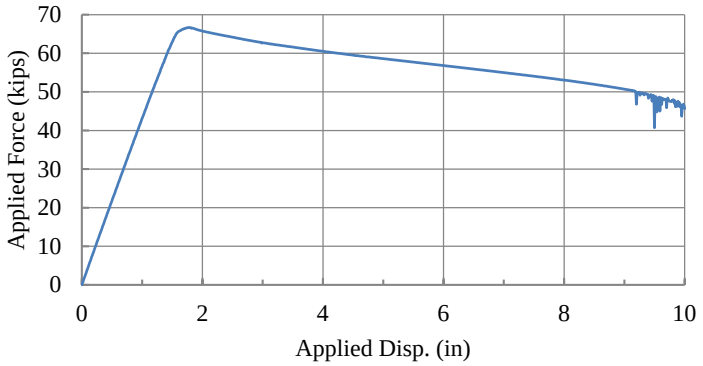

Maximum applied force: 54.54 kips
Story drift at maximum applied force: 0.86%
Yield displacement δy: 1.85 in.
Maximum out-of-plane displacement of panel zone: 2.71 in.

Model 6A: Applied Force vs. Applied Disp.

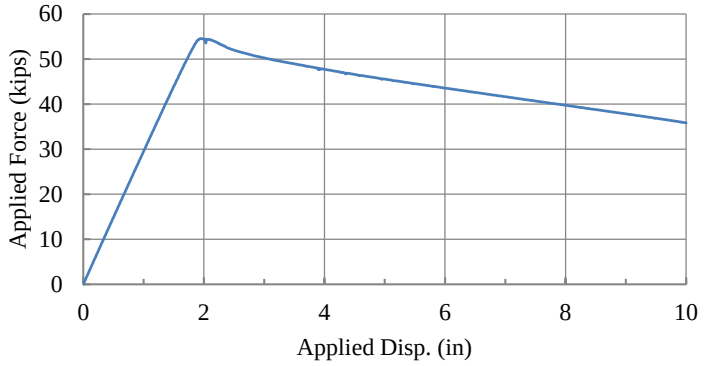

Maximum applied force: 55.30 kips
Story drift at maximum applied force: 0.90%
Yield displacement δy: 1.98 in.
Maximum out-of-plane displacement of panel zone: 2.88 in.

Model 6B: Applied Force vs. Applied Disp.

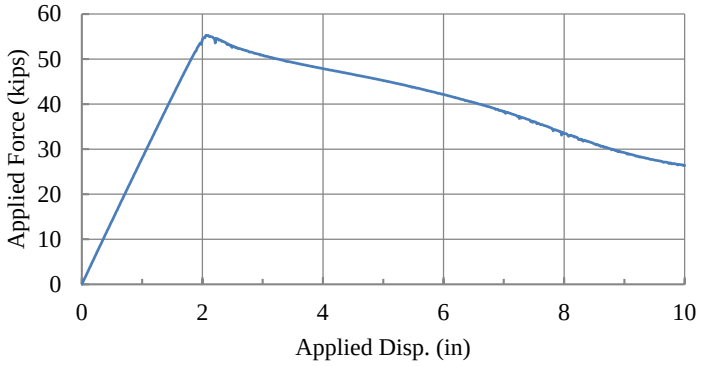

Maximum applied force: 41.05 kips
Story drift at maximum applied force: 0.73%
Yield displacement δy: 1.39 in.
Maximum out-of-plane displacement of panel zone: 2.51 in.

Model 7A: Applied Force vs. Applied Disp.

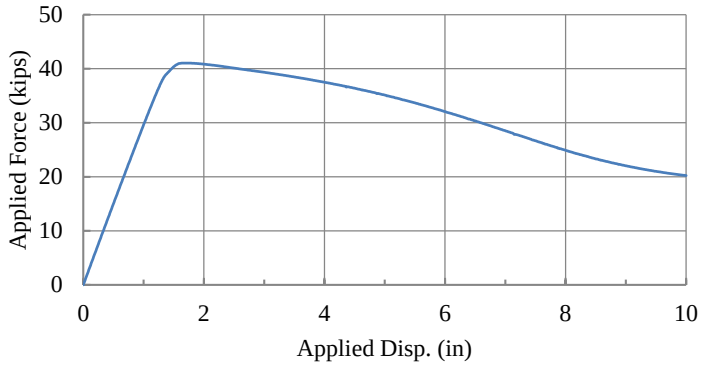

Maximum applied force: 41.01 kips
Story drift at maximum applied force: 0.71%
Yield displacement δy: 1.26 in.
Maximum out-of-plane displacement of panel zone: 2.40 in.

Model 7B: Applied Force vs. Applied Disp.

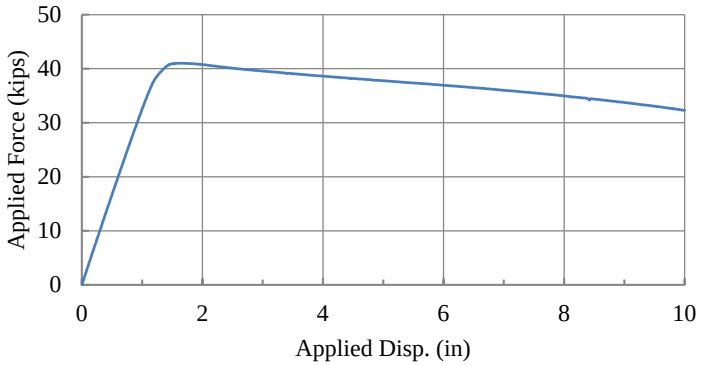

Maximum applied force: 45.73 kips
Story drift at maximum applied force: 0.70%
Yield displacement δy: 1.25 in.
Maximum out-of-plane displacement of panel zone: 2.69 in.

Model 8A: Applied Force vs. Applied Disp.

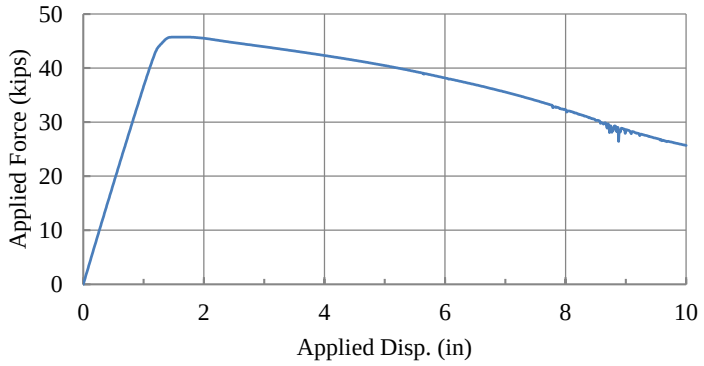

Maximum applied force: 45.62 kips
Story drift at maximum applied force: 0.80%
Yield displacement δy: 1.34 in.
Maximum out-of-plane displacement of panel zone: 2.72 in.

Model 8B: Applied Force vs. Applied Disp.

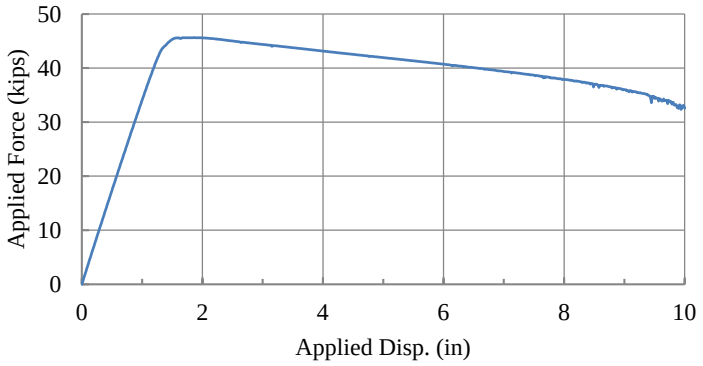

Maximum applied force: 36.71 kips
Story drift at maximum applied force: 0.69%
Yield displacement δy: 1.43 in.
Maximum out-of-plane displacement of panel zone: 2.14 in.

Model 9A: Applied Force vs. Applied Disp.

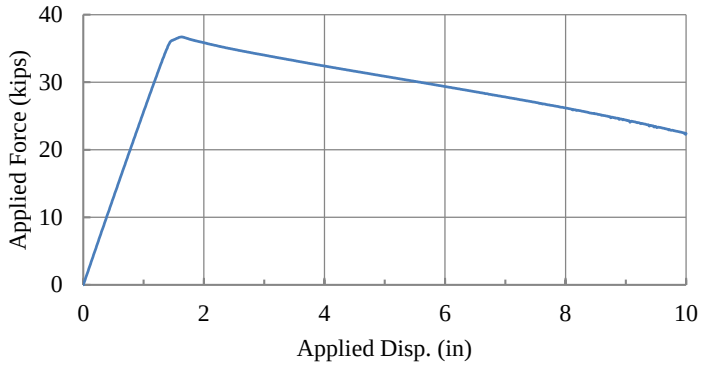

Maximum applied force: 36.77 kips
Story drift at maximum applied force: 0.70%
Yield displacement δy: 1.46 in.
Maximum out-of-plane displacement of panel zone: 2.58 in.

Model 9B: Applied Force vs. Applied Disp.

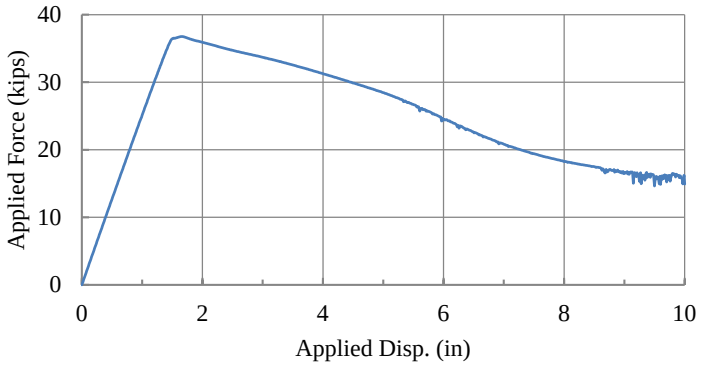

Maximum applied force: 31.23 kips
Story drift at maximum applied force: 0.76%
Yield displacement δy: 1.23 in.
Maximum out-of-plane displacement of panel zone: 2.46 in.

Model 10A: Applied Force vs. Applied Disp.

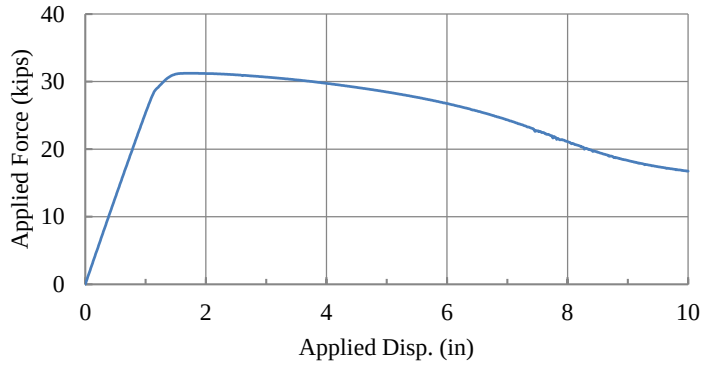

Maximum applied force: 31.38 kips
Story drift at maximum applied force: 0.78%
Yield displacement δy: 1.13 in.
Maximum out-of-plane displacement of panel zone: 2.29 in.

Model 10B: Applied Force vs. Applied Disp.

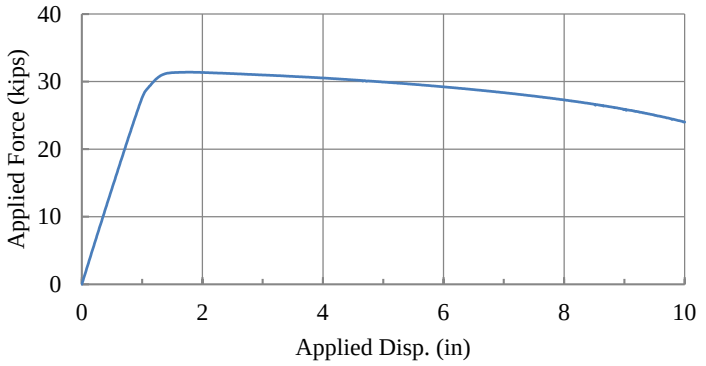

Maximum applied force: 35.00 kips
Story drift at maximum applied force: 0.82%
Yield displacement δy: 1.11 in.
Maximum out-of-plane displacement of panel zone: 2.55 in.

Model 11A: Applied Force vs. Applied Disp.

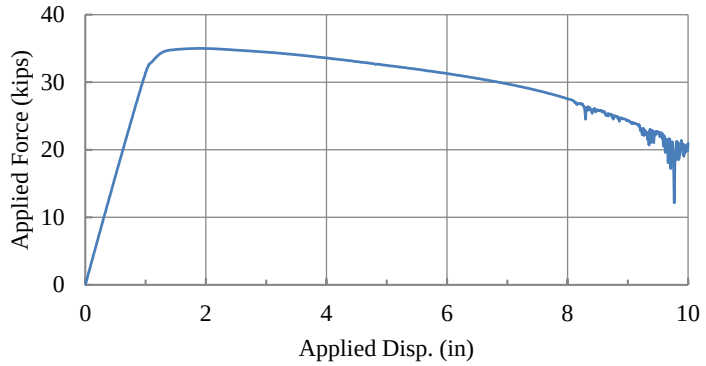

Maximum applied force: 35.42 kips
Story drift at maximum applied force: 0.92%
Yield displacement δy: 1.07 in.
Maximum out-of-plane displacement of panel zone: 3.54 in.

Model 11B: Applied Force vs. Applied Disp.

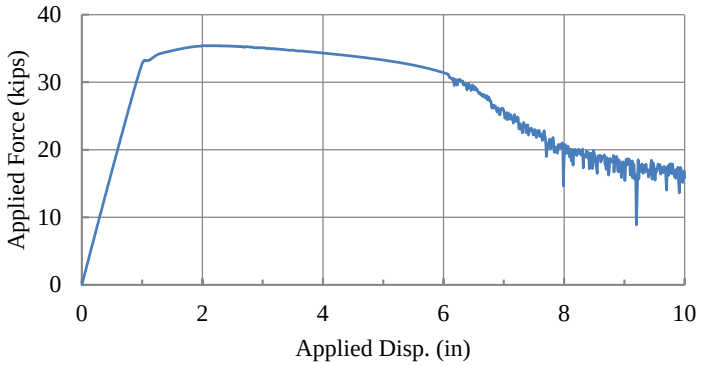

Maximum applied force: 28.11 kips
Story drift at maximum applied force: 0.60%
Yield displacement δy: 1.14 in.
Maximum out-of-plane displacement of panel zone: 2.48 in.

Model 12A: Applied Force vs. Applied Disp.

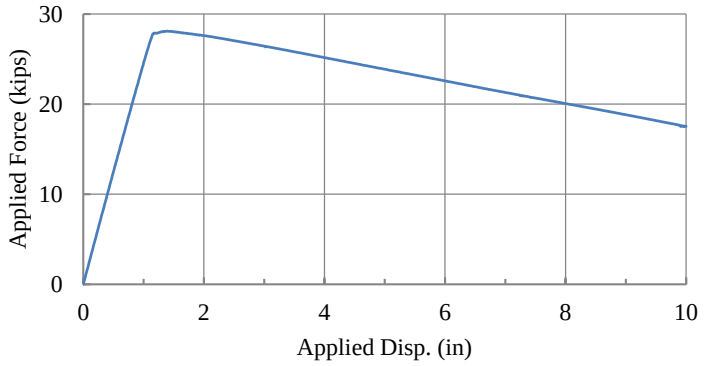

Maximum applied force: 28.38 kips
Story drift at maximum applied force: 0.52%
Yield displacement δy: 1.18 in.
Maximum out-of-plane displacement of panel zone: 2.77 in.

Model 12B: Applied Force vs. Applied Disp.

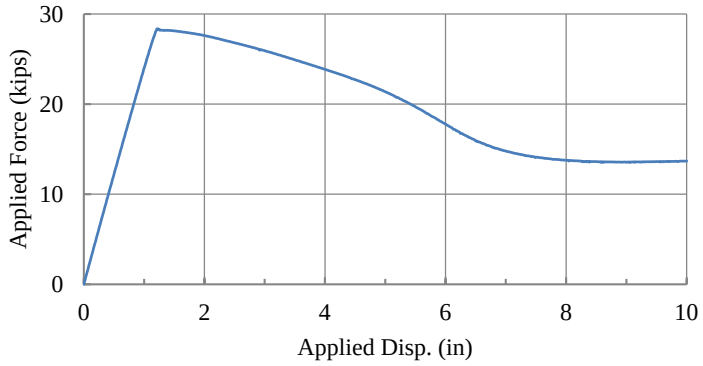

C2.3 Sub-study on Orientation of End-Plate Connection

Maximum applied force: 43.46 kips
Story drift at maximum applied force: 0.99%
Yield displacement δy: 1.90 in.
Maximum out-of-plane displacement of panel zone: 2.40 in.

Model 6H: Applied Force vs. Applied Disp.

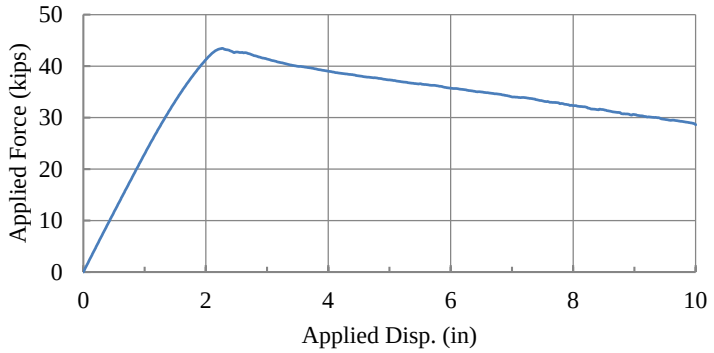

Maximum applied force: 44.39 kips
Story drift at maximum applied force: 1.29%
Yield displacement δy: 1.90 in.
Maximum out-of-plane displacement of panel zone: 2.28 in.

Model 6S: Applied Force vs. Applied Disp.

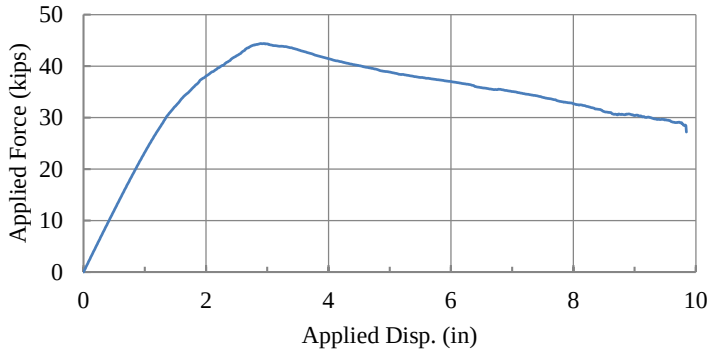

Maximum applied force: 49.47 kips
Story drift at maximum applied force: 1.54%
Yield displacement δy: 1.99 in.
Maximum out-of-plane displacement of panel zone: 2.09 in.

Model 25H: Applied Force vs. Applied Disp.

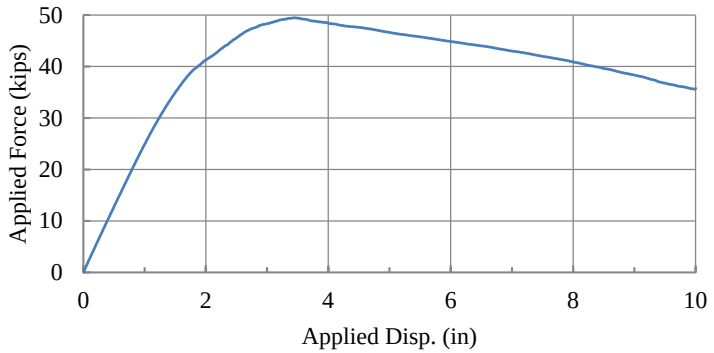

Maximum applied force: 50.55 kips
Story drift at maximum applied force: 1.53%
Yield displacement δy: 1.90 in.
Maximum out-of-plane displacement of panel zone: 2.36 in.

Model 25S: Applied Force vs. Applied Disp.

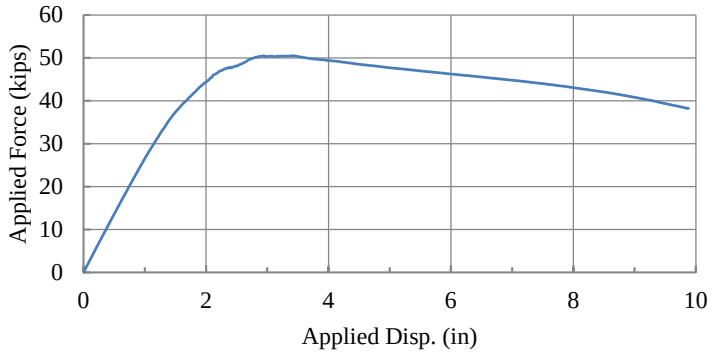

C2.4 Sub-study on Roof Slope

Maximum applied force: 46.99 kips
Story drift at maximum applied force: 1.07%
Yield displacement δy: 2.30 in.
Maximum out-of-plane displacement of panel zone: 2.64 in.

Model 6C: Applied Force vs. Applied Disp.

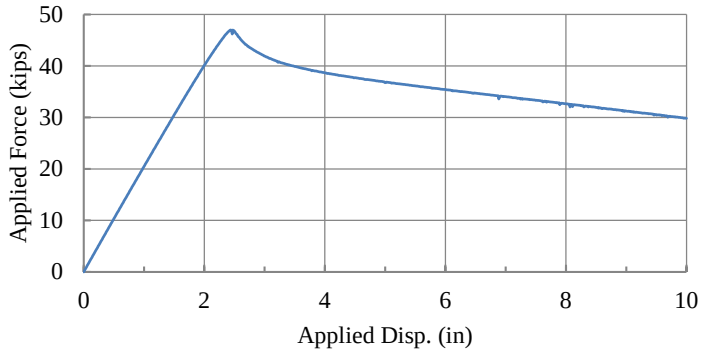

Maximum applied force: 49.89 kips
Story drift at maximum applied force: 0.86%
Yield displacement δy: 1.68 in.
Maximum out-of-plane displacement of panel zone: 2.25 in.

Model 6D: Applied Force vs. Applied Disp.

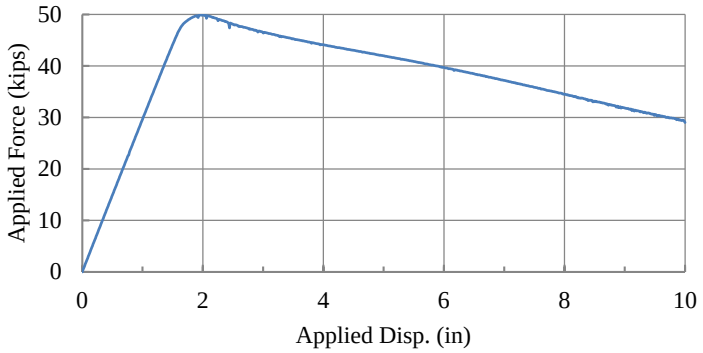

Maximum applied force: 52.25 kips
Story drift at maximum applied force: 1.09%
Yield displacement δy: 2.24 in.
Maximum out-of-plane displacement of panel zone: 2.73 in.

Model 25C: Applied Force vs. Applied Disp.

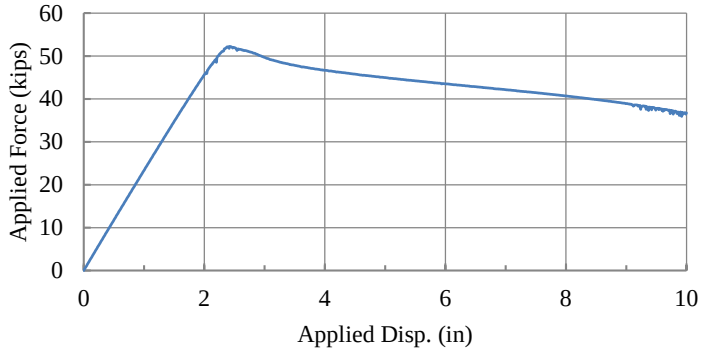

Maximum applied force: 58.72 kips
Story drift at maximum applied force: 0.99%
Yield displacement δy: 1.75 in.
Maximum out-of-plane displacement of panel zone: 2.35 in.

Model 25D: Applied Force vs. Applied Disp.